THESIS

ASSESSING IMPACTS OF RAINFALL PATTERNS, POPULATION GROWTH, AND SEA LEVEL RISE ON GROUNDWATER SUPPLY IN THE REPUBLIC OF MALDIVES

Submitted by

Chenda Deng

Department of Civil and Environmental Engineering

In partial fulfillment of the requirements

For the Degree of Master of Science

Colorado State University

Fort Collins, Colorado

Summer 2016

Master's Committee:

Advisor: Ryan Bailey

Neil Grigg
William E. Sanford

ABSTRACT

ASSESSING IMPACTS OF RAINFALL PATTERNS, POPULATION GROWTH, AND SEA LEVEL RISE ON GROUNDWATER SUPPLY IN THE REPUBLIC OF MALDIVES

Groundwater resources of the Republic of the Maldives are threatened by a variety of factors including variable future rainfall patterns, continued population growth and associated pumping demands, rising sea level, and contamination from the land surface. The Maldives is composed of approximately 2,000 coral islands residing in 26 atolls in the Indian Ocean, with each coral island less than a few square kilometers in surface area and less than a few meters in elevation. This thesis uses numerical modeling techniques to assess the influence of variable rainfall patterns, increased pumping due to population growth, and sea level rise on fresh groundwater supply of the coral islands that comprise the Maldives. The density-dependent groundwater flow and solute transport model SUTRA (Saturated Unsaturated Transport) is used for all simulations, with the model simulating the spatial extent of the freshwater lens in the aquifer of the coral islands.

The thesis first assesses changes in groundwater supply due to variable rainfall patterns in the coming decades, a key component of water resources management for the country. Using a suite of two-dimensional vertical cross-section models, time-dependent thickness of the freshwater lens is simulated for a range of island sizes (200 m to 1100 m) during the time period of 2011 to 2050, with recharge to the freshwater lens calculated using rainfall patterns provided by General Circulation Models (GCM) for the three distinct geographic regions (north, central, south) of the Maldives. Results show that average lens thickness of islands in all three geographic regions

during the 2031-2050 time period is slightly greater than during the 2011-2030 time period, indicating a mild increase in future available groundwater supply under predicted conditions. Average lens thickness during 2011-2030 for islands of 200 m, 400 m, 600 m, and 1100 m width is 0.5 m, 3.0 m, 7.0 m, and 12.2 m, respectively, with these values increasing by 1-5% during 2031-2050 time period. However, these results do not include the effect of sea level rise.

To quantify the total available groundwater on a representative island and to provide accurate simulation of the effect of radial pumping on the freshwater lens, a three dimensional model is created for the island of Gan (Area: 598 ha, Population: 4,280) to evaluate the impact of increasing pumping and sea-level rise on future groundwater resources. Simulations covering the 2012-2050 period are used to compare scenarios of future rainfall, pumping vs. non-pumping, varying rates of population growth and hence of groundwater pumping, and sea level rise (0.5 m by 2100) vs. no sea level rise. Results indicate that the total freshwater volume increases about 19% under the effects of future rainfall patterns. If moderate pumping is included, with rates increasing at 1.76% to correspond with increasing population, the volume increases only by 12%. If just considering sea level rise, then the volume decreases by 14%. With aggressive pumping, corresponding to an annual population growth rate of 9%, but no sea level rise, the volume decreases by 24%. With aggressive pumping and sea level rise, the freshwater lens is rapidly depleted.

This study quantifies the major future impacts on groundwater of the atoll islands in Maldives. Similar methodologies using output from GCMs can be used for other atoll island nations, such as the Republic of Marshall Islands, Federated States of Micronesia, and Gilbert Islands. For the Maldives, results from this study can be used in conjunction with population

growth estimates to determine the feasibility of including groundwater in water resources planning and management for the country.

TABLE OF CONTENTS

LIST OF TABLES

LIST OF FIGURES

CHAPTER 1: INTRODUCTION OF ATOLLS IN THE REPULIC OF MALDIVES

This first chapter gives an introduction about atoll islands, atoll island hydrogeology, and groundwater resource of the coral islands of the Republic of Maldives. The problem statement regarding groundwater resources will be discussed, and objectives of the thesis will be outlined.

1.1 Geography and Population of the Maldives

The Republic of the Maldives (Figure 1) consists of approximately 2000 coral islands, each located in one of 26 atolls within the region of 5^0S -10^0N latitude in the Indian Ocean (Karthikheyan, 2010). An atoll (Figure 1C) is a circular chain of small islands and coral reef surrounding a shallow lagoon, underpinned by carbonate platforms that extend downward to a volcanic edifice. The central lagoon is the result of the outgrowth of the coral reef due to a preference for sediment-free waters (Falkland and Custodio, 1991), and usually is shallow and assumed to have the same salinity as the surrounding ocean (Terry and Ting, 2012). The total land area of the Maldives is approximately 300 km^2 (MEE, 2011), with many of the inhabited islands having a land surface area of less than 1 km^2. Island widths range between 100 m to about 1200 m. Maximum ground surface elevation is 2.4 m above sea level, and 90% of the land area has an elevation of less than 1 m. Approximately 200 islands are inhabited, with a total population of 320,000 (The World Bank, 2011).

1.2 Climate and Water Resources of the Maldives

The Maldives experiences a warm and tropical climate year-round, with an average annual temperature of 28.0 ^{o}C and an average relative humidity of 80%. The rate of rainfall increases from north to south, with three distinctive regions of 5^0N -10^0N, 0^0 -5^0N, and 5^0S -0^0 having

average annual rainfall rates of 1715 mm, 1940 mm, and 2380 mm respectively, over the 1998-2011 period. A distinct dry season occurs during from January to April, particularly for the northern regions. As the high permeability of islands soils precludes the formation of streams or surface water bodies, typical of atoll islands (Urish, 1951), the communities rely on a combination of water from rooftop catchment systems, desalinized water, and groundwater.

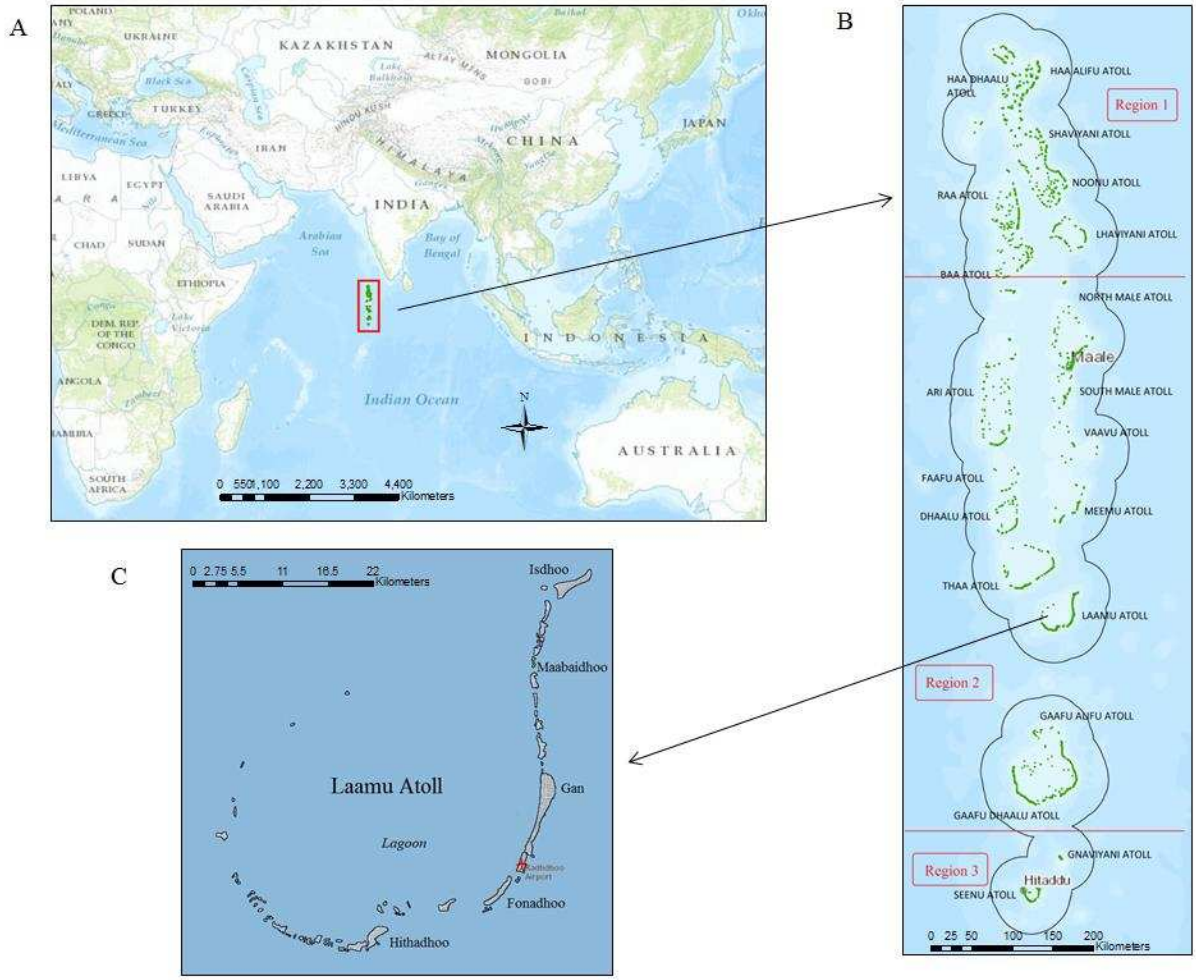

Figure 1. (A) Maldives geographical position in the Indian Ocean; (B) the atolls of the Maldives, divided into three geographic regions used in this study: Region 1 is the area above 5° N, Region 2 is between 5°N and 0° and Region 3 is below 0°; (C) a close-up of an example atoll (Laamu Atoll), showing the coral islands surrounding the lagoon.

1.3 Geology of Atoll Islands in the Republic of Maldives

The island's aquifer usually consists of two layers, the Holocene aquifer resting on the Pleistocene aquifer (Figure 2A). Many studies have found the existence of these two layers on the atoll islands in the Indian Ocean before including Cocos Islands (Woodroffe and Falkland, 1997). During 2000 to 2001, Falkland did lots of coring on 16 islands in the Maldives; white coral rock was found that might belong to the Pleistocene age. They also estimated that the contact between the two layers, which is termed as "Thurber Discontinuity" (Thurber et al., 1965), ranges from 9.5-24 m (Falkland, 2000, 2001). The contact is an important factor in limiting the freshwater lens in large atoll islands because of the large difference between the aquifer hydraulic conductivities (Hunt, 2007). The permeability (typically 5-10m/day) of upper aquifer has been estimated to be one to two orders of magnitude less than that of the Pleistocene aquifer(typically 50-1000m/day) (Falkland, 2000).

1.4 Freshwater Lens

Fresh groundwater is mostly contained in the Holocene aquifer. Rainfall that does not runoff directly into the ocean and is not transpired by vegetation percolates through the shallow unsaturated zone of the island and recharges the water table. The body of fresh groundwater in the aquifer is referred to as a "freshwater lens" due to its geometrical shape (Figure 2), with the maximum thickness of the lens typically occurring under the center of the island. Due to the mounding of the water table and the resulting hydraulic gradient, the fresh groundwater flows towards the perimeter of the island and discharges into the sea (Glover, 1964). Vertical infiltration of precipitation expends the thickness of freshwater, which varies under a dynamic equilibrium between moving freshwater and sea water. To simply quantify the thickness of the

freshwater lens, Badon and Herzberg used the difference in density between freshwater and seawater to determine that the thickness of the freshwater lens is approximately forty times the height of the freshwater level above sea level (Badon Ghyhen, 1889; Herzberg, 1901). However, Ghyben-Herzberg principle is not always applicable because the interface of freshwater and seawater is not a sharp sharp interface; instead, there is a mixing zone of freshwater and seawater, which makes estimating the freshwater boundary very difficult. Various modeling methods used to simulate the freshwater/seawater dynamics and the depth of this interface will be presented in Chapters 2 and 3 of this thesis.

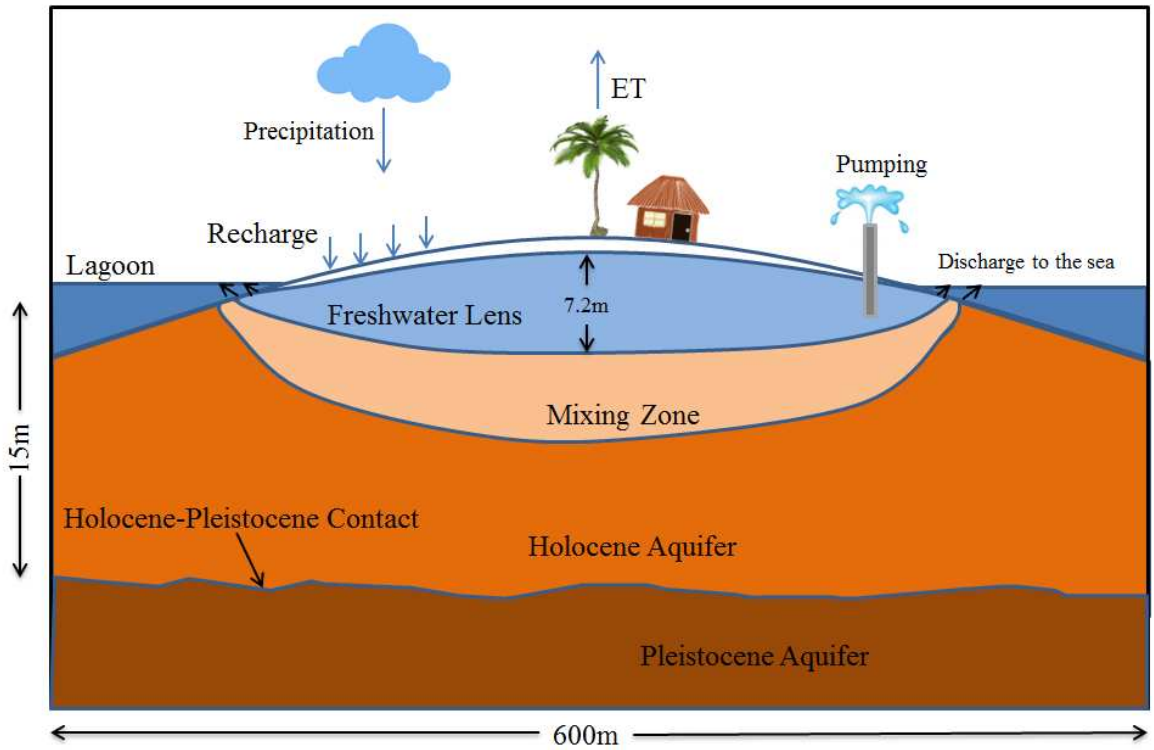

Figure 2. Hydrogeological cross section of a typical atoll island in the Maldives region;

The amount of fresh groundwater, which often is quantified by the metrics of freshwater lens volume and maximum freshwater lens thickness, is controlled principally by the width of the island, the permeability of the aquifer, the recharge rate to the water table resulting from

precipitation (Mather, 1975), and (if any) groundwater extraction through vertical wells or horizontal infiltration galleries (White et al., 2007). Generally, freshwater lens volume and thickness correlate positively with island size; for example, small coral islands (cross-section width < 600 m) generally have thin (< 5 m) lenses, whereas larger coral islands (> 600 m) generally have thick (5-20 m) lenses. As mentioned before, the input of freshwater recharge and discharge to the sea establishes the dynamic equilibrium. A change in rainfall patterns can have a significant impact on the volume of fresh groundwater in the aquifer. In addition, sea-level rise, population growth and associated increase in groundwater extraction, and groundwater contamination from leaching land surface pollution results in the freshwater lens being an extremely fragile resource for small coral islands (Pernetta, 1992; Presley, 2005; Church et al., 2006).

1.5 Water resources in the Republic of Maldives

This section summarizes all possible water resources used in Maldives and quantifies their usages. It gives an overview of present situation and management of those water resources in Maldives, followed by discussing all kinds of threats to freshwater lens of Maldives. One of the objectives of this thesis is to evaluate some of the threats.

1.5.1 Water resources and usages in Maldives

Freshwater mainly comes from three resources in Maldives: rainwater, groundwater, and desalinated seawater. The government's goal is to provide 10 liters of safe water per person per day for drinking and cooking purposes (MPHRE, 1998), with the majority of water coming from rainwater catchment systems. Rainwater is usually collected into water tanks through a house roof and gutter system. According to UNEP (United Nations Environment Programme), in 2005,

75% of the population collected rainwater from communal rainwater storage tanks or individual household tanks (UNEP, 2005). Since 1994, the government has focused on providing 2914 high-density polyethylene (HDPE) tanks (capacity of 5000L) for community use on over 200 inhabited islands and implemented a program to provide household tanks (capacity of 1500~2500L) for each household in 2006 (WHO,2009). Besides rainwater, desalinated water is a source for drinking water. The use of desalinated water is increasing, especially in the capital Male. 35% of the population in Maldives has access to desalinated water with desalination plants in 51 islands (MEE, 2011). However, after the Indian Ocean Tsunami of 2004, 30% of the population had drinking water shortages (MPND, 2004). From the year of 2005 to 2011, More than about 70 out of 200 inhabited islands reported water scarcity every year, ranging from 2.1 ML to 7.5 ML (MEE, 2011).

According to Beswick (2000), groundwater fulfills for non-potable usages such as sanitary cleansing and toilet flushing, bathing and clothes washing. Estimates of total water usage are as high as 175L/p/d (Beswick, 2000). However, after reviewing other studies, Falkland (2010) recommended water usage as 120L/p/d, in which only 5-10L is from rain catchment, and the bulk of water is from pumping. Groundwater is still the main domestic water resource for most islands of the Maldives. There is still no adequate data for assessing fresh groundwater quantities in all islands (MEE, 2011), although some groundwater investigations have been done for nineteen islands (Falkland, 2000 2001; Bangladesh Consultants, Ltd., 2010a,b,c,d). The average freshwater lens and sustainable yield for each of the studied island from these studies are listed in Table 1. Adequate fresh groundwater resources exist in most islands. The data from these islands, particularly the freshwater lens thickness, are used to test the model applications described in Chapters 2 and 3.

Before 2005, Male Water and Sewerage Company (MWSC) were in charge of the promotion of best practice water supply and sanitation provision for all the islands, especially providing potable water to Male residents. The outer islands of Male managed their own water at the household level. After July 2005, a new ministry, the Ministry of Environment, Energy and Water (MEEW), share the authority with MWSC on national water sector management. MEEW is now in charge of overall water policy for Maldives. However, the outer islands communities are still responsible for the operation and maintenance of these new systems (GWP Consultants, 2006).

Table 1. Lens thickness and sustainable yield for 19 islands in Maldives from groundwater investigations (Falkland, 2000 2001; Bangladesh Consultants, Ltd., 2010a,b,c,d)

Atoll	Island Name	Area (ha)	Average Freshwater Lens Thickness (m)	Sustainable Yield (kL/Day)
Addu Atoll	Hithadhoo	544	8	3,680
	Maradhoo	87	2	322
	Feydhoo	60	6	441
	Gan	290	15	2,880
Haa Alifu Atoll	Hoarafushi	63	0.5	140
	Ihavandhoo	60	3	135
	Dhidhdhoo	51	2	205
	Kelaa	213	8	480
	Filladhoo	226	0.5	35
	Baarah	249	6	375
Haa Dhaalu Atoll	Hanimaadhoo	260	4	775
	Nolhivaranfaru	151	0.5	125
	Nolhivaram	221	4	515
	Kulhudhuffushi	172	7	475
	Kumundhoo	178	8	545
Gaafu Dhaalu Atoll	Thinadhoo	118	5.5	1000
Laamu Atoll	Gan	598	8.4	5600
Noonu Atoll	Holhudhoo	19.8	1.28	100
	Velidhoo	44.2	1.93	240

1.5.2 Threat to the freshwater lens in the Maldives

Fresh groundwater can be a valuable water resource, however, it is very vulnerable. Sea-level rising, changing rainfall pattern, shoreline erosion, sea water intrusion, pumping, and groundwater contamination are all threats to freshwater lens.

Climate change is a huge concern for the Republic of Maldives. The rising sea-level and seawater temperature are threats to the freshwater lens. The sea-level rise is predicted to rise a half meter for the Maldives during 21st century (Woodworth, 2005), which will result in significant shoreline recession. The general shoreline recession is 100 m corresponding to 1 m of sea-level rise (1% slope) (Tysban et al., 1990). As a result, massive land areas will erode and inundate due to the rising seawater; in turn, the thickness of the freshwater lens decreases as land surface area shrinks (Volker et al. 1985). Another major concern from climate change is the increase in water temperature. Coral bleaching would increase due to temperature increase in lagoon water (Pernetta and Elder, 1990). Current death of corals is associated with thermal stress (Pernetta, 1992). In 1998, 70-90% mortality of coral was reported in Maldives due to climate related bleaching events (Rajasuriya et al., 2000). The reasons of this bleaching event, including high temperatures, are discussed (Wilkinson et al., 1999). Global-mean land temperatures are projected to increase about 5.5K by 2100 (Cox et al., 2000), which might make the bleaching events more frequent and widespread. Death of coral reefs will accelerate the erosion of shorelines and damage to the freshwater lenses.

Human activities influence shoreline erosion, in addition to climate changes. In the Maldives, human activities like construction of causeways between islands, construction of wharves, grouynes and breakwater, dredging, harbour works, sea defences and sand mining cause severe erosion (Mörner et al., 2004; Rajasuriya et al., 2000; Richmond et al., 2006). Furthermore, human activities tend to negatively impact the coral reefs. As mentioned before, as a country of 1192 coral islands with its great diversity and extent in corals, the reefs are essential for its shoreline protection for Maldives (Rajasuriya et al., 2000). However, intensive coral mining has caused dramatic reduction in coral varieties and abundance in some areas. For example, the

living coral reef in North Male is estimated to be exhausted within few decades (Brown and Dunne, 1988). There is no complete evaluation of shoreline erosion for all atolls in Maldives, however, with the evidence above, it is reasonable to conclude that the shorelines of the Maldives are a severe risk of erosion.

Climate controls the rainfall patterns, so a change in climate results in more frequent inordinate events, such as extreme rainfall, winds, storm surge tide and droughts (White et al., 2007; Peinhardt, 2014; Sovacool, 2012; Hay, 2006). A long-term drought can deplete the freshwater lenses since fresh groundwater continually discharges to the sea. During the dry season of a normal year, from January to March in Maldives, the freshwater lens of small coral islands almost depletes. In addition, surges of seawater during storms and typhoons can cause damage to the freshwater lens. A storm surge is a high rise of seawater that erodes the freshwater aquifer and overtops low-laying islands, causing seawater intrusion (Terry and Thaman 2008; Spennemann 2006). It can take up to eleven months for a freshwater lens to recover from the seawater intrusion (Terry and Falkland, 2010).

All of the above examples are natural stressors. However, anthropogenic stress, such as population growth and groundwater contaminations, has already done a lot of damage to the freshwater resources in Maldives (SOE, 2011; Pernetta, 1992). The relatively high-population capital, Male, has run out of potable, fresh groundwater (Pernetta, 1992). Water scarcity occurs often with significant population increase (SOE, 2004). The population of Maldives has tripled in the last 35 years with an above average growth rate of 1.76% (World average: 1.17%) (SOE, 2011). High population growth creates a higher water demand via pumping.

Groundwater contamination is detected in sampled wells of all islands. Fecal coliform, salinity, ammonia, nitrate and nitrite and phosphate are found at different levels for each island, which renders fresh groundwater to be non-potable or highly unsafe for domestic use. From the report "State of the Environment for Maldives" (2004), only 39 of the 198 islands' groundwater is suitable for drinking (MEE, 2004).

1.6 Brief Historical review of estimating freshwater lenses

There are several ways to estimate the freshwater lens thickness in atoll islands. A traditional way of performing these estimates is through field measurements. Historically, the principal means of measuring the thickness of the lens is through drilling monitoring wells and measuring the salinity concentration of the groundwater through the depth of the profile. Recently, geophysical methods were used (Falkland 2000, 2001) to estimate lens thickness and, if enough measurements were taken, the volume of the lens. For example, during 2000 to 2001, Falkland did salinity surveys on 10 islands in the Maldives using Electromagnetic (EM) surveying (Falkland, 2000; Falkland, 2001). Falkland tested water salinity from several boreholes to estimate the lens thickness with supplemental (EM) surveying. Thus, the relationship of EM readings and lens thickness from salinity survey was developed and used to estimate the total groundwater resources for each island. In 2009, Bangladesh Consultants performed groundwater investigations on the islands of Gan, Thinadhoo, Holhudhoo and Velidhoo. They used the EM method at more than 20 locations on each island to make contour maps and estimate the total freshwater volume (Bangladesh Consultants, Ltd., 2010a,b,c,d). The advantage of this method is that sufficient data can be obtained without drilling boreholes.

Another way of estimating lens thickness and lenses volume is through analytical and numerical modeling, with these models solving mass balance equations for groundwater flow and solute transport in coastal and island aquifers. Whereas analytical models can estimate lens thickness while assume a sharp interface between freshwater and seawater in a homogeneous aquifer (Fetter, 1972; Vacher, 1988; Bailey et al., 2013), numerical models can include spatially-varying aquifer properties, time-dependent fluid source terms (e.g. recharge to the freshwater lens), horizontal and vertical flow patterns, and spatially-varying salt concentration in the groundwater. Numerical models are able to assess the impact of drought, sea level rise, and varying rainfall patterns on the dynamics of the freshwater lens.

1.7 Objectives of this study

In relation to the groundwater resources of the Republic of Maldives, the two main objectives of this thesis are as follows:

1. Estimate the effects of future rainfall patterns on the freshwater lens for the islands of the Maldives. Future rainfall patterns, which are necessary to compute future recharge patterns for the islands, come from a set of General Circulation Models (GCMs) that statistically compare favorably to historical rainfall patterns in the three geographic regions of the Maldives.
2. Estimates the impacts of future rainfall, population and groundwater pumping growth, and sea level rise on the volume and extent of the freshwater lens for a representative island of the Maldives. The island selected is Gan island due to its moderate population and potential for groundwater use.

A suite of 2D and 3D numerical models using the SUTRA (Saturated Unsaturated Transport) modeling code and tested against field data from the Maldives will be used to accomplish these objectives. The 2D modeling applications are summarized in Chapter 2, whereas the 3D model application to the island of Gan is presented in Chapter 3. Summary and concluding remarks are presented in Chapter 4.

CHAPTER 2: ASSESSING GOURNDWATER SUPPLY OF THE MALDIVES WITH 2-D MODELING

This chapter illustrates how to use two-dimensional numerical modeling to assess groundwater supply for different island sizes for Maldives. First, it gives a brief introduction and review about 2-D modeling. Then, it shows how to use 2-D modeling to simulate density-dependent flow. Finally, the results give the prediction of lens thickness changes under climate change from 2012 to 2050.

2.1 Introduction

Lam first started the numerical modeling for atoll islands by creating a model of pressure field in an atoll using Darcy's law (Lam, 1974). Then the model was developed for next decades by several researchers (Lloyd et al., 1980; Falkland, 1983). Lloyd et al. developed the non-steady solutions for the modeling for a Pacific Ocean atoll by finding out that steady state solutions cannot be realistically applied (Lloyd et al. 1980). In 1984, Herman and Wheatcraft improved the accuracy of the modeling by dividing the atoll aquifer into two aquifers that have large differences in hydraulic conductivity (Herman and Wheatcraft, 1984). A finite-element code SUTRA (Saturated and Unsaturated Transport) was developed by Voss (Voss, 1984) and has been continuously used by many researchers for last 30 years on atoll islands (Hogan 1988; Griggs 1989; Oberdorfer et al. 1990; Underwood et al. 1992; Griggs and Peterson 1993; Peterson and Gingerich 1995; Gingerich and Voss, 2005; Bailey et al, 2009 ; Ketabchi et al. 2014). SUTRA is also used for this study.

More recently, freshwater lens thickness was estimated for the islands of the Maldives during the 1998-2011 time period (Bailey et al., 2014a) and during the coming decades under different scenarios of sea level rise (Bailey et al., 2014b), with model results tested against the data from Falkland (2000, 2001) and Bangladesh Consultants, Ltd. (2010a,b,c,d). Bailey et al. (2014a) used code SUTRA (Voss and Provost, 2010) and daily recharge rates to simulate time-dependent lens dynamics in a two-dimensional (2D) vertical cross-section of the islands, whereas Bailey et al. (2014b) used an empirical model to calculate steady-state lens thickness according to island width, aquifer hydraulic conductivity, depth to the contact between the Holocene and Pleistocene aquifer units, and average annual recharge rate, with island width in future decades decreasing depending on the rate of sea level rise. Results from both studies suggest that groundwater is a viable option for water supply both now and in the future, with average lens thickness estimated to be approximately 2.5 m for 400 m wide islands, 4.0 m for 600 m islands, and 12.0 m for 1100 m islands. Neither study, however, accounted for the effects of future rainfall patterns on groundwater resources.

The objective of this study is to assess groundwater resources of the Republic of Maldives under future climate conditions (through the year 2050) with a focus on the influence of future variable rainfall patterns.

2.2 Methodology

This section presents the methodology for estimating freshwater lens thickness under future rainfall patterns for the islands of the Maldives. Models are constructed for islands of varying widths (200 m, 400 m, 600 m, 1100 m), with rainfall and recharge applied for the three different geographic regions. Rainfall is obtained from GCMs that accurately replicate historical rainfall patterns in the region of the Maldives. Whereas results will be analyzed in detail for 2011-2050,

simulations are run from 1998 so that results for 1998-2011 can be compared to results from using historical daily rainfall data as a test of the GCM rainfall output.

2.2.1 Construction of Island Subsurface Models using SUTRA

Freshwater lens dynamics, i.e. freshwater-seawater interaction within the atoll island aquifer system, were simulated using the SUTRA, which uses the finite element method to solve the coupled density-dependent groundwater flow and solute transport governing equations. Required parameters include porosity, permeability, specific yield, porous matrix compressibility, and dispersivity. Model output includes nodal pressure, saturation, and solute concentration. Salt is used as the solute in this study. Salt concentration of fresh groundwater is limited to 0.00089 kg_{salt}/kg_{water}. This corresponds to a chloride concentration of approximately 550 mg/L and an overall salt concentration equal to 2.5% of the salt contained in seawater, which is a slightly lower than the World Health Organization (WHO, 1972) recommended of 600mg/L. The body of groundwater with salt concentrations less than this limit defines the freshwater lens.

Four different 2D finite-element meshes representing islands with widths of 200 m, 400 m, 600 m and 1100 m were constructed to represent the vertical cross-section of generic atoll islands from lagoon side of the island to the ocean side (see Figure 3A). The outline of the model domain is shown in Figure 3B for the model representing the 600 m island, with the top layer of mesh nodes corresponding to mean sea level. Each mesh was finely discretized within the immediate vicinity of the island subsurface, with particularly high refinement along the upper model layers and within the approximate location of freshwater lens development (Bailey et al., 2009). For example, node spacing in the top 4 m of the model is between 0.2 m and 0.3 m, then 1 m between 4 and 15 m below sea level, and then 0.75 m between 15 m and 25 m below sea level. The 400 m island has 7,832 elements and 8,055 nodes and the 1100 m island has 18424 elements

and 18850 nodes, with the other models for 200 m and 600 m containing numbers of elements and nodes commensurate with the island width.

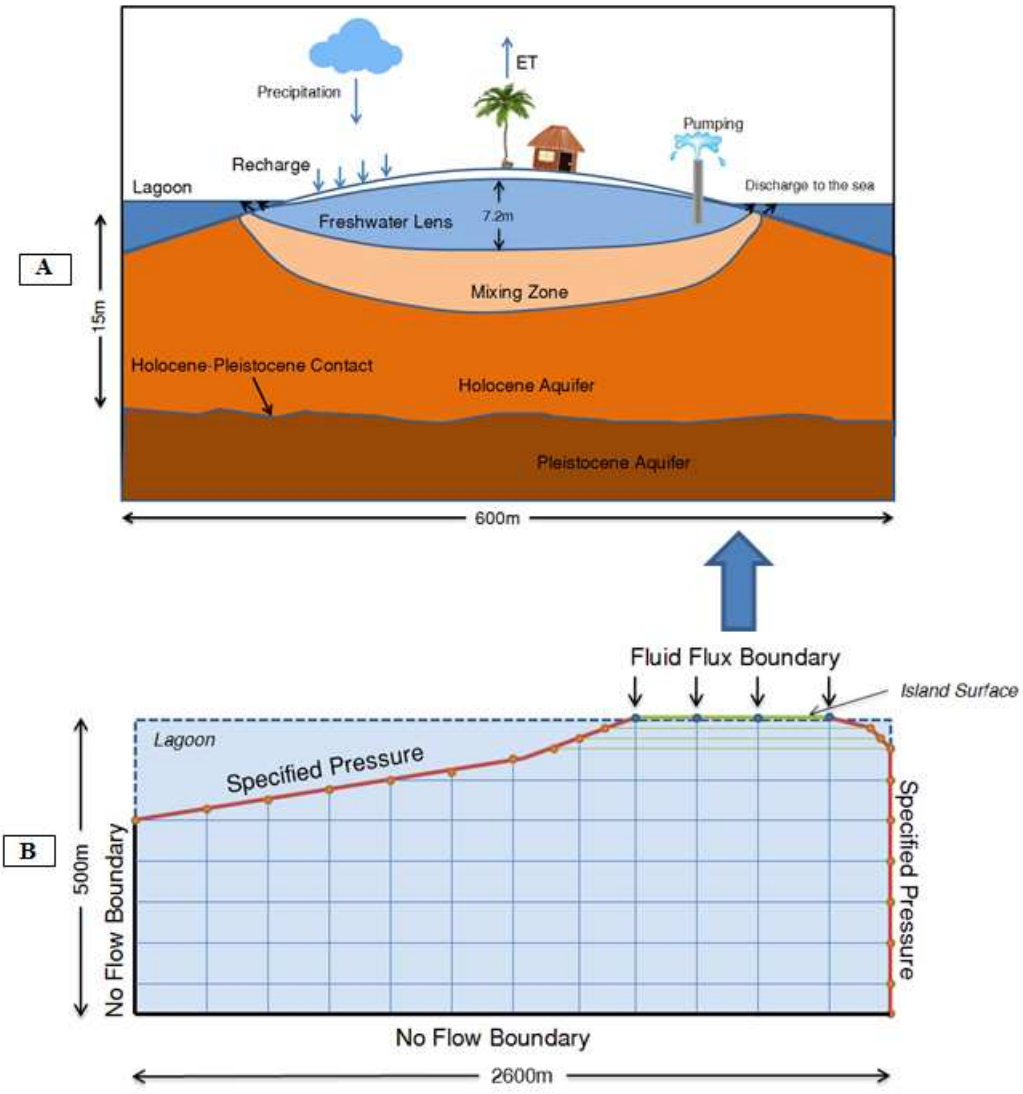

Figure 3: (A) Typical island cross section for coral islands (B) Model domain adopted for the SUTRA modeling simulations, with boundary conditions and fluid flux boundary (recharge at the water table).

Each island model received the same aquifer properties, assuming uniform geologic formation across the region of the Maldives. This seems appropriate given the similarity between estimated *K* values in the southern region (Falkland, 2000) and the northern region (Falkland, 2001). General aquifer properties (Table 2) include compressibility of the porous matrix, specific

yield, and longitudinal and transverse dispersivity for salt transport. The subsurface is divided into an upper Holocene aquifer (13 m thick on ocean side, increasing to 18 m thick on the lagoon side) and a lower Pleistocene aquifer (485 m thick). Holocene aquifer *K* (horizontal *K* and vertical *K* equal to 75 m/d and 15 m/d, respectively) was determined in a previous study (Bailey et al., 2014b) through comparing model simulation results with observed lens thickness values for the 1998-2011 period. Results are shown in Supplementary Data. Due to Pleistocene aquifer *K* estimated to be 1 to 2 orders of magnitude higher than Holocene aquifer *K* (Woodroffe and Falkland, 1997), Pleistocene aquifer *K* is set to 5000 m/d. Water table storage was accounted for by setting the nodal specific storage values to the specific yield divided by half of the element vertical thickness (Griggs and Peterson, 1993). The nodes along the lagoon basement and reef are assigned specified pressure based on the depth of each node below sea level, and a constant specified concentration of 0.0357 kg/kg to represent seawater. The bottom of the mesh and the boundary simulating the limit of the lagoon were assigned no-flow boundaries.

Table 2. Properties of the atoll island aquifer system, including general properties, and properties for the Holocene and Pleistocene aquifer units (after Bailey et al., 2014a).

Parameters	Value	Units	Source
General Aquifer Properties			
Compressibility of Porous Matrix	1.00×10^{-9}	m^2/N	Peterson and Gingerich 1995
Specific Yield	0.20	m^3/m^3	Griggs and Peterson 1993
Longitudinal Dispersivity α_L	6.0	m	
Transverse Dispersivity α_T	0.05	m	Griggs and Peterson 1993
Holocene Aquifer			
Holocene Porosity	0.2	m^3/m^3	Anthony 1997
Holocene thickness	13 to 18	m	Hamlin and Anthony 1987
Holocene horizontal *K*	75	m/d	Calibrated value (this study)
Holocene vertical *K*	15	m/d	Calibrated value (this study)
Pleistocene Aquifer			
Pleistocene Porosity	0.3	m^3/m^3	Swartz 1962
Pleistocene thickness	485	m	

Pleistocene horizontal *K*	5000	m/d	Oberdorfer et al. 1990
Pleistocene vertical *K*	1000	m/d	Oberdorfer et al. 1990

2.2.2 Assigning Recharge Rates during 1998-2050

2.2.2.1 Overall procedure of using General Circulation Models

Recharge derived from rainfall is applied to the nodes along the top of the model (see Figure 3B), with spatially-uniform recharge rates assumed across the width of the island. Daily recharge rates from 1998 to 2050 are calculated by statistically downscaling monthly output from GCMs participating in the Coupled Model Intercomparison Project 5 (CMIP5) (Meehl et al., 2009; Taylor et al., 2012). Rainfall output from both the lowest emission scenario [Representation Concentration Pathway (RCP) 2.6, corresponding to a limited radiative forcing of 2.6 W/m^2 by the year 2100] and the highest emission scenario RCP8.5 are used to provide end-member climate conditions. We acknowledge the World Climate Research Programme's Working Group on Coupled Modelling, which is responsible for CMIP, and we thank the modeling groups (Table 3) for producing and making available their model output. 24 GCMs are used in total.

The overall process of calculating daily recharge is as follows:

1) Retrieve monthly rainfall depths as simulated by the GCMs
2) Statistically compare patterns of rainfall between the GCMs and historical monthly rainfall depths over the 1998-2011 time period, to either accept or reject each GCM
3) For the accepted GCMs, downscale the monthly rainfall depths to daily rainfall depths using a Markov chain algorithm
4) Use daily rainfall depths to calculate daily recharge using a soil water balance model (Falkland, 1994).

The process is performed for both RCP2.6 and RCP8.5 and for each of the three geographic regions of the Maldives: Region 1 (5^0N-10^0N, 70^0E-75^0E), Region 2(0^0-5^0N, 70^0E-75^0E), and Region 3(5^0S-0^0, 70^0E-75^0E). Steps 2), 3), and 4) will now be described.

Table 3. General Circulation Models (GCM) and their organizations.

Modeling Center (or Group)	**Institute ID**	**Model Name**	**Model Index**
Beijing Climate Center, China Meteorological Administration	BCC	BCC-CSM1.1	1
National Center for Atmospheric Research	NCAR	CCSM4	2
Community Earth System Model Contributors	NSF-DOE-NCAR	CESM1(CAM5)	3
Commonwealth Scientific and Industrial Research Organization in collaboration with Queensland Climate Change Centre of Excellence	CSIRO-QCCCE	CSIRO-Mk3.6.0	4
The First Institute of Oceanography, SOA, China	FIO	FIO-ESM	5
NOAA Geophysical Fluid Dynamics Laboratory	NOAA GFDL	GFDL-CM3	6
		GFDL-ESM2G	7
		GFDL-ESM2M	8
NASA Goddard Institute for Space Studies	NASA GISS	GISS-E2-H-p1	9
		GISS-E2-H-p2	10
		GISS-E2-h-p3	11
		GISS-E2-H-p1	12
		GISS-E2-H-p2	13
		GISS-E2-H-p3	14
National Institute of Meteorological Research/Korea Meteorological Administration	NIMR/KMA	HadGEM2-AO	15
Met Office Hadley Centre (additional HadGEM2-ES realizations contributed by Instituto Nacional de Pesquisas Espaciais)	MOHC (additional realizations by INPE)	HadGEM2-ES	16
			17
Institut Pierre-Simon Laplace	IPSL	IPSL-CM5A-LR	18
		IPSL-CM5A-MR	19
Atmosphere and Ocean Research Institute (The University of Tokyo), National Institute for Environmental Studies, and Japan Agency for Marine-Earth Science and Technology	MIROC	MIROC5	20
Japan Agency for Marine-Earth Science and Technology, Atmosphere	MIROC	MIROC-ESM	21

and Ocean Research Institute (The University of Tokyo), and National Institute for Environmental Studies		MIROC-ESM-CHEM	22
Norwegian Climate Centre	NCC	NorESM1-M	23
		NorESM1-ME	24

2.2.2.2 Statistical Comparison between GCMs and Historical Rainfall

Seven statistical criteria (Table 4) are used to assess the performance of each GCM (Fu et al., 2013). To eliminate bias, the overall performance is assessed using the combined effects of all criteria. Each individual criterion is associated with weighting factors, with some having weights of 0.5 because they are complementary to another criterion. The total rank score of a GCM is calculated as follows, with low scores indicating a closer agreement between the GCM output and historical data (RC represents Ranking Score):

$$RC_{total} = RC_{mean\ RE} + RC_{Std\ RE} + RC_{NRMSE} + RC_{Corr} + \left(0.5 \times RC_{BS}\right) + \left(0.5 \times RC_{S\ score}\right) + RC_{Kendal\ Slope} \quad (1)$$

Table 4. Statistical criteria for evaluating GCMs. The weighting factor assigned to each criterion also is shown.

Statistic Criterions	Formula	Weighting factor
Mean Relative Error (Mean RE)	$\frac{\left\|u_{model} - u_{ob.}\right\|}{u_{ob.}}$	1.0
Standard Deviation Relative Error (Std RE)	$\frac{\left\|Std_{model} - Std_{ob.}\right\|}{Std_{ob.}}$	1.0
Normalized Root Mean Square Error (NRMSE)	$\frac{\sqrt{\frac{1}{n}\sum_{i=1}^{n}(X_{mi} - X_{oi})^2}}{\sqrt{\frac{1}{n}\sum_{i=1}^{n}(X_{Oi} - \bar{X}_O)^2}}$	1.0
Correlation Coefficient (Corr)	Calculation in Matlab	1.0
Brier Score (BS)	$\frac{1}{n}\sum_{i=1}^{n}(P_{mi} - P_{oi})^2$	0.5
Skill Score	$\sum_{i=1}^{n} Minimum\left(P_{mi}, P_{oi}\right)$	0.5

Kendall Slope	Calculated in Pro-UCL	1.0	

Monthly mean relative error (*mean RE*) and standard deviation relative error (*Std RE*) are used to quantify the similarity between modeled and historical rainfall depths; the Normalized Root Mean Square Error (*NRMSE*) is used to compare the similarity of two time series by considering both mean value and standard deviation; the Correlation Coefficient (*Corr*) is to evaluate both the annual cycle and the spatial distribution of monthly rainfall; the Brier Score (*BS*) and Skill Score (S_{score}) are used to evaluate the GCM probability density functions (PDFs) of monthly rainfall; and the Mann-Kendall Slope determines the magnitude of long-term trends of time series. The resulting total scores (RC_{total}) for each GCM are ranked and sorted, and the moving range, i.e. the difference in scores between two successive GCMs, is used to detect change points (Fu et al., 2013). In this study, any substantial increase in score between successive GCMs constituted a change point, with the group of GCMs having a score lower than the change point accepted for use in calculating recharge, and the remaining GCMs rejected. This process is performed for both RCPs (RCP2.6 and RCP8.5) and for each of the three geographic regions.

2.2.3 Statistical Downscaling to Daily Rainfall Depths

To obtain daily precipitation depths, the monthly data from the accepted GCMs are downscaled statistically according to patterns of historical daily rainfall depths. A Markov chain algorithm (Todorovic and Woolhiser, 1975; Srikanthan and McMahon, 2001) generates daily wet/dry sequences for each month of historical data, fits shape parameters for gamma distributions that describes the classifications, and then uses these distributions to provide rainfall depths for future wet days. The Gamma distribution is used since it is a common

statistical model for days with non-zero precipitation (Coe and Stern, 1982; Srikanthan, 2005). Simulated daily rainfall depths are scaled so that monthly sums equal monthly rainfall depths from the GCM output. The algorithm is expressed by:

$$X_t \mid X_{t-1} \sim Markov\left(\boldsymbol{P}, p_1\right) \tag{2}$$

where $\boldsymbol{P}$ is the transitional probability matrix whose elements p_{ij} are defined by:

$$p_{ij} = \Pr(X_t = i \mid X_{t-1} = j) \qquad i,j = \text{wet or dry} \tag{3}$$

and p_1 is the probability distribution vector of the wet/dry classifications (Srikanthan and McMahon, 2001). Classification (wet/dry) for each historical month is determined by comparing the monthly rainfall depth with the median of average rainfall across all years of data, after which each month of the GCM simulation time also is assigned a wet/dry classification. The wet/dry conditions of each day are determined using the same methodology and applied to the days of each future month, with values drawn from Gamma distributions created for each monthly of the year.

2.2.2.3 Calculating Daily Recharge from Daily Rainfall Depths

Daily recharge to the freshwater lens is estimated using the downscaled daily rainfall depths and the daily soil water balance model of Falkland (1994), which accounts for canopy interception, evapotranspiration (ET), soil field capacity, and soil wilting point, with recharge to the water table occurring when soil water storage exceeds soil field capacity. On days when soil water storage is below field capacity, ET is limited to 20% of the potential value (Lloyd et al., 1980). The soil water balance equation (Falkland, 1994) is described as below. It does not count for surface runoff which does not usually happen because of high infiltration capacity of the coral soils. The recharge to the water table only happens when soil moisture content exceeds field capacity. Precipitation is the daily value from downscaled monthly data. Evaporation is

usually estimated from using both Penman and Pan Methods. Transpiration rates is estimated from measurement of coconut tree transpiration rate which is about 400mm-750 mm/year/tree.

$$R = P - ET_a + dV \quad (4)$$

R (mm) is the daily recharge

P (mm/day) is the daily rainfall

ET_a (mm/day) is the actual evaporation from all surfaces which included evaporation from interception storage

dV (mm) is the change in storage within the soil moisture zone. Maximum and minimum limits are set for soil moisture to calculate the storage change

As with previous atoll modeling studies in the Federated States of Micronesia (Bailey et al., 2009) and the Maldives (Bailey et al., 2014a), interception depth is set to 1.0 mm, field capacity and wilting point are set to a soil water content of 0.15 and 0.05, respectively, and potential ET is set to a constant daily value of 3.5 mm/day, which is the average value of ET in Maldives.

2.2.3 Summary of Simulations

Simulations are run for each accepted GCM for both RCPs (RCP2.6, RCP8.5), for each of the four island width models and for each of the three geographic regions. The initial conditions (salinity concentration and pressure at each mesh node) for each 1998-2050 simulation are achieved by imposing a steady recharge rate until the freshwater lens reaches steady-state conditions, followed by a transient simulation from 1991-1998 using recharge calculated from historical daily rainfall rates. Results of each model simulation are processed to determine the thickness of the freshwater lens under the center of the island.

2.3 Results

2.3.1 Accepted GCMs for the Maldives Region

Table 5 shows the statistical scores and total score for each GCM for Region 1 and RCP 2.6. Tables summarizing GCM scores for each region for both the RCP 2.6 and RCP 8.5 scenarios are contained in Supplementary Data. $RC_{mean\ RE}$ ranges from 0.5% to 58%, with most GCMs having a small value. However, most RC_{NRMSE} values are larger than 1.0, signifying a poor match with the historical rainfall series in terms of both mean value and standard deviation. RC_{Corr} ranges from 0.3 to 0.7, with MIROC5 having the highest value. RC_{BS} and $RC_{S\ score}$ values range from 3.3 to 16.6 and from 85 to 110, respectively, with NorESM1-ME having the best match (i.e. lowest RC_{BS} and highest $RC_{S\ score}$).

The GCM scores for the three geographic regions for RCP2.6 are plotted in Figure 4 in ascending order, with the GCMs divided into groups according to identified change points. For each region there are three groups, with the GCMs within Group 1 accepted for use in the groundwater modeling simulations. The accepted GCMs each of the three regions and for both RCP scenarios are listed in Table 6. In general, there are more accepted GCMs in Region 1 than the other regions, and in Region 2 than in Region 3. Several GCMs are consistently accepted in most or all regions, such as CESM1-CAM5 and MIROC5. To demonstrate the difference between accepted and rejected GCMs for a particular region, Figure 5 compares the times series and PDF of historical and GCM rainfall data, with an accepted model (CSIRO-Mk3-6-0) shown in Figure 5a,b and a rejected model (bcc-csm1-1) shown in Figure 5c,d. The time series of historical rainfall shows a strong wet season – dry season pattern, with magnitude of rainfall rate approximately uniform across all years. CSIRO-Mk3-6-0 matches the historical pattern very well, whereas bcc-csm1-1 greatly over-predicts the rainfall in the region. These trends can also be seen in the accompanying PDFs.

Table 5. Model performance results for monthly rainfall rates in Region 1 and RCO Scenario 2.6, ranking best to worst according to the total score.

GCM	Mean RE(mm)	Std RE	NRMSE	Corr	BS	S score	Kendal Slope (mm/year)	Total Score
MIROC5	-0.07	0.05	0.85	0.66	4.11	103	0.0032	28
GFDL-CM3	0.09	0.17	0.56	0.56	5.03	109	0.003	43
CSIRO-Mk3-6-0	-0.12	-0.07	0.87	0.61	6.03	88	0.0011	47.5
IPSL-CM5A-MR	-0.01	0.90	0.90	0.56	4.41	99	0.003	50
GFDL-ESM2M	-0.03	0.05	1.01	0.51	3.34	102	0.009	51.5
FIO-ESM	0.07	0.04	1.12	0.40	3.81	99	0.0024	53
NorESM1-M	-0.03	0.18	1.12	0.48	6.59	98	0.0013	55.5
CESM1-CAM5	0.26	0.01	1.01	0.56	4.81	92	0.0019	56
HadGEM2-ES	-0.19	0.00	1.06	0.47	6.26	95	0.0026	63
CCSM4	0.24	0.10	1.08	0.53	4.53	93	0.0044	73
NorESM1-ME	0.01	0.18	1.28	0.32	3.32	110	0.005	73
GISS-E2-H p3	-0.05	0.33	1.23	0.47	4.67	107	0.0054	75.5
GFDL-ESM2G	-0.22	-0.27	0.99	0.44	4.13	98	0.0041	76
GISS-E2-R p3	-0.09	0.23	1.19	0.45	5.03	91	-0.0003	77
IPSL-CM5A-LR	-0.16	-0.44	0.87	0.54	5.21	87	0.0037	77.5
GISS-E2-R p2	-0.11	0.29	1.19	0.49	6.09	93	-0.0019	81.5
MIROC-ESM	0.54	0.45	1.38	0.62	4.41	100	0.0034	87.5
MIROC-ESM-CHEM	0.58	0.35	1.36	0.63	4.19	94	0.0047	93
MRI-CGCM3	-0.21	0.26	1.27	0.43	16.58	85	0.0005	93
GISS-E2-H p2	-0.06	0.46	1.33	0.47	5.93	92	0.0046	96.5
GISS-E2-R p1	-0.09	0.32	1.28	0.42	5.25	97	-0.0036	98
GISS-E2-H p1	-0.09	0.38	1.29	0.45	7.81	97	-0.0033	101
HadGEM2-AO	-0.23	0.11	1.25	0.35	8.81	89	0.0067	108.5
bcc-csm1-1	0.25	0.86	1.84	0.32	9.71	92	0.0091	135

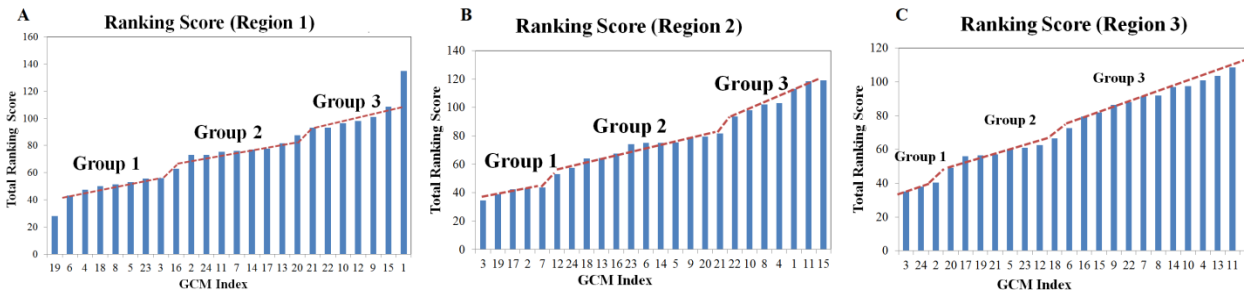

Figure 4. Bar chart A, B, C of sorted ranking score for the three geographic regions for the RCP2.6 scenario. All GCMs are grouped by identified change points.

Table 6. Accepted GCMs for the three regions for RCP2.6 and for RCP8.5.

	Scenario 2.6	**Scenario 8.5**
Region 1	MIROC5	IPSL-CM5A-MR
	GFDL-CM3	GFDL-ESM2M
	CSIRO-Mk3-6-0	MIROC5
	IPSL-CM5A-MR	CSIRO-Mk3-6-0
	GFDL-ESM2M	CESM1-CAM5
	NorESM1-M	GFDL-CM3
	CESM1-CAM5	GFDL-ESM2G
	HadGEM2-ES	
Region 2		CESM1-CAM5
	CESM1-CAM5	MIROC5
	MIROC5	CCSM4
	IPSL-CM5A-LR	IPSL-CM5A-MR
	CCSM4	GISS-E2-R p1
	GFDL-ESM2G	GFDL-ESM2G
		GFDL-CM3
Region 3	CESM1-CAM5	CESM1-CAM5
	CCSM4	MIROC-ESM
	MIROC-ESM	CCSM4

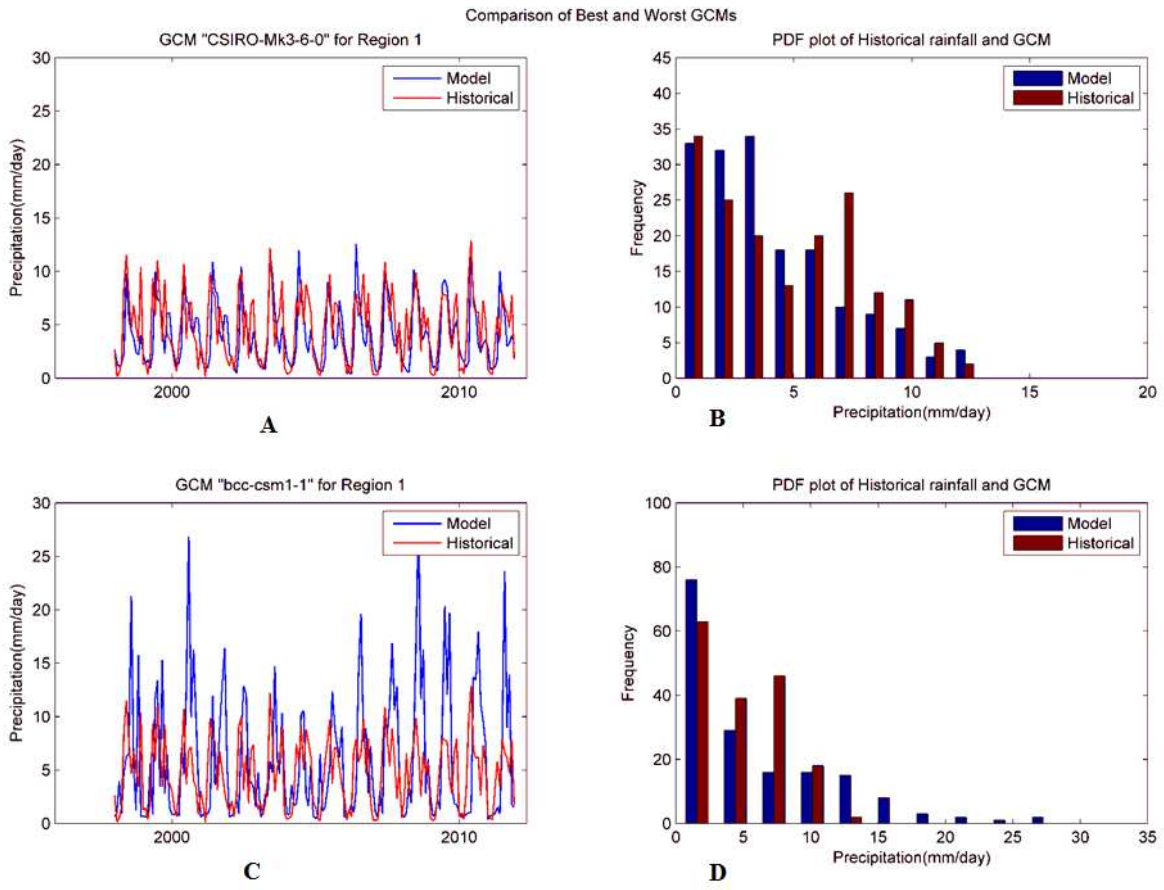

Figure 5. Comparison of time series plots and a PDF plot for an accepted GCM (CSIRO-Mk3-6-0) (A, B) and a rejected GCM (bcc-csm1-1) (C, D) in Region 1 for RCP2.6.

2.3.2 Lens Thickness Fluctuation and Trends through 2050

The time series of simulated monthly lens thickness for each accepted GCM for both RCP2.6 and RCP5 is shown in Figure 6 for each island width within Region 1. Similar plots can be made for Regions 2 and 3. Each GCM is depicted by a light gray line, with the average monthly value shown with a dark line. Model results using historical daily rainfall depths are shown in dotted lines from 1998-2011, demonstrating the close match between using historical data and the average of the accepted GCMs. Results show that larger islands (e.g. 600 m and 1100 m islands) have much larger freshwater lenses than smaller islands (200 m and 400 m), with overall average

thickness of 0.3 m, 2.3 m, 5.6 m, and 11.7 m for 200 m, 400 m, 600 m, and 1100 m islands, respectively. Overall, the islands with width of 200 m and 1100 m have a smaller scatter than 400 m and 600 m islands. The standard deviation of average lens thicknesses across the GCMs is 0.066 m, 0.22 m, 0.40 m and 0.19 m for 200m, 400m, and 600m and 1100m islands, respectively.

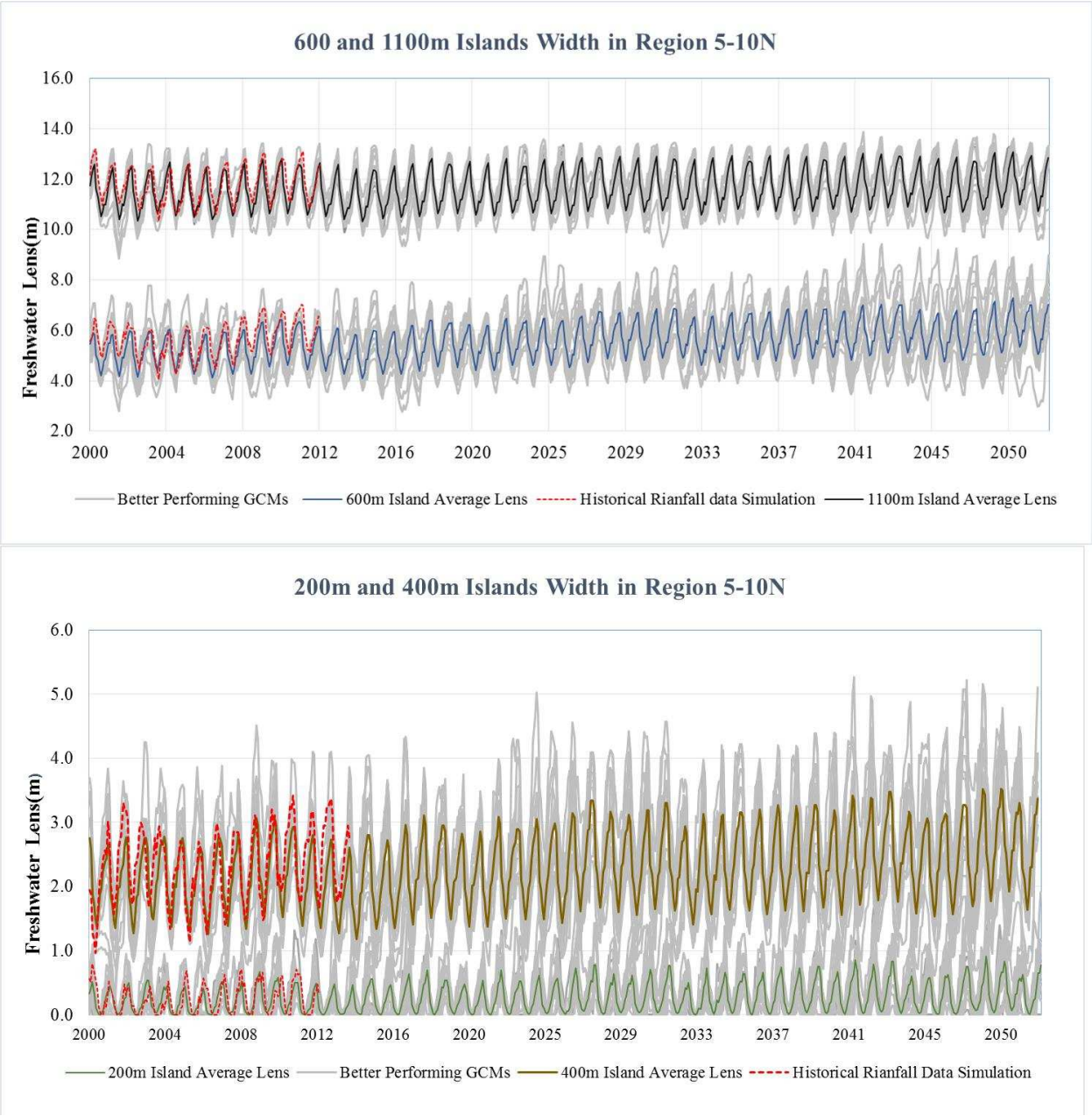

Figure 6. Time series plot of lens thickness for each accepted GCM in Region 1 for (A) the 600 m and 1100 m islands, and (B) the 200 m and 400 m islands. Solid lines in each series represent the average values of all simulations for a given island size from both RCP 2.6 and RCP.8.5. The dashed lines are results from using historical daily rainfall data in the SUTRA models from 1998-2011.

Average simulated lens thickness for each simulation is shown in Table 7. Values are shown for each island width within each of the three regions (R1, R2, R3), and for each accepted GCM. The GCM index corresponds to the order listed in Table 6. Lens thickness for each island width and for each region is averaged across the accepted GCMs for two time periods: the first 20 years (2011-2030) and the second 20 years (2031-2050). For example, the average lens thickness for a 400 m island in region 2 (R2) is 2.81 m during 2011-2030 and 2.84 m during 2031-2050, whereas the average lens thickness for an 1100 m island in R2 is 12.16 m during 2011-2030 and 12.13 m during 2031-2050.

The time series plot of lens thickness in Figure 6 shows that the freshwater lens responds quickly to the distinct wet/dry season pattern of rainfall. The average lens thickness during the wet season considering each accepted GCM for different size islands in Region I are 0.71 m, 3.1 m, 6.46 m and 12.73 m for 200 m, 400 m, 600 m, and 1100 m islands, respectively. The average lens thickness during the dry season is 0.0 m , 1.4 m, 4.5 m and 10.57 m, corresponding to decreases of 100%, 55%, 30%, and 17%, for the four island sizes, demonstrating that the effect of the dry season is less for larger islands. Salt distribution in the subsurface during wet and dry seasons is shown in Figure 7 for a 200 m island (a,b) and for a 600 m island (c,d). Blue represents portions of the aquifer with a salt concentration less than the freshwater limit (2.5% of the salt in seawater), and therefore the freshwater lens, and red represent portions of the aquifer with seawater in the pores, with a mixing zone that grades from freshwater to seawater. The lens of the 200 m island during the wet season (Figure 7a) is much thicker (0.71 m) than during the dry season (0.003 m). Similar results occur for the 600 m island, comparing the lens during the wet season (Figure 7c, lens thickness: 6.5 m) with the lens during the dry season (Figure 7d, lens thickness: 4.4 m).

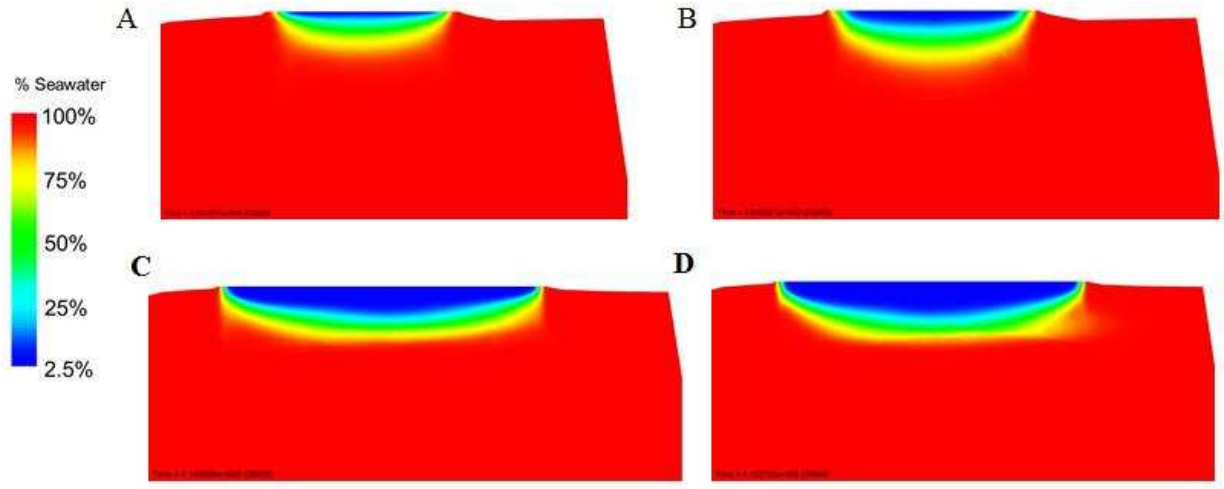

Figure 7. Salinity distribution in the island subsurface, with the contour colors corresponding to the percent of salt in the groundwater related to the salt content of seawater. Dark blue corresponds to freshwater. Red corresponds to seawater, with a mixing zone between. The top two graphs show the freshwater lens during the (A) dry season and (B) wet season for the 200 m island. The bottom two graphs show the freshwater lens during the (C) dry and (D) wet season for the 600 m island.

The difference in groundwater resources between the three geographic regions of the Maldives is demonstrated in PDF plots of lens thickness (Figure 8). The plots for 400 m islands in the three regions for RCP2.6 are shown in the upper plots (a,b,c), and the plots for 1100 m islands are shown in the lower plots (d,e,f). The freshwater lens is thickest in the southern region (R3: 5-10S) followed by the central region (R2: 0-5S), which is in agreement with the rainfall patterns of the Maldives' region with rates increasing north to south. Similar patterns (not shown) occur for the 200 m and 600 m islands. The bi-modal shape of the distribution for the northern region (Figure 8a,d) denotes the sharp contrast in rainfall and associated lens thickness between the wet season and dry season. The southern regions do not experience as pronounced of a dry season, and hence the distribution is uni-modal (Figure 8c, f).

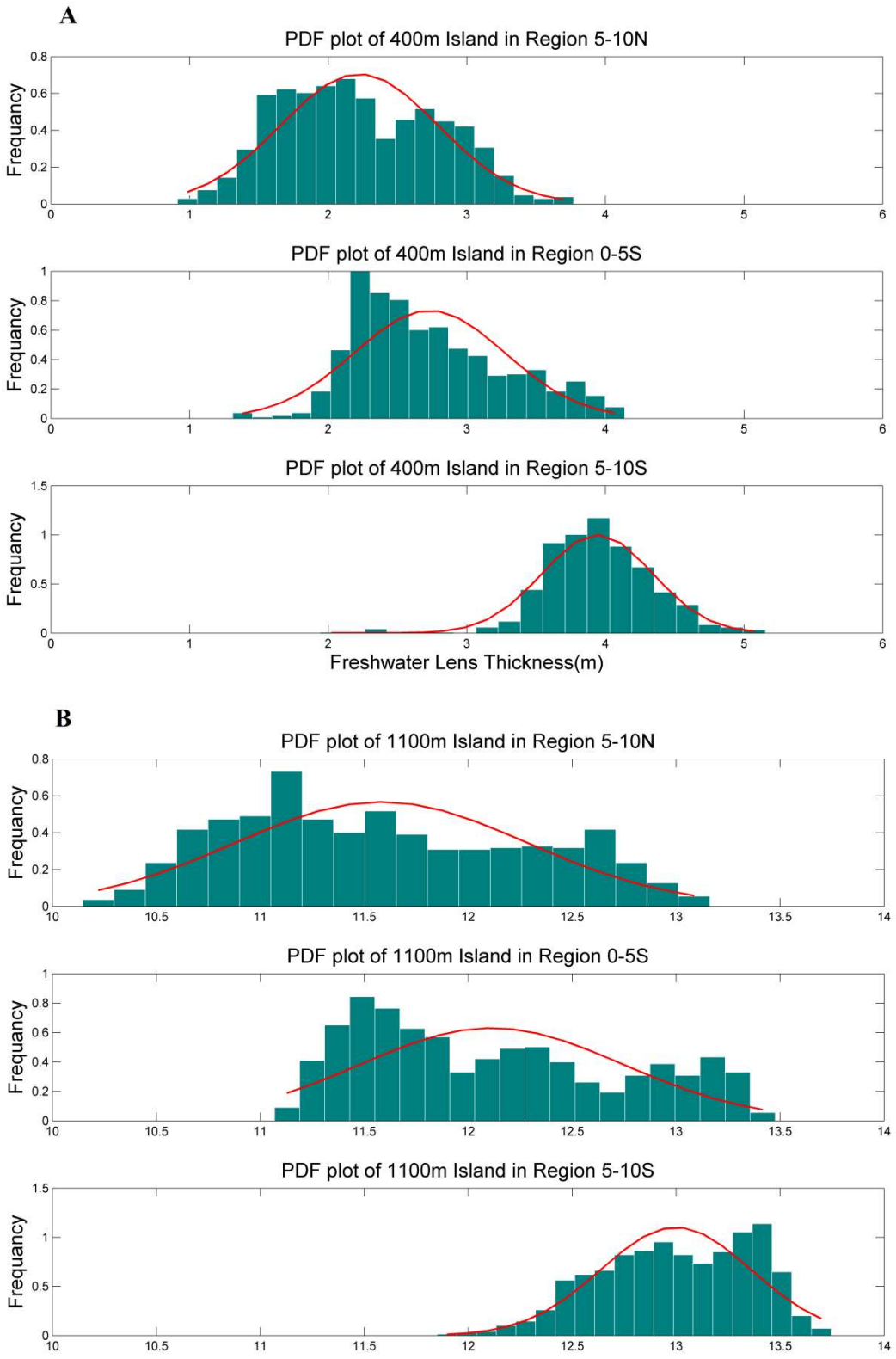

Figure 8. Lens thickness PDF plot for 400 m and 1100 m islands in the three regions, for the RCP2.6 scenario.

The difference between the RCP2.6 and RCP8.5 scenarios is shown in Figure 9 for 600 m islands in each of the three regions. The mean value of maximum lens thickness for RCP2.6 and RCP8.5 for all three regions is 5.45 m and 5.43 m, 6.39 m and 6.28 m, 8.75 m and 8.81 m, respectively. Average standard deviations of all GCMs in each of these two scenarios are 0.93 and 0.97, 0.90 and 1.02, 0.94 and 0.86, signifying the close agreement between the two pathway scenarios.

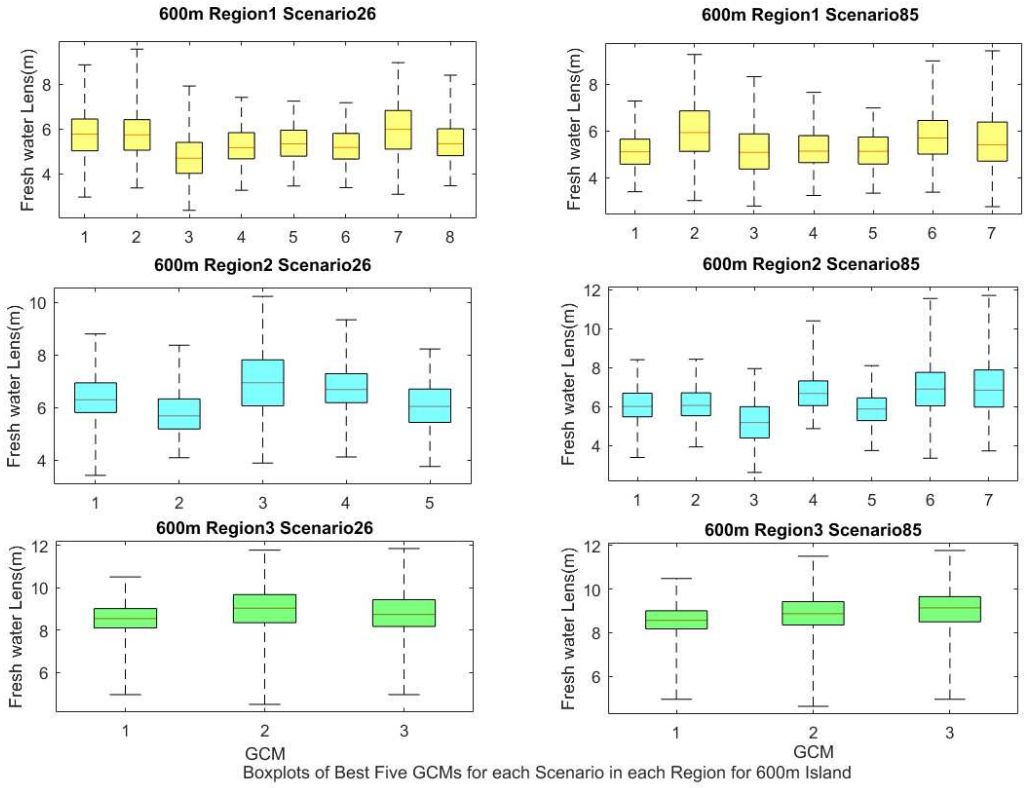

Figure 9. Boxplots of freshwater lens thickness comparing simulation results from RCP 2.6 and RCP 8.5 for the 600 m islands. The graphs on the left show results for the three regions using scenario RCP 2.6; the graphs on the right show results for the three regions using scenario RCP8.5. The GCM index corresponds to the order listed in Table 6

In terms of the effects of changing rainfall patterns on groundwater resources, the results shown in Table 7 indicate an increase in lens thickness between the first 20 years of the study

period (2011-2030) and the second 20 years (2031-2050). The majority of average values in the second 20 years are larger than during the first 20 years, with the only exception being 1100 m islands in region 2 (12.16 m in 2011-2030 compared to 12.13 m in 2031-2050). Overall average increase in lens thickness is 3.8%, with 7.4%, 4.2%, 2.9%, and 0.6% for 200 m, 400 m, 600 m, and 1100 m islands, showing the higher sensitivity of small islands to changes in temporal rainfall and recharge patterns. These results suggest a slow natural increase in lens thickness, and hence groundwater resources, over the next 40 years. This increase of course can be tempered by anthropogenic influences such as groundwater pumping. Also, groundwater could become contaminated in the short-term or long-term due to surface contamination or overwash events. In general, however, results can be used by country officials in water resources management decisions over the coming decades.

2.4 Summary and Concluding Remarks

This study provides an assessment of groundwater resources considering only changing rainfall patterns, and does not consider the exploitation of these resources from a growing population. Current population growth is estimated to be approximately 1.76 % in the Maldives, which could impose a significant burden on groundwater resources. Three-dimensional modeling approaches using estimates of population growth and water demand are needed to quantify the maximum use of groundwater supply in future decades. Furthermore, groundwater quality must be considered when assessing potable groundwater supply. These aspects can be conducted in future studies, but likely not at the broad geographic scale assessed in this current study.

Table 7. Average lens thickness under the center of the island for each island width and geographic region, across all accepted GCMs from the RCP2.6 and RCP8.5 scenarios. The first set of values is averages through the years 2011-2030, and the second set is for the years 2031-2050. The GCM index corresponds to the order listed in Table 6.

Average Lens		**Island Width (m)**											
Thickness (m)		**200**			**400**			**600**			**1100**		
		R1	R2	R3	R1	R2	R3	R1	R2	R3	R1	R2	R3
First 20 Years (2011-2030)	GCM 1	0.22	0.24	0.91	1.96	2.39	3.44	6.00	5.74	8.75	11.29	11.87	12.99
	GCM 2	0.27	0.30	0.87	2.11	2.56	4.10	5.72	6.11	9.27	11.49	12.00	13.05
	GCM 3	0.29	0.41	0.80	2.15	2.82	4.11	5.65	6.60	9.02	11.54	12.15	13.10
	GCM 4	0.21	0.42		2.17	2.98		5.48	6.85		11.57	12.34	
	GCM 5	0.19	0.57		2.18	3.28		5.37	7.37		11.61	12.43	
	GCM 6	0.25			2.29			5.32			11.64		
	GCM 7	0.21			2.39			5.20			11.69		
	GCM 8	0.37			2.54			5.03			11.79		
	Mean	0.25	0.39	0.86	2.23	2.81	3.88	5.47	6.53	9.01	11.58	12.16	13.01
		R1	R2	R3	R1	R2	R3	R1	R2	R3	R1	R2	R3
Last 20 Years (2031-2050)	GCM 1	0.25	0.27	0.95	1.95	2.41	3.84	6.37	5.77	8.69	11.29	11.83	13.00
	GCM 2	0.38	0.36	0.78	2.22	2.75	3.95	6.50	6.47	9.17	11.57	12.14	13.11
	GCM 3	0.40	0.43	0.92	2.23	2.77	4.28	4.95	6.55	9.41	11.62	12.16	13.14
	GCM 4	0.25	0.38		2.24	3.05		5.62	7.07		11.64	12.39	
	GCM 5	0.19	0.51		2.32	3.21		5.47	7.36		11.72	12.40	
	GCM 6	0.26			2.73			5.46			11.99		
	GCM 7	0.23			2.73			6.70			12.01		
	GCM 8	0.46			2.90			5.43			12.06		
	Mean	0.30	0.39	0.88	2.41	2.84	4.02	5.81	6.64	9.09	11.74	12.13	13.09

CHAPTER 3: ASSESSING IMPACTS OF RAINFALL PATTERNS, POPULATION GROWTH, AND SEA LEVEL RISE ON GROUNDWATER SUPPLY IN THE REPUBLIC OF MALDIVES USING 3-D MODEING

This chapter assesses the groundwater resources in one of the islands in Maldives by using three dimensional modeling. It also examines the effects of changing rainfall pattern, increasing pumping demand and rising sea level on the groundwater resources.

3.1 Introduction to Three-Dimensional modeling on atoll islands

To more accurately simulate the dynamics of freshwater-seawater interactions in island and coastal aquifers, three-dimensional models have been used in groundwater modeling during the past years. Compared to 2D vertical cross-section modeling, which was the method used in the study detailed in Chapter 2, three dimensional models have the advantage of being able to specify natural boundary conditions and the actual shape of the coast or island surface area, include 3D spatial variability of material properties, and represent pumping in three dimensions (Ghassemi et al., 1996; Ghassemi et al., 2000). Pumping can be represented in 2D models, but major simplifications and assumptions must be employed since the actual cone of depression cannot be simulated.

Several studies have used 3D modeling techniques to assess fresh groundwater supplies on coral islands during the past two decades, using the modeling codes SUTRA (Voss and Provost, 2003;), HST3D (Kipp, 1987) SALTFLOW (Molson and Frind, 1994), and SEAWAT (Langevin et al., 2007). Each has the capability to simulate density-dependent groundwater flow. A HST3D model was built for Nauru Island in the Central Pacific Ocean to simulate the freshwater lens

(Ghassemi et al., 1996), although it is found to be inefficient in dealing with large islands and fine grids even with the advanced version (Meurant, 1990). The SALTFLOW modeling code was used for the aquifer on Home Island in the Indian Ocean (Ghassemi et al., 1998), although the calibration was not very successful due to inadequate data for groundwater quality and quantity.

SEAWAT was used to simulate freshwater responses to climate change for a coral island named Grande Glorieuse in Western Indian Ocean (Comte et al., 2014). A 3-D model with dual aquifer system is created with total 67,830 cells to simulate the groundwater flow in a 14.7 km^2 island. 0.35 m of sea-level rise with a 0.64 km^2 loss of land area was considered in the model. Rainfall and potential evaporation is projected to increase 3% and 6%, respectively. It also evaluated the combination effect of climate change and vegetation on groundwater salinity. However, a different groundwater modeling tool SUTRA is used in this thesis. This 3-D model is created with seven times more cells for smaller island (6 km^2). GCMs (General Circulation Models) with different scenarios predict future rainfall and temperature. 0.5 m of sea-level rise is projected by the end of 21st century with 12% land area loss. Besides, this thesis includes pumping effects. SUTRA has been used successfully to simulate three-dimensional variable-density flow in a coastal aquifer in southern Oahu in Hawaii by Gingerich and Voss (2005).

In December of 2009, the Bangladesh Company performed a groundwater investigation survey in Gan using the EM method at more than 20 locations on each island. Three best-fit mathematical relationships used in the past were applied to translate the EM readings to lens thickness. They were used to provide contours of lens thickness (Figure 10) and a total volume of fresh groundwater. The total volume of fresh groundwater at the time of the study was estimated to be 14.2 million m^3, with an average freshwater lens thickness of 8.4 m (Bangladesh Consultants, Ltd., 2010a,b,c,d).

Figure 10. Freshwater lens thickness contour plot after groundwater investigation by Bangladesh Consultants, Ltd (2010a, b, c, d).

The main objective of this study is to assess fresh groundwater quantity of a major coral island of the Maldives under future climate threats. The island chosen for the assessment is Gan Island, located on Laammu atoll. Fresh groundwater lens thickness and volume are estimated for Gan from 2012 to 2050. This study examines the effects of changing rainfall patterns, increasing pumping needs and sea-level rise on lens thickness and volume. The SUTRA modeling code (Voss and Provost, 2010) was selected as the tool to quantify lens dynamics in the 3D subsurface

of Gan Island during the 2012-2050 time period due to its recent successful application to coral island aquifer systems. As compared to other full-island modeling studies, this study is the first to quantify the effect of a growing population on the groundwater resources of the aquifer in a changing climate. Methods of this study can be used for other oceanic islands, and results can be valuable to the government of Gan Island specifically and to the government of the Maldives generally for better water resources management.

3.2 Methods:

3.2.1 Gan of Laammu Atoll

As the biggest island in the Maldives, Gan in the Laammu atoll has a land area of 598 ha with length of 7.8 km and width of 3.4 km (GoM, 2010). It is located in the eastern side of Laamu atoll with latitude $1°55'$and longitude$73°32''30'$. Gan's population has grown rapidly from 2,537 persons (AFD, 2007) in 2005 to 4,208 persons in 2009. The population for each of its three villages (Thundi, Mathimaradhoo and Mukurimagu) were 2539, 748 and 921 (Bangladesh, 2010) (Figure 12). Gan falls into geographic Region II (see Chapter 1). Tropical Rainfall Measuring Mission (TRMM) provides fourteen years of historical daily rainfall data from 1998 to 2011. Figure 11 displays the time series plot. The average annual rainfall is 1930 mm/year. Wet and dry season are pronounced. High rainfall and very dry events are found around 2007.

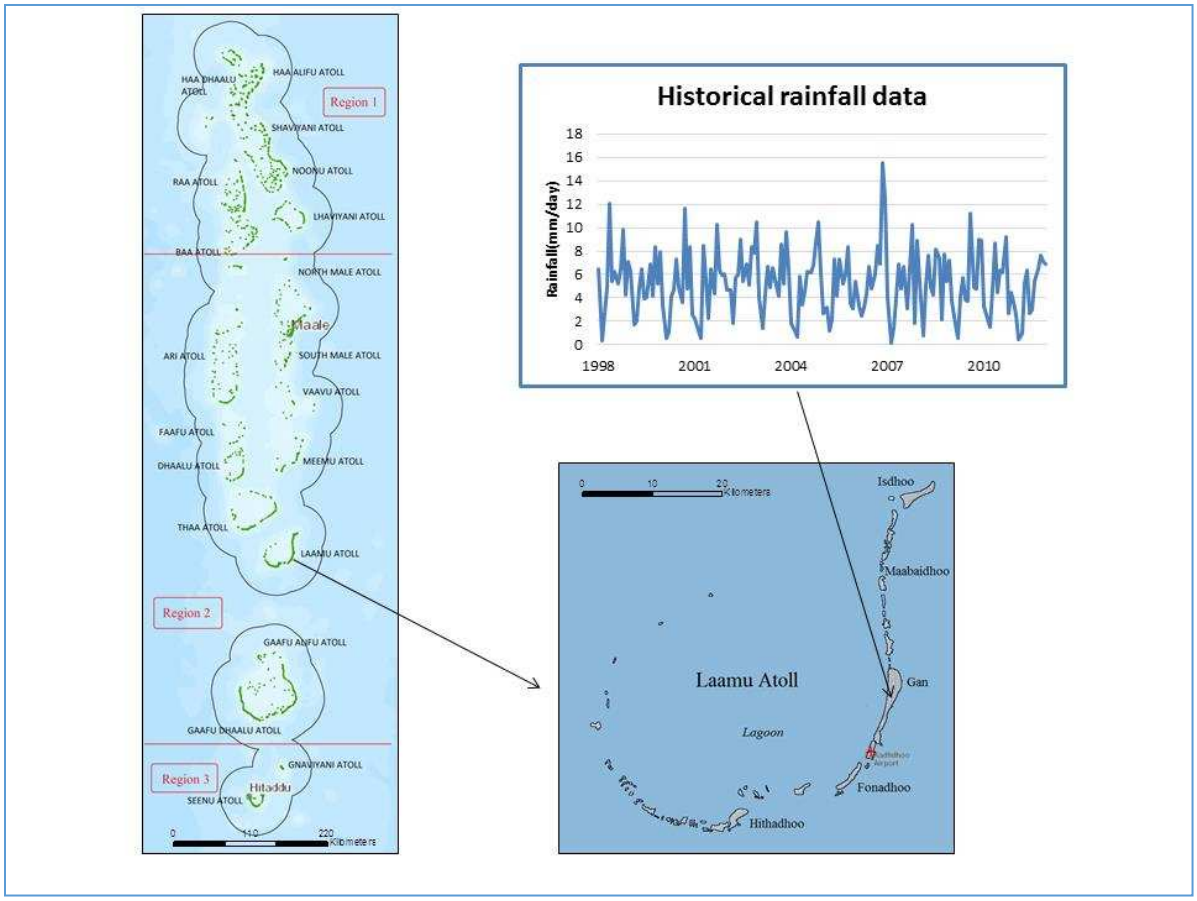

Figure 11. Geographic location of island of Gan and its historical monthly average rainfall

Figure 12: Map of Gan and the location of three villages.

3.2.2 Model development

3.2.1.1 Model Construction

This study uses ModelMuse (Winston, 2009)—a graphical user interface for constructing numerical models for USGS-based codes such as MODFLOW and SUTRA, is used to construct the 3-D SUTRA finite element mesh and to generate the necessary input files containing node-

by-node aquifer properties, boundary conditions, initial conditions, and fluid source/sink terms such as recharge and pumping (i.e. extraction). The procedure of constructing the model is as follows:

a) Draw the domain of the island – this is accomplished by importing the island GIS shapefile generated within ArcMap and then drawing the outline of the island. The effect of the ocean is simulated in the model, with the model domain extending out to the ocean on all sides of the island. The ocean domain is big enough to minimize the influence of the boundary conditions on groundwater dynamics within the island aquifer. In this study, the size of ocean is set as double the size of the island, with the shape similar to the island.

b) Generate the finite element mesh –SUTRA uses irregular quadrilateral elements, which are refined locally along the top of the model and along the coastal boundary where large changes in groundwater hydraulic head and salt concentration are expected during the model simulations. The elevation of island surface in the model is set to be 0, since the study only simulates saturated flow (i.e. aquifer below mean sea level) is simulated in this study. The slope on the coast is set to 1% which is the most common island slope in Maldives. The surface mesh and vertical discretization of the mesh are shown in Figure 13. The layer thickness near surface is < 1m while layers toward the bottom of the mesh are between 20 – 30 m.

c) Aquifer properties - the layers of the mesh are assigned to either the Holocene aquifer (0 m to 20 m below sea level) or the Pleistocene aquifer (20 m to 200 m below sea level). The Holocene aquifer is assigned a porosity of 0.2, whereas the Pleistocene aquifer is assigned a porosity of 0.3. Its permeability is much higher than the first layer. (Table 8)

Table 8: Properties of the atoll island aquifer system, including general properties, and properties for the Holocene and Pleistocene aquifer units for 3-D model construction

Parameters	Value	Units	Source
General Aquifer Properties			
Compressibility of Porous Matrix	1.00 x 10^{-9}	m^2/N	Peterson and Gingerich 1995
Specific Yield	0.20	m^3/m^3	Griggs and Peterson 1993
Longitudinal Dispersivity α_L	6.0	m	
Transverse Dispersivity α_T	0.05	m	Griggs and Peterson 1993
Holocene Aquifer			
Holocene Porosity	0.2	m^3/m^3	Anthony 1997
Holocene thickness	13 to 18	m	Hamlin and Anthony 1987
Holocene horizontal *K*	75	m/d	Calibrated value (this study)
Holocene vertical *K*	15	m/d	Calibrated value (this study)
Pleistocene Aquifer			
Pleistocene Porosity	0.3	m^3/m^3	Swartz 1962
Pleistocene thickness	485	m	
Pleistocene horizontal *K*	5000	m/d	Oberdorfer et al. 1990
Pleistocene vertical *K*	1000	m/d	Oberdorfer et al. 1990

d) Boundary conditions and Initial Conditions – the mesh nodes within the ocean domain have a specified pressure which represents the pressure from overlying seawater. The nodes along the island top (i.e. the top layer of the mesh) are a fluid flux boundary and represent locations of recharge to the freshwater lens. The freshwater inputs to each node are the product of the recharge rate and the spatial area of the node.

Fifteen meshes were constructed to create a mesh that provided minimized error of the results as well as the model run-time. The final mesh contained elements of 45 m within the interior of the island and 18 m along the coast. It has thirty layers for the upper (Holocene) aquifer and eight layers for the lower (Pleistocene) aquifer, with a total of 480,000 nodes. Part of the process of making the mesh is showed in the following Figure 14. Using a time step of one day, approximately 10 days are required to run a 39-year simulation on a 8-professor, 6G computer.

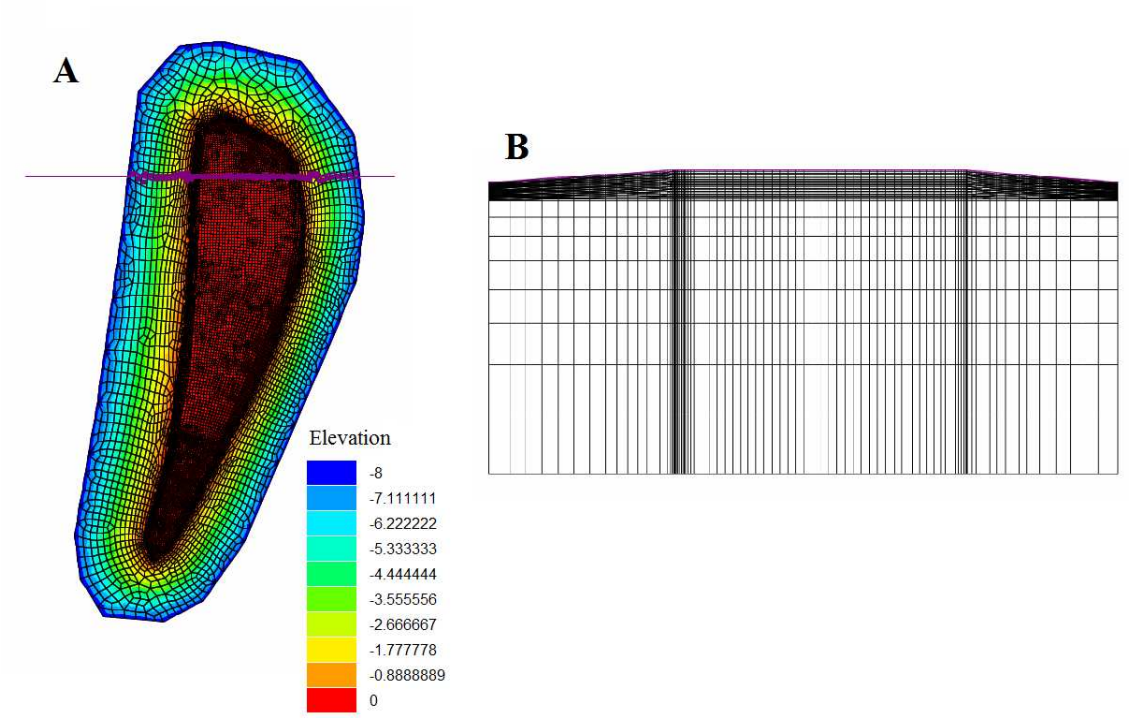

Figure 13. Top view and cross section view of the mesh of Gan. The island surface is the red area in Graph A with elevation of 0 m. Other colors presents the elevation change of the islands extent under the ocean.

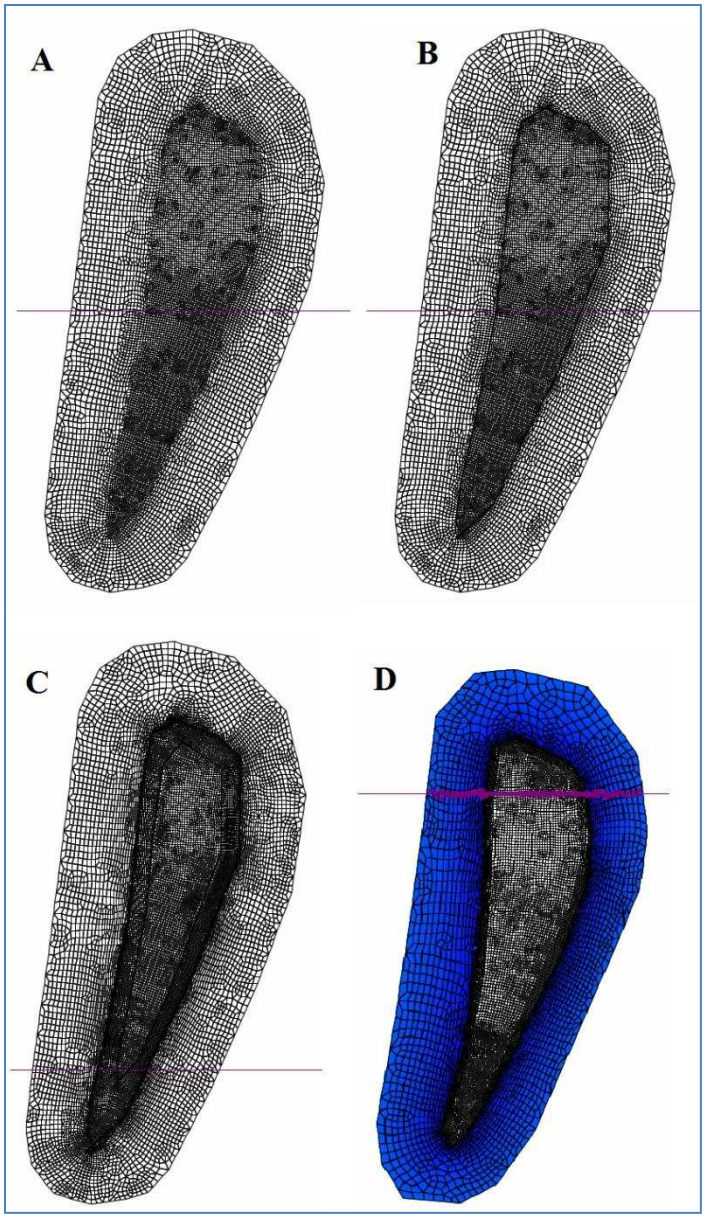

Figure 14. Graph A, B, C, D shows the process of making the mesh. In Graph A, the mesh is fine everywhere and even more fine for island surface but it takes 2.3 minutes to run one time step. Graph B decreased the size of the mesh but it still take about 1.7 minutes/ time step. In Graph C, it remains the fine grid size near the coast but coarsen the grid far from coast. It takes about 1.3 minutes/ time step. In the last graph, it enlarged the ocean grids. The farther the grid is from coast, the coarser they are. The grids in the center are coarsened but the ones around coast line remain fine. It takes about 1minutes/ time step.

3.2.1.2 Pumping in Model and SUTRA code modification

In the island of Gan, groundwater recharges from rainfall and is pumped out for anthropogenic use. There are three villages in Gan. One is in the northwest of the island, one is in

the mideast and the other is located in the south. The estimate of total number of occupied houses is 691, as of October 2009, and each house has one or two pumping wells (Bangladesh, 2010). That mean there are about 700-1300 pumping wells. Adding each individual well to the model is too time consuming. So, rather than specify individual pumping nodes, this study defines pumping areas (Figure15A). The nodes in pumping areas are all considered as pumping nodes with uniform pumping rates. The three main pumping areas correspond to the three villages in Gan. Three polygon objects are created to simulate pumping (Figure15B). Based on the Bangladesh report, estimated groundwater usage is 120L/day/person. The total water pumped out for each village is approximated as the product of pumping rate and population. As a result, the pumping rate in each pumping area is total water usage divide by the number of nodes in pumping area (See equations below).

$$total\ water\ usage_{village\ 1} = 120L/d/p \times population_{village\ 1}$$

$$pumping\ rate = \frac{total\ water\ usage_{village\ 1}}{No\ of\ Pumping\ nodes_{village\ 1}}$$

The SUTRA executable provided within the downloaded software package from the USGS is a 32-bit software that can only allocate a maximum of 2 GB instant memory for each model simulation. When the mesh is too large and the running process required more than 2GB, it cannot be executed. Therefore, GFortran was used to recompile SUTRA code into a 64-bit executable. Also, subroutines within the code were implemented to allow for time-dependent fluid source/sinks terms (i.e. recharge and pumping).

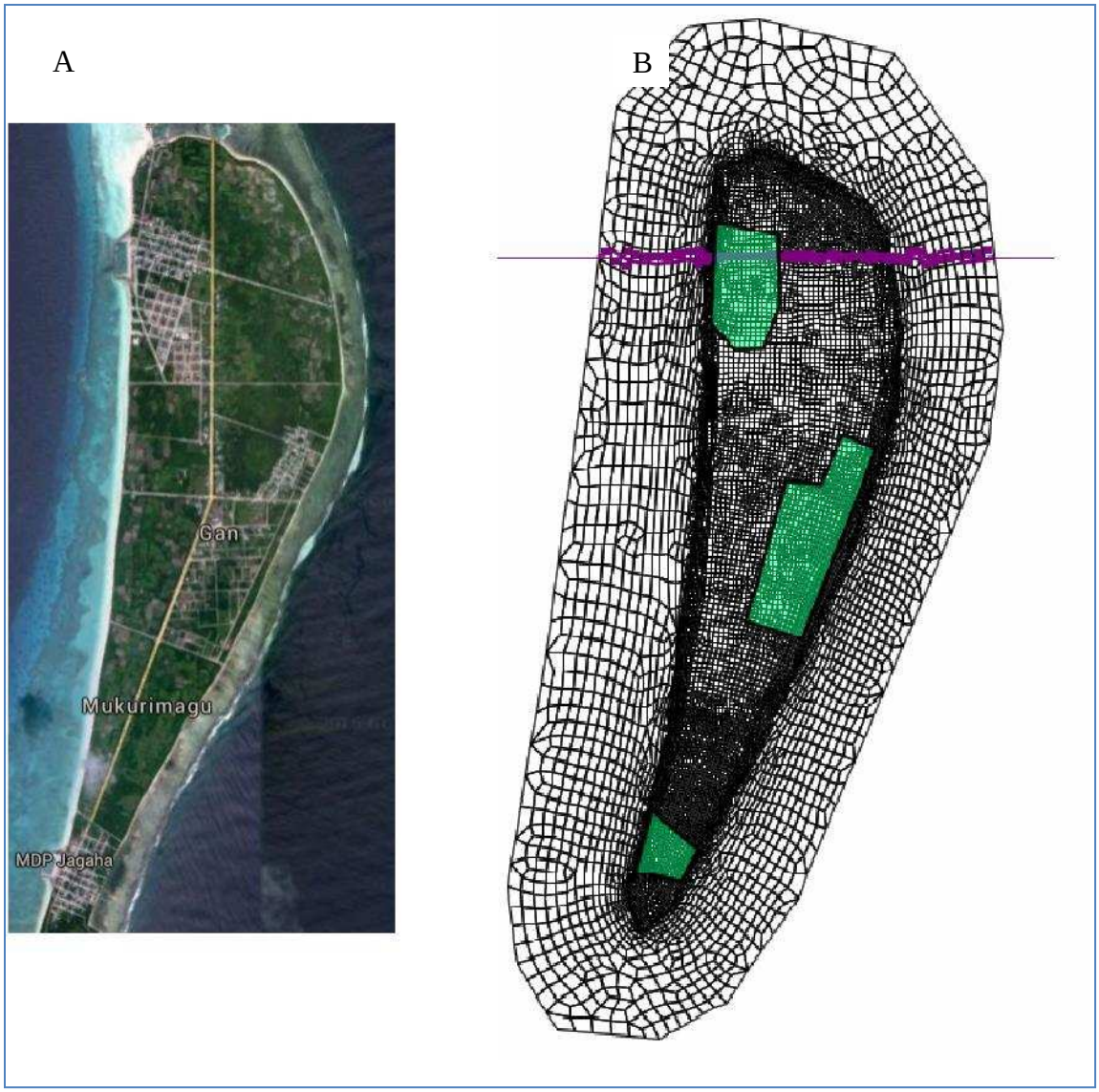

Figure 15. Pumping area (Green colors) in the model (Figure 15B) that represents the pumping in Gan (Figure 15A). Three green areas simulate the pumping in three villages in Gan.

3.2.3 Model Calibration

Even though all the values of aquifer properties are from calibrated 2-D SUTRA model, 3-D model might be different. Geological investigation also only gave general range of these properties. In consideration of many factors, vertical permeability is the key factors to determine freshwater lens thickness—especially in the Holocene aquifer, which contains most of the freshwater.

There is limited historical data to calibrate the model. The Bangladesh Company did a groundwater survey in Gan in December 2009, which gave freshwater lens thickness in 25 locations (Table 1) and estimated freshwater volume. The model uses historical rainfall data from 1998 to 2012 as an input. Recharge is calculated using the same method as Chapter II. To calculate the pumping rate (See Section 2.1.1), the population figures in 2006 are used. Thus, the pumping rate in the village Thundi, Mathimaradhoo and Mukurimagu are 7.80E-03 kg/s, 1.54E-03 kg/s and 4.19E-03 kg/s, respectively. The simulation starts with the model completely filled with seawater, with a freshwater influx over many years, and runs until the freshwater lens is stable. Then, the results of that stable freshwater lens are used as the initial condition for the final model. The final run uses calculated recharge from 1998-2012 and transient pumping rate. The results of freshwater lens thickness taken in December, 2009 are compared to the investigated results at the same location. The simulation attempts many vertical permeability ranges from 1-10 m/day with an interval of 1 m/day. The value which best matches the practical data is considered the calibrated model.

3.2.4 Estimating the Effect of Future Climate Scenarios on Gan's Freshwater Lens

This section lists the methods which estimate the effects of rainfall pattern, population growth and sea-level rise on the groundwater resources in Gan. All the GCMs used for each of the simulations are listed in Table 9.

Table 9: All the GCMs used for simulations of each scenario.

	Rcp2.6	Rcp8.5
Rainfall Pattern	CESM1-CAM5 MIROC5 IPSL-CM5A-LR CCSM4 GFDL-ESM2G	CESM1-CAM5 MIROC5 CCSM4 IPSL-CM5A-MR GISS-E2-R p1 GFDL-ESM2G GFDL-CM3
Conservative Pumping	CESM1-CAM5 MIROC5 IPSL-CM5A-LR CCSM4 GFDL-ESM2G	
Aggressive Pumping	CESM1-CAM5 MIROC5 IPSL-CM5A-LR CCSM4 GFDL-ESM2G	CESM1-CAM5 MIROC5 CCSM4 IPSL-CM5A-MR GISS-E2-R p1 GFDL-ESM2G GFDL-CM3
Sea-level Rise	Steady recharge	
Sea-level Rise and Aggressive Pumping	CCSM4 IPSL-CM5A-LR	

3.2.4.1 Future Estimated Precipitation

GCMs are used to estimate future climate change. In Chapter II, five better-performing GCMs are selected for in Region 2— where Gan is— for scenario Rcp2.6 and seven GCMs are selected for scenario Rcp8.5. The same procedures are used to downscale to daily rainfall data and calculated recharge (Figure 16A) using mass balance. Time series of predicted rainfall data for 2012-2050 from these five GCMs are plotted in Figure 16A. SUTRA uses this data to predict future lens thickness. The output gives salt concentrations at all locations for every two months. The freshwater lens is limited at 0.00089 $kg_{salt}/kg_{water.}$ The average lens thickness of whole islands is calculated by MATLAB.

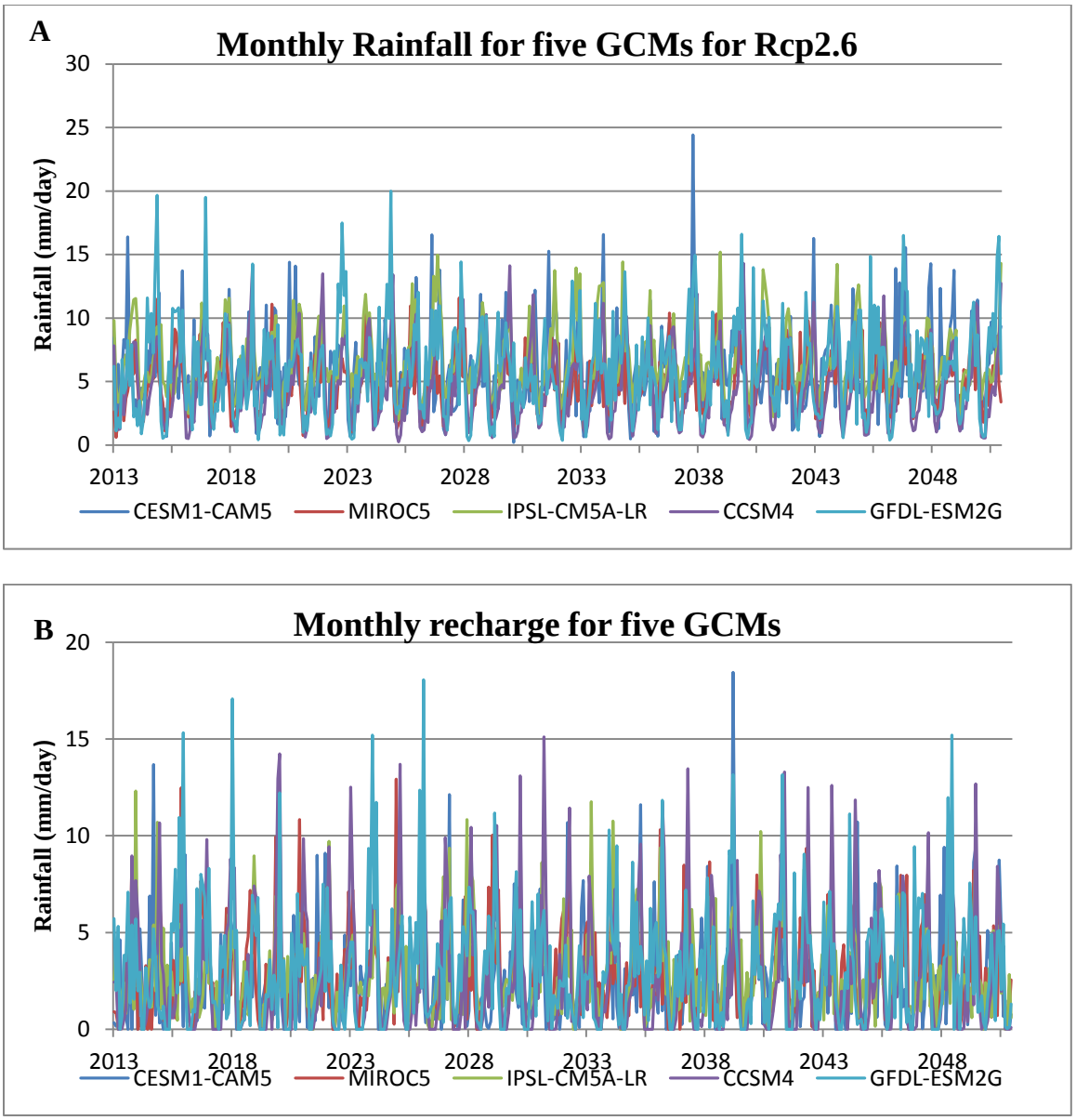

Figure 16. Time series plots of precipitation (A) and corresponding recharge (B) from five selected GCMs with scenario Rcp2.6 from the year of 2013 to 2050 for island of Gan.

3.2.4.2 Future Estimated Pumping

Pumping needs varies with population. The Maldives has a high annual population growth rate of 1.76%. The island of Gan is even worse. The average annual growth rate from 2006 to 2010 was 13.5%. The Government of Maldives (GoM) estimates that the population could rise to 20,000 (Bangladesh, 2010). Gan is the largest island in Maldives. Its population density (11.2 /ha)

is much lower than the capital Malé (260/ha). As population stress increasing in the future, it is very possible that more people will move to Gan. In this study, in order to estimate future pumping, conservative and aggressive estimation are both considered for population growth. The conservative estimate uses a population growth of 1.76%; the aggressive estimation uses 9%. Population growth and pumping rates are plotted in Figure 17. These two different pumping rates both run with all GCMs from scenario Rcp2.6 and Rcp8.5. the resulting data is compared with regards to the effects on groundwater resources. Also, one example that uses climate data from CCSM4 is used to compare no pumping with conservative pumping and examine the pumping effects on groundwater resources.

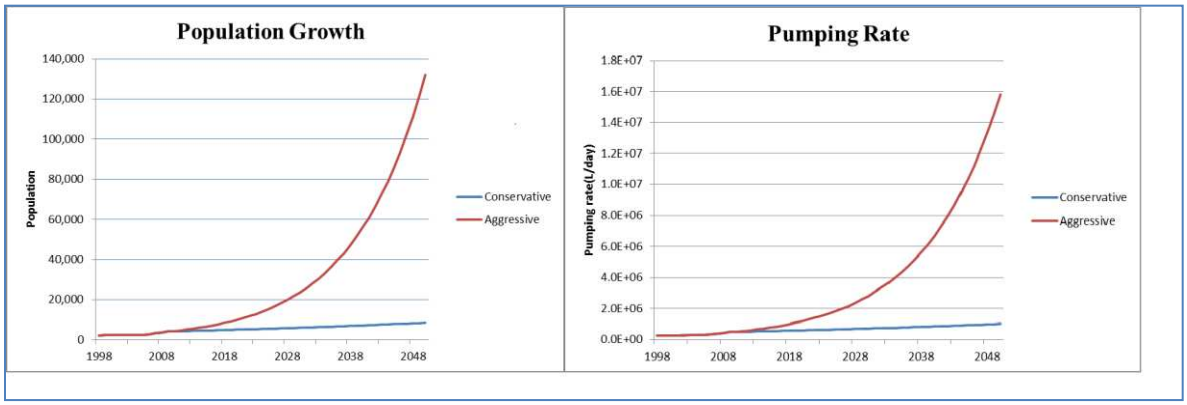

Figure 17. Estimated conservative and aggressive population growth and pumping rate in the future for Gan

3.2.4.3 Future Sea-Level Rise

Sea-level rise has been a big issue for Maldives. As the sea level rises, massive land areas in Maldives are inundated by seawater, especially for Maldives. It has the lowest average elevation of about 1.5 m above sea level and the slope of the islands is about 1:100. The sea-level is predicted to rise a half meter for Maldives during 21st century (Woodworth, 2005). As a result, about 50 m of shoreline would be inundated. Some islands may disappear.

For Gan, the sea level rise is a serious problem for its fresh groundwater. As the sea level

rises, the seawater pressure underground increases and pushes up the freshwater lens upward. The island's shrunken surface would discharge more freshwater to the sea and would receive less precipitation. The model simulates the effect of sea level rise on groundwater by building a new model with a smaller islands surface (Figure 18). About 50m of coastline is lost to the ocean in the model. The green line is the surface before sea-level rise, whereas the red one marks the surface after. The sea level rise decrease land area by about 12.5%. In that simulation, pumping is not applied and rainfall rate is kept steady in order to isolate the effects of sea level rise. The rainfall rate is about 2.73 mm/day which is the average of the rainfall rate from 2011 to 2050. Two models are simulated to contrast with each other: before and after sea level rise. The models assume the island is full of seawater as initial condition, then run until a steady state for about 20 years. The results give us the percent of freshwater lens volume lost according to the amount of land area.

3.3 Results

3.3.1 3-D views of simulation results

The simulation results give the salt distribution at each mesh node in each time step. The Figure showed below is a 3-D view of the salt distribution in the groundwater of island Gan (Figure 19). In Figure 19A, it shows the whole island model grid. The red part is seawater, which has the highest salt concentration. The blue part is mostly fresh water, which has a very low salt concentration. Other colors, like yellow and green, represent the parts with salt concentration between seawater and freshwater. A mix of seawater and freshwater is not potable. Figure B and C show the cross section of the island. The blue part is the freshwater lens and its thickness. It gives the lens thickness in each point of the island. Freshwater volume can be calculated from that under certain limits of salt concentration for each time step.

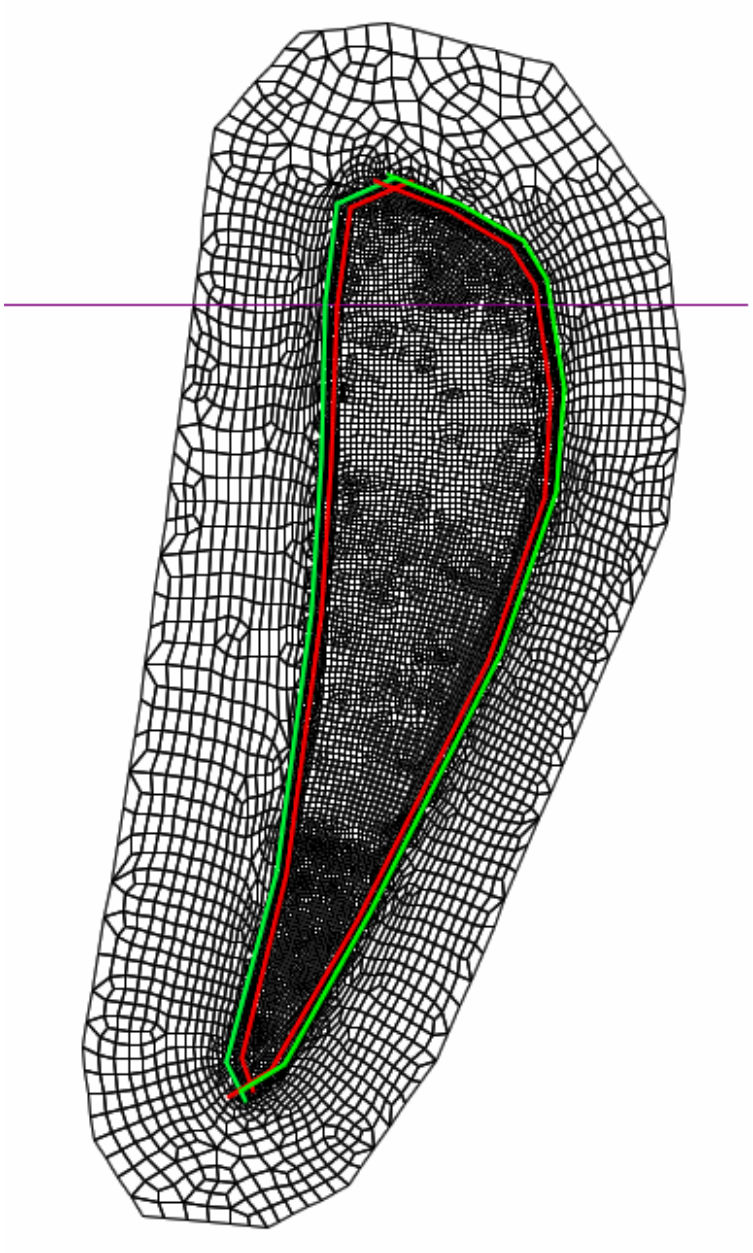

Figure 18. Land surface comparison before and after sea-level rise. The blue line is the contour before sea-level rise whereas the red one is after sea-level rise.

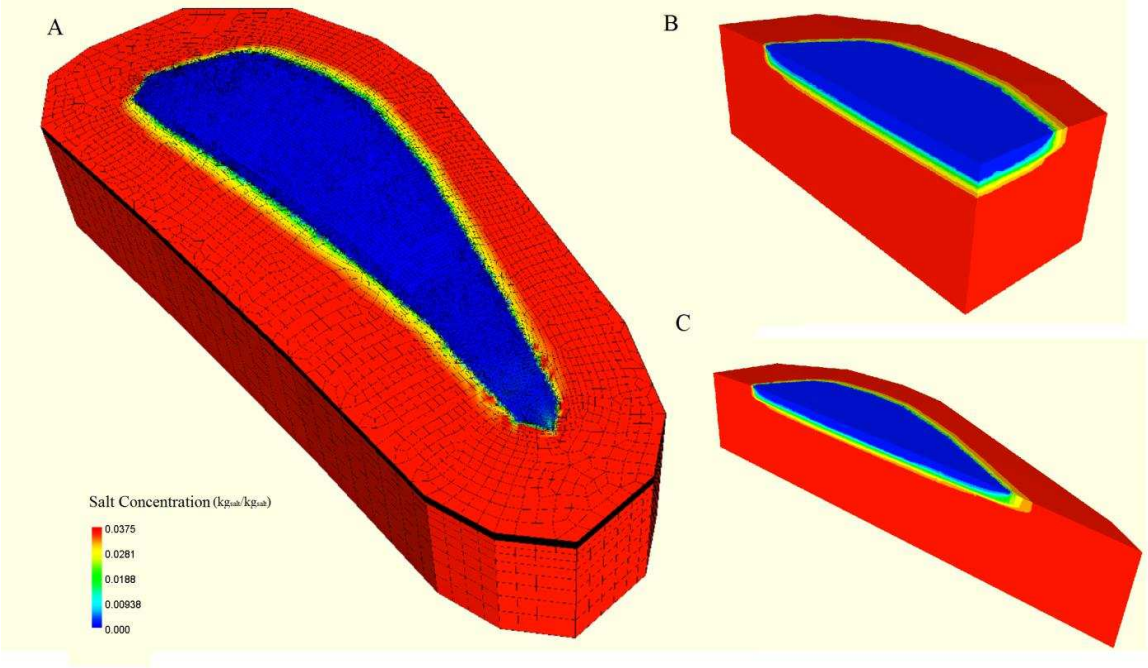

Figure 19. Three dimensional review of the SUTRA modeling results. The color represents the salt concentration. The red color has highest salt concentration that represents seawater. The blue color is freshwater. Other colors are the mixture of fresh and seawater.

3.3.2 Calibration Results

The model is calibrated with different vertical permeability in the time of December 2009. Few plots of observed freshwater lens thickness on certain points of Gan versus modeled values are showed as below. $K_v = 3m/day$ looks the best match for historical data (Figure 20). With the best match, the difference of the mean of the observed and modeled value is pretty small about 0.033 m, which can be reasonable approximation to be unbiased, but the relative error is still large with about 58%. The total estimated freshwater is very close to field measurement estimate, which is about 14300 million liter versus 14200 million m^3 from groundwater investigation report (Bangladesh Ltd., 2010). Overall, the model might perform better if there are more available historical measurements.

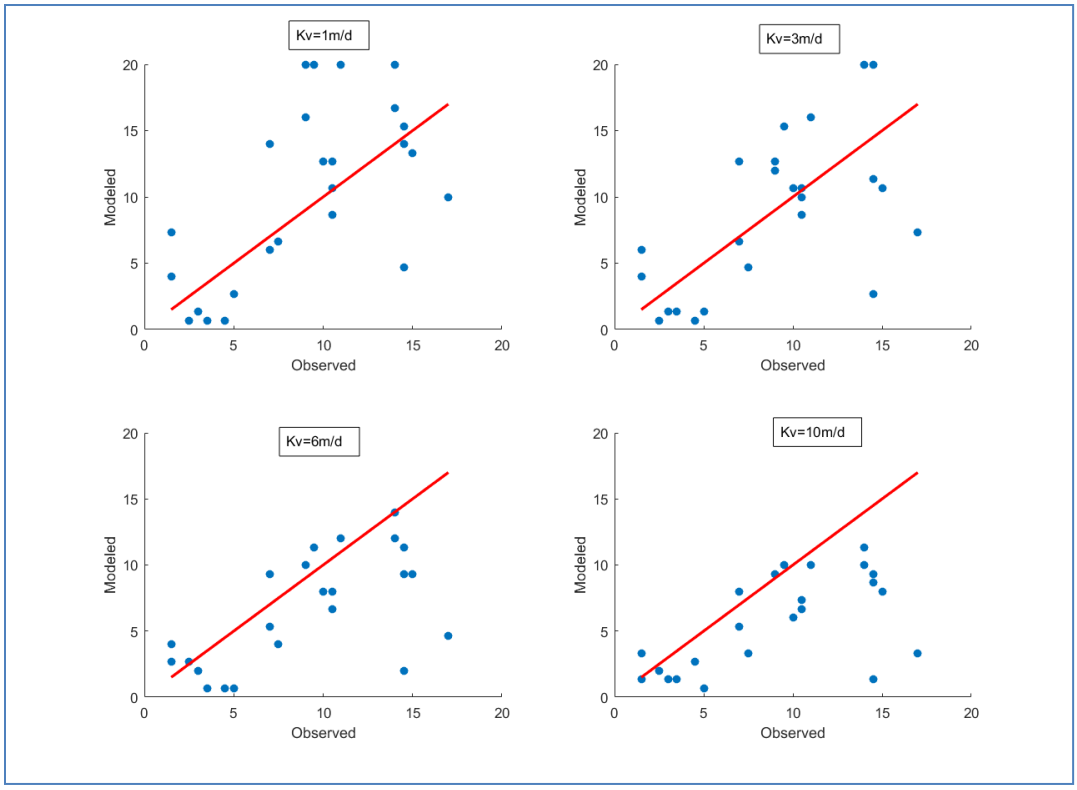

Figure 20. Observed vs. modeled lens thickness plot with different vertical permeability. The red line the y=x line. The $\boldsymbol{k_v = 3\ m/d}$ shows the best match.

3.3.3 Pumping effects

3.3.3.1 Pumping vs. Non pumping

One model is simulated to generally show the pumping effect on freshwater volume by using one of the GCMs (CCSM4). Figure 21 shows the freshwater volume time series plot and compares pumping to no pumping. With the conservative pumping, volume decline is observed at the beginning of pumping and increased later as pumping increased. Comparing to non-pumping simulation, the average loss of fresh groundwater volume is about 6.77% and the highest is 10.5% (Figure 22). At the end of 2050, the total loss of fresh groundwater from pumping is 1.73 million m^3. However, the total water pumped out for 39 years during 2012-2050 are much greater than that, which is 10536 million m^3. The water loss of fresh groundwater from

pumping is less than 0.02% of the water pumped out, which is not significant at all. In addition, in the beginning five or six years, the losses increase linearly. However, after that, the losses are not a linear progression because it changes with wet and dry seasons.

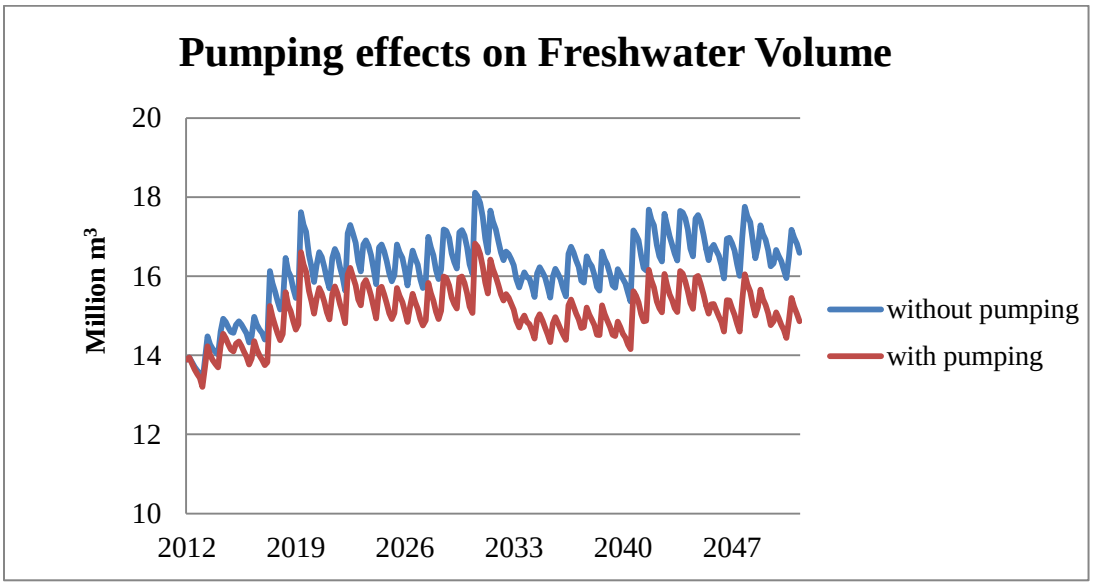

Figure 21. Comparison of freshwater volume time series plots from the scenarios with pumping and without pumping.

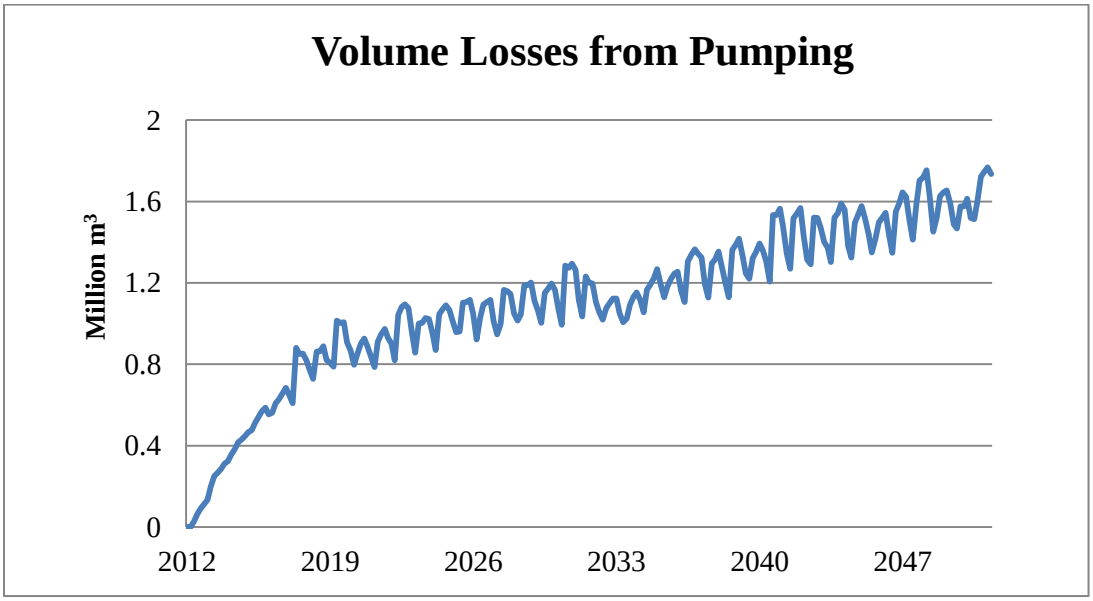

Figure 22. Time series plot of freshwater volume plot from pumping. The loss is the freshwater volume difference between pumping scenario and non-pumping scenario.

3.3.3.2 Conservative pumping

The conservative pumping demands grow at a rate of 1.76%, due to population growth. The results show that the freshwater volume increases in the future even with more pumping. The Figure 23A is the time series plot of freshwater lens volume for five different GCM scenarios. The GCM scenarios give similar results. CCSM4 and MIRCO5 are close to each other, but there is a large difference between CESM-CAM5 and IPSL-CM5A-LR. The range of the volume is within about 10 to 20 million m^3 and the average is about 15.3 million m^3. At the end of 2050, three of them reached a point of 16 million m^3 and the other two meet at 15 million m^3. Fluctuation of volumes corresponding to wet and dry season are observed. CCSM4, MIRCO5 have small fluctuations whereas the other three have much larger fluctuations. For example, GFDL-ESM2G has 3-6 large fluctuations that some of them are over a period of ten years. This causes a larger range for freshwater volume and more extreme wet and dry season, correspondingly. A slight uptrend in freshwater volume is observed for all the GCM scenarios. These increases of freshwater volume, for GCMs are 6.9%, 5.6%, 15.9%, 15.1% and 18.1%, respectively, with an average increase of 12%. The Figure 23B shows the average lens thickness of the whole island for the simulation time period, 2012-2050. The range of average lens is from 5 meter to 8 m and the average of all scenarios across the simulation period is about 6.6 meters. The fluctuation of lens thickness can be as larger as 2 meters. Overall, with conservative pumping, the fresh groundwater would still satisfy the pumping needs in the future.

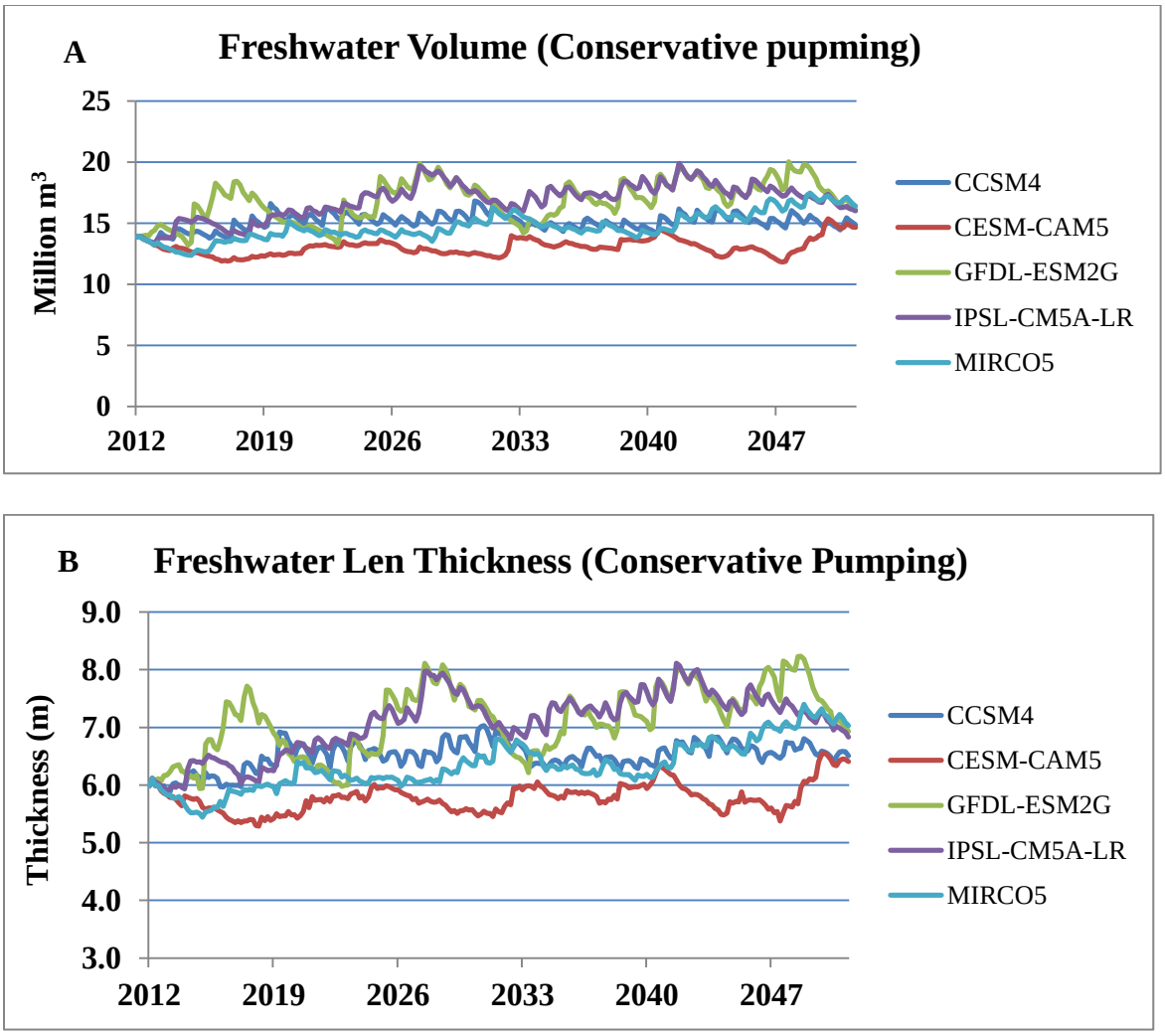

Figure 23. Time series plots of freshwater volume and lens thickness for all selected GCMs

3.3.3.3 Aggressive pumping

With aggressive pumping, the pumping rates increase by 9% per year. A large decrease in fresh groundwater volume is predicted (Figure 24). All GCMs have decreasing trend. By the end of 2050, the freshwater volume would decrease by 23.7% on average for scenario Rcp2.6. The average freshwater value is about 10.6 million m^3. The average lens drops from 6 m to 5.56 meters. However, the lens area, which held freshwater, shrank about 20% from 6 km^2 to 4.79km^2, parts of shoreline area do not have fresh groundwater anymore. The results for

scenario Rcp8.5 are more diverse. The time series pattern of freshwater volume for all GCMs is less consonant than Rcp2.6. and the range for volume at the end of 2050 is much larger. The average decrease of freshwater volume is about 20.88%. The lens area shrinks about 21.6% at the end of simulation. Overall, with aggressive pumping, the freshwater lens would essentially be destroyed.

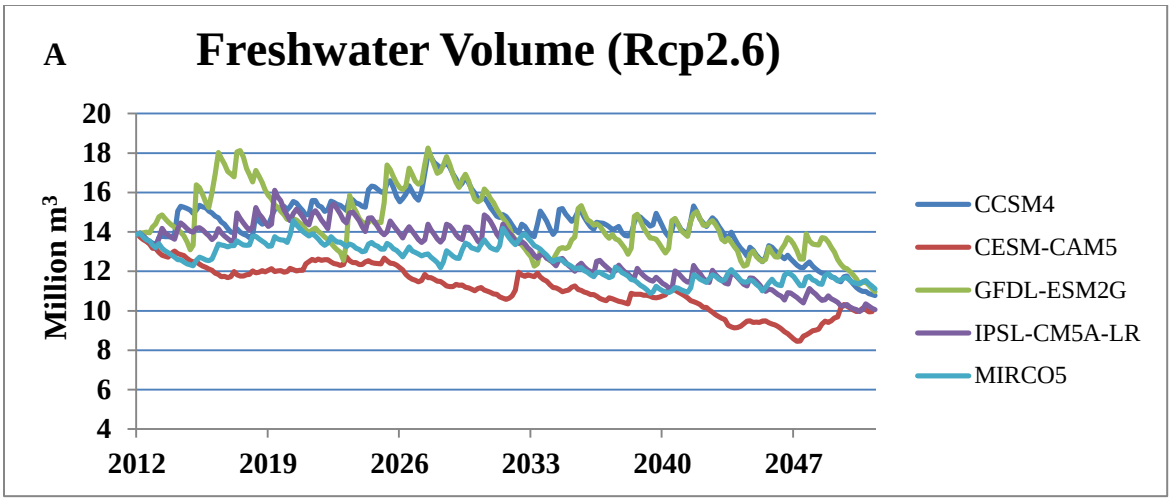

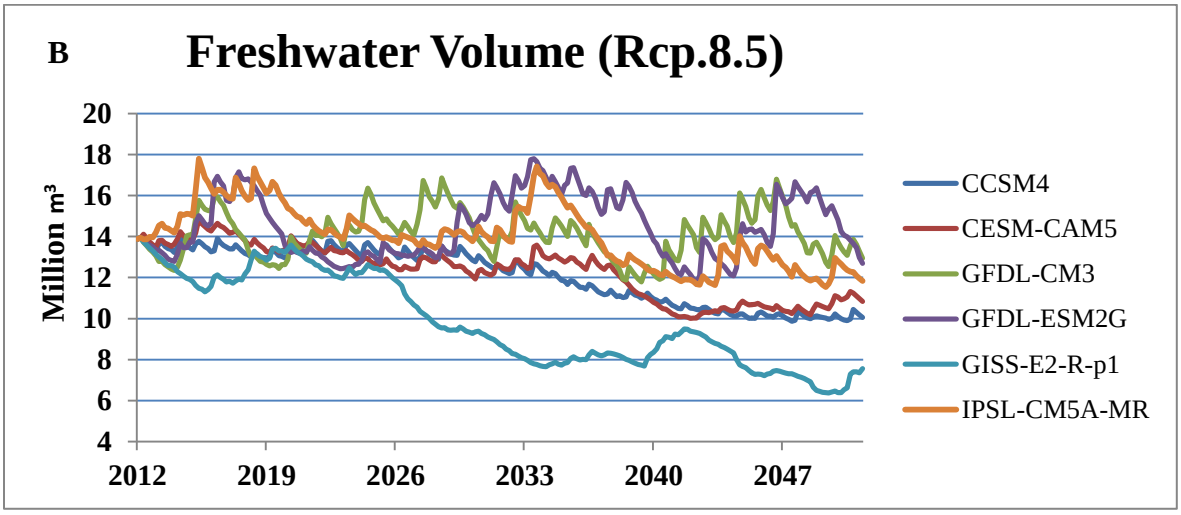

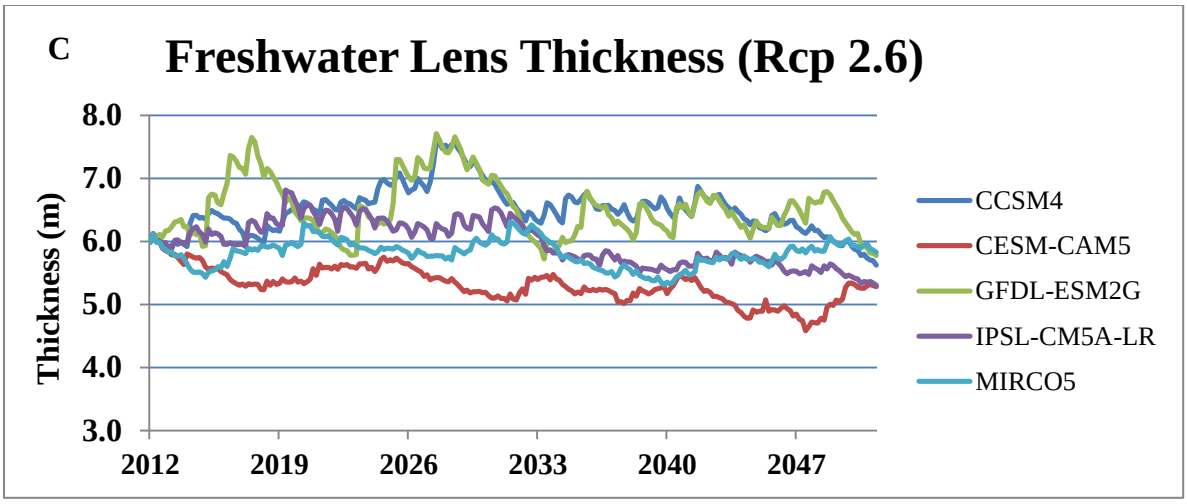

Figure 24. Plot A and B show the time series plots of freshwater volume from scenario Rcp2.6 and Rcp8.5. Plot C shows the time series plot of freshwater lens thickness.

3.3.4 Sea-level rise effects

The land area of Gan was about 6.57 km^2 in 1998, but it will drop to 5.75 km^2 during the 21st century. The freshwater volume will decrease in response to smaller land area. With an inundation of 12.5% of Gan's land area, it loses 13.73% of freshwater volume. Figure 25 shows a time series plot which compares freshwater volume before and after sea level rise. At the beginning of simulation with 100% seawater, there is no fresh water. As rainfall is applied on the models, the freshwater volume starts to increase. For the first few years, two models have a similar increasing trend. After seven years, a gap develops between them. After about fourteen years, the trends approach a steady gap. At the end of simulation, the before sea level rise model has a freshwater volume of 16.1 million m^3 whereas after sea rise model has 13.9 million m^3. To conclude, the effects of sea-level rise on freshwater lens in Gan are bigger than moderate population growth but smaller than aggressive population growth.

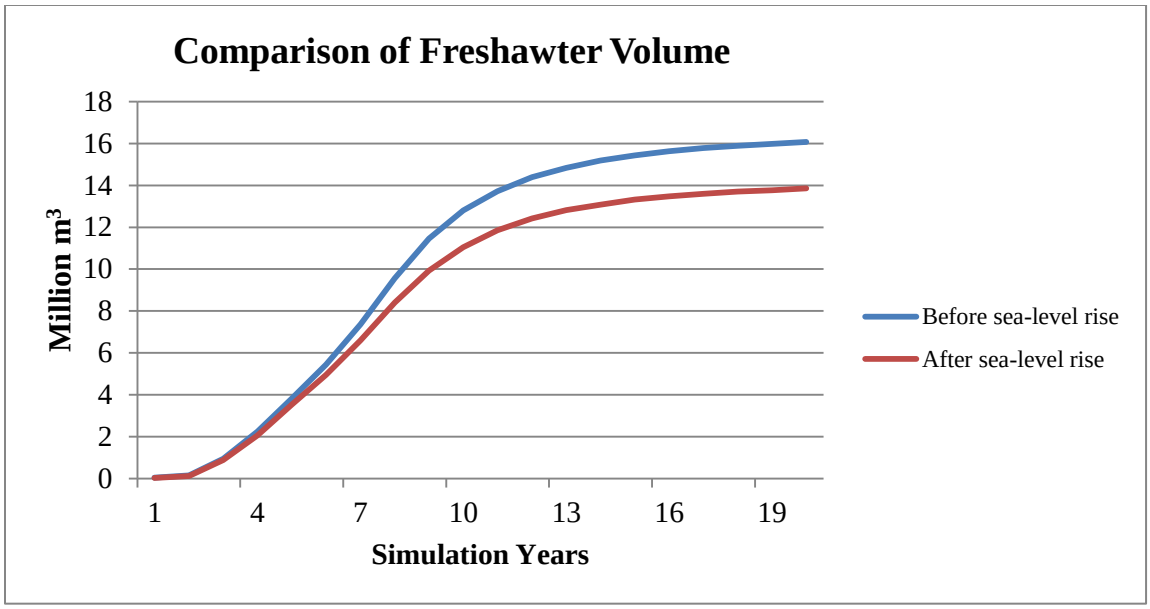

Figure 25. Time series plot comparison of freshwater volume between simulations before sea-level rise and after sea-level rise.

3.3.5 Combined effects of sea-level rise and aggressive pumping

Under the impact of sea level rise and aggressive pumping, the freshwater volume drops tremendously. At the end of 2050, the freshwater volume decreased about 87% from about 14.1 to 1.8 million m^3. The area that has freshwater is decreased to 10% of the total land area. The average lens thickness decreased from 6.8 m to about 1.1 m. With less than 2 meters of lens thickness, pumping is not viable. The freshwater lens is effectively destroyed even with some remaining fresh water. These results are only valid at the year of 2050.

3.4 Discussion

3.4.1 Advantage and disadvantage of the model

The model mesh is fine enough to give a good resolution for the results but model runs slowly. The model mesh is built in ModelMuse. It has approximately a half-million elements or nodes with thirty layers in the Holocene aquifer and eight layers in Pleistocene aquifer. It takes a

long time to run and lots of computation memory. For the simulation from 2012-2050 with about 14235 daily time steps, it takes about two weeks to run and 1.7 GB computer memory. This study ran about forty models. Lots of computers resources or super computers are needed to do this research. Another way to shorten the running time would be to improve the SUTRA model performance such as optimizing the algorithm or changing it to parallel processing, which may be too difficult. However, improvement of model performance is necessary and can be done in future modeling.

The boundary condition is simplified to ease processing. The rainfall rate is assumed to be homogenous for the island. The model top is mean sea level, not the island's surface, which means unsaturated zones are not simulated. The island's topography is unknown, so the slope of shoreline is estimated. Technically, the north and south ends are connected with other islands. However, they are assumed surrounded by seawater. This can affect the model results. All these simplifications of boundary conditions can be improved in the future modeling,

The assumption of homogeneity of the two aquifers would also affect the model results. And it can be significant. With limited geographic data, it is impossible for us to accurately estimate the aquifer properties. Accordingly, more geographic investigation of freshwater lens is necessary to improve the model performance. The model calibration is limited by the available data. Only one groundwater investigation in 2009 has estimated the freshwater lens thickness. Obviously, more field data are needed to improve calibration results too. Current field data could be used to validate the model. Overall, more investigation and field data are needed in the future.

3.4.2 Effects of changing rainfall pattern

The fresh groundwater would increase in the future according to model results. This is because the rainfall is predicted to increase in the future by GCMs. As a result, there will actually be more fresh groundwater available for the island of Gan. This conclusion also coincides with 2-D modeling. However, more rainfall could contribute to more frequent extreme events. Extreme rainfall or dry seasons are predicted to be likely in the future too.

3.4.3 Effects of pumping

3.4.3.1 Pumping vs. non pumping

A mild increase of pumping rates does decrease the freshwater volume. However, compared to the total fresh water volume pumped out, the decrease freshwater volume is insignificant. The main reason is that the water discharge to the sea is being replaced by the pumping. In other words, much less water is discharged to the sea at the edge of the island when it is pumping because the water table stays low. Otherwise, the freshwater from rain could discharge to the sea without being used. Hence, it is safe to pump a reasonable amount of fresh groundwater for use by residents. In addition, it is interesting to see the losses (Figure 22) change seasonally instead of by a positive linear progression.

3.4.3.2 Conservative pumping vs. aggressive pumping

With conservative pumping, the freshwater lens keeps its shape and is not affected much by the pumping. The population growth assumed in this scenario is 1.76% per year. At the end of 2050, the population doubles, which is not a small amount of stress. However, the population stress does not outweigh the projected increase in rainfall: the freshwater volume increases even with conservative pumping stress. The average lens thickness remains around 6-7 m, which is thick enough for pumping. This indicates that with high population growth rate of 1.76% in Gan,

there is enough fresh groundwater for their usage for next forty years. However, aggressive pumping with a population growth rate of 9% cause severe seawater intrusion: the freshwater would become exhausted. Moreover, the land area near the shoreline would run out of fresh groundwater first. All three villages are very close to the shoreline, so pumping issues would occur very quickly. This scenario requires a shallower pump or a central location for pumping on the island. Even though the freshwater volume decreases a lot, the lens is thick enough for pumping. The population growth did stress on the groundwater in Gan. The assumed population growth in Bangladesh Consultants reports may be too high, but it could happen in the future. Consider the capital Male: it has nearly 200,000 people and they run out of fresh groundwater. To avoid this situation happens again, sever results from population stress needs to be taken into account by the government of Gan. The number of people who live in Gan should be limited for the sake of groundwater quantity and quality.

3.4.3.3 Sea-level rise

Sea-level rise does have a huge effect on the groundwater in Gan. First, the shoreline of Gan will be pushed inward 50-80 m by seawater. All three villages are very close to the shoreline and the closest roads or houses are within 50 m of shoreline. If sea-level rise happens, these houses would have to be moved. Second, with 12.5% of land area inundated, 12.5% less rainfall recharged is received by the smaller land area. Third, freshwater is lost because the freshwater is pressurized by the raised sea level. The advantage of the model is that it can quantify the freshwater losses from sea-level rise. However, the model simplified the sea-level rise process. In reality, the sea level rises slowly and continuously. So, the land area changes alongside the sea level change. Nevertheless, in this study, the model only simulates the situation at the end of 21st century by making a smaller land surface model while the rainfall is assumed steady. The results

can only give the final stage of sea level rise effects. The process of sea level rise is not simulated, which could have impacts on the final results.

The combined effects of sea-level rise and aggressive pumping will exhaust freshwater resources in Gan very quickly. In a short time there would be no potable water for drinking or domestic use. The government of Gan should be prepared to preserve groundwater resources to prevent this scenario from happening.

CHAPTER 4: SUMMARY

This study helps assess current and future groundwater resources in Maldives by using 2-D and 3-D numerical modeling. 2-D modeling gives an overall assessment of fresh groundwater quantity for 4 different sizes of islands (200, 400, 600 and 1100 m) in Maldives. Estimations of lens thickness and its fluctuation from the year of 2012 to 2050 are provided by 2-D modeling. A mild increase in lens thickness in the future is found under the effects of changing rainfall pattern. 3-D modeling is used to evaluate the effects of changing rainfall pattern, increasing pumping and sea-level rising on the groundwater resources for a specific island, Gan. Same results from 2-D modeling are found on the effects of changing rainfall pattern in 3D modeling. An increase in fresh groundwater volume is estimated in the future for Gan since more rainfall is predicted by GCMs. In terms of pumping, conservative pumping with a normal population growth of 1.76%/yr would not have negative effects on the quantity of groundwater resources. Instead, freshwater groundwater can be a very valuable water resource for Gan with reasonable pumping. More freshwater could be pumped out for usage instead of discharging to the sea without destroying the freshwater lens. However, with aggressive pumping, it will exceed the capacity and sustainability of the groundwater. The lens would essentially be destroyed essentially. Under the effects of sea-level rise, the groundwater volume shrinks as land area shrinks. It will have a significant effect on groundwater resource in atoll islands if it happens. The worst case is that sea-level rise and aggressive pumping all happens. In this case, the groundwater resources in Gan are exhausted within few years. Overall, this study gives an estimation and evaluation of major impacts on groundwater resources for the future of Maldives.

This study would also help the water management for the government of Maldives. The overall assessment and estimation of groundwater resources can give them a general understanding of freshwater quantity in different islands. Especially, estimation of future groundwater resources can help with future water resources planning. Residents also can plan the pumping according to the seasonal fluctuation of lens thickness in case of pumping seawater out. The results from 3-D modeling give them a more clear and mathematic understanding of effects of pumping and sea-level rising on groundwater resources. With these quantified impacts, it makes easier for the government of Gan in Maldives to manage pumping, population and water resources. Knowing the negative results of aggressive pumping and sea-level rise, they can come up with better solutions of water management to prepare for that happening. Modeling results can develop improved the understanding of groundwater resources in Maldives and also help with water supply management for the Ministry of Environment, Energy and Water (MEEW) and Male Water and Sewerage Company (MWSC).

The 3-D modeling can be applied for other islands in the Maldives or other atolls. 3-D modeling is better simulates on radial pumping than 2-D modeling. However, there are still lots of things to be improved. The model can be improved significantly by inputting more detail information about geology, topography and local rainfall data of the island. Unsaturated zone can also be simulated in the future. Evapotranspiration can be calculated more accurately by knowing the plants or vegetable type on the islands. The tide can be simulated by applying transient pressure boundary along the shoreline. The simulation methods can be improved by specifying pumping location and pumping rates in different time, changing the sea-level rising to a transient process. The future research would focus on the accuracy of the modeling.

REFERENCE

Ablain, M., Cazenave, A., Valladeau, G., & Guinehut, S. (2009). A new assessment of the error budget of global mean sea level rate estimated by satellite altimetry over 1993–2008. *Ocean Science*, 5(2), 193-201.

AFD (2007). Sewerage System Creation in 4 Islands, Maldives Tsunami Infrastructure Rehabilitation Project, Final Report. *Prepared by BRL Ingénierie for Agence Française de Développement*, November 2007.

Ayers, J.F., and H.L. Vacher (1986), Hydrogeology of an atoll island: A conceptual model from detailed study of a Micronesian example. *Ground Water* 24, 2-15.

Bailey, R., Khalil, A., & Chatikavanij, V. (2014a). Estimating transient freshwater lens dynamics for atoll islands of the Maldives. *Journal of Hydrology*, 515, 247-256.

Bailey, R., Khalil, A., & Chatikavanij, V. (2014b). Estimating Current and Future Groundwater Resources of the Maldives. *JAWRA Journal of the American Water Resources Association*, 51(1), 112-122.

Bailey, R.T., Jenson, J.W., and A.E. Olsen (2009), Numerical Modeling of Atoll Island Hydrogeology. *Ground Water* 47, 184-196.

Bangladesh Consultants, Ltd. 2010a. Groundwater Investigations Report for GDh. Thinadhoo, *Ministry of Housing, Transport and Environment Republic of Maldives*.

Bangladesh Consultants, Ltd. 2010b. Groundwater Investigations Report for L.Gan, *Ministry of Housing, Transport and Environment Republic of Maldives.*

Bangladesh Consultants, Ltd. 2010c. Groundwater Investigations Report for N.Holhdhoo, *Ministry of Housing, Transport and Environment Republic of Maldives.*

Bangladesh Consultants, Ltd. 2010d. Groundwater Investigations Report for N.Velidhoo, *Ministry of Housing, Transport and Environment Republic of Maldives.*

Barthiban, S., Lloyd, B., & Maier, M. (2012). Sanitary Hazards and Microbial Quality of Open Dug Wells in the Maldives Islands. *JWARP Journal of Water Resource and Protection*, 4(7), 474-486.

Beswick R. (2000). Water Supply and Sanitation, A Strategy and Plan for the Republic of Maldives, Parts 1 & 2, *Ministry of Health, Republic of Maldives*, March 2000.

Brown, B. E. & Dunne, R. P. (1988). The environmental impact of coral mining on coral reefs in the Maldives. *Environ. Conserv.*, 15, 159-66.

Church, J.A., N. White and J. Hunter (2006), Sea level rise at tropical Pacific and In-dian Ocean islands. *Global Planet.Change* , 53 , 155-168.

Coastal Aquifers, U.S. Geol. Surv. *Water Supply Pap*. 1613-C, 35-69, 1964.

Coe, R., and R. D. Stern. "Fitting models to daily rainfall data." *Journal of Applied Meteorology* 21.7 (1982): 1024-1031.

Comte, J. C., Join, J. L., Banton, O., & Nicolini, E. (2014). Modelling the response of fresh groundwater to climate and vegetation changes in coral islands. *Hydrogeology Journal,* 22(8), 1905-1920.

Cox PM, Betts RA, Jones CD et al. (2000) Acceleration of global warming due to carbon-cycle feedbacks in a coupled climate model. *Nature*, 408 , 184-187

Dickinson, W.R. (2004), Impacts of eustasy and hydro-eustasy on the evolution and landforms of Pacific atolls. *Palaeoecology* 213, 251-269.

Drabbe, J., and Badon Ghyben, W., 1889, Nota in verband met de voorgenomen putboring nabij Amsterdam [Notes on the probable results of the proposed well drilling near Amsterdam]: *The Hague, Koninkl. Inst. Ing. Tijdschr*., 1888-89, p. 8-22.

Falkland, A., & Custodio, E. (1991). Conditions for freshwater occurrence in small islands. In Hydrology and water resources of small islands: *A practical guide: A contribution to the International Hydrological Programme*, IHP-III, Project 4.6. Paris: Unesco.

Falkland, A.C. (1994), Climate, Hydrology and Water Resources of the Cocos (Keeling) Islands. *Atoll Research Bulletin No. 400*, Smithsonian Institute, Washington, D.C., 23 pp.

Falkland, A.C. 1983. Christmas Island (Kiritimati) Water Resources Study. Vol. 1. Victoria, Australia: *Australian Department of Housing and Construction*.

Falkland, T. 2000. Report on Groundwater Investigations in Southern Development Region (ADB Regional Development Project). *Report for Ministry of Planning and National Development.*

Falkland, T. 2001. Report on Groundwater Investigations in Northern Development Region (ADB Regional Development Project). *Report for Ministry of Planning and National Development.*

Fu, G., Liu, Z., Charles, S., Xu, Z., & Yao, Z. (2013). A score-based method for assessing the performance of GCMs: A case study of southeastern Australia. Journal of Geophysical Research: *Atmospheres J. Geophys. Res. Atmos*., 118, 4154-4167.

Ghassemi, F., Alam, K., & Howard, K. (2000). Fresh-water lenses and practical limitations of their three-dimensional simulation. *Hydrogeology Journal*, 8(5), 521-537.

Ghassemi, F., Jakeman, A. J., Jacobson, G., & Howard, K. W. F. (1996). Simulation of seawater intrusion with 2D and 3D models: Nauru Island case study. *Hydrogeology Journal*, 4(3), 4-22.

Ghassemi, F., Molson, J. W., Falkland, A., & Alam, K. (1998). Three-dimensional simulation of the Home Island freshwater lens: preliminary results. *Environmental modelling & software*, 14(2), 181-190.

Gingerich, S. B., & Voss, C. I. (2005). Three-dimensional variable-density flow simulation of a coastal aquifer in southern Oahu, Hawaii, USA. *Hydrogeology Journal*, 13(2), 436-450.

Glover, Robert E., The pattern of fresh-water flow in a coastal aquifer. Sea Water in Coastal Aquifers, U.S. Geol. Surv. *Water Supply Pap*. 1613-C, 35-69, 1964.

GoM (2010). Website "Isles" (http://isles.egov.mv), *Government of Maldives*.

Griggs, J.E. and Peterson, F.L. (1993), Ground-water flow dynamics and development strategies at the atoll scale. *Ground Water* 31(2), 209-220.

GWP Consultants (2006), Maldives water and sanitation authority five year activity plan 2006-2010.

Hamlin, S.N. and S.S. Anthony (1987), Ground-water resources of the Laura area, Majuro Atoll, Marshall Islands. *USGS Water Resources Investigation Report* 87-4047.

Han, W., Meehl, G.A., Rajagopalan, B., Fasullo, J.T., Hu, A., Lin, J., Large, W.G., Wang, J.-w., Quan, X.-W., Trenary, L.L., Wallcraft, A., Shinoda, T., and S. Yeager (2010), Patterns of Indian Ocean sea-level change in a warming climate. *Nature Geoscience Letters*, doi: 10.1038/NGEO901.

Hay, J. (2006). Climate Risk Profile for the Maldives. *Maldives: National Disaster Management Center*.

Herman, M.E., and S.W. Wheatcraft. 1984. Groundwater dynamics investigation of Enjebi Island, Enewetak Atoll: An interpretive computer model simulation. *In Finite Elements in Water Resources: Proceedings*, vol. 5, 133–142, ed. J.P.Laible, C.A.Brebbia, W. Gray, G. Pinder. London, England: Springer-Verlag.

Herzberg, Alexander, 1901, Die Wasserversorgung einiger Nordseebader [*The water supply on parts of the North Sea coast*]: Munich, Jour. Gasbeleucht. u. Wasserversorg., v. 44, p. 815-819, 842-844.

Hogan, P.J. 1988. Modeling of fresh water-saltwater interaction on Enjebi Island, Enewetak Atoll. *M.S. thesis, Department of Geology*, San Jose State University, San Jose, California.

Hunt, C.D., Jr. 1997. Hydrogeology of Diego Garcia. In Geology and Hydrogeology of Carbonate Islands. *Developments in Sedimentology* 54, eds. H.L. Vacher and T. Quinn, 909-931.

J C Pernetta and D.L. Elder, 1990, Climate, Sea Level Rise and the Coastal Zone: Management and Planning for Global Changes, *International Union for the Conservation of Nature and Natural Resources*, Gland.

Karthikheyan, T. (2010). Environmental Challenges for Maldives. *South Asian Survey*, 343-351.

Kench, P.S., McLean, R.F., Brander, R.W., Nichol, S.L., Smithers, S.G., Ford, M.R., Parnell, K.E., and M. Aslam (2006), *Geological effects of tsunami on mid-ocean atoll islands: The Maldives before and after the Sumatran tsunami. Geology*, 34(3), 177-180.

Ketabchi H., Mahmoodzadeh D., Ataie-Ashtiani B., Werner A. D., and Simmons C. T. (2014), Sea-level rise impact on fresh groundwater lenses in two-layer small islands, Hydrol. Process., 28; pages 5938–5953, doi: 10.1002/hyp.10059

Kipp, K. L. (1987). HST3D; a computer code for simulation of heat and solute transport in three-dimensional ground-water flow systems.

Lam, R.K. 1974. Atoll permeability calculated from tidal diffusion. Journal of Geophysical Research 79, 3073–3081.

Lloyd, J.W., J.C. Miles, G.R. Chessman, and S.F. Bugg. 1980. A ground water resources study of a Pacific Ocean atoll—Tarawa, Gilbert Islands.Water Resources Bulletin16, no. 4: 646–653.

Mather, J.D., 1975, Development of the groundwater resources of small limestone islands: Quarterly Journal of Engineering Geology, v. 8, p. 141-150.

MEE, 2004. State of the Environment Maldives 2011. Ministry of Environment and Energy, The Republic of Maldives, Male.

MEE, 2011. State of the Environment Maldives 2011. Ministry of Environment and Energy, The Republic of Maldives, Male.

Meehl, G., Goddard, L., Murphy, J., Stouffer, R. J., Boer, G., Danabasoglu, G., . . . Stockdale, T. (2009). Decadal Prediction: Can It Be Skillful? American Meteorological Society, 1467-1485.

Meurant, G. (1987). Multitasking the conjugate gradient method on the CRAY X-MP/48. Parallel Computing, 5(3), 267-280.

Molson, J. W., & Frind, E. O. (1994). SALTFLOW: Density dependent flow and mass transport model in three dimensions. User Guide, Waterloo Centre for Groundwater Research, University of Waterloo, Ontario.

Mörner , N.-A., Tooley, M., Possnert, G., 2004. New perspectives for the future of the Maldives. Global Planet. Change 40, 177–182.

MPHRE (1998). Fifth National Development Plan 1997-2000, Volume II, Ministry of Planning, Human Resources and Environment, Government of Maldives. UNEP,(2005) Post-Tsunami Environmental Assessment, Male, Maldives

MPND, 2006, Census 2006, Ministry of Planning and National Development, Male, Republic of Maldives.

Oberdorfer, J.A., P.J. Hogan, and R.W. Buddemeier. 1990. Atoll island hydrogeology: Flow and freshwater occurrence in a tidally dominated system. Journal of Hydrology 120, 327–340.

Peinhardt, K. A. (2014). Climate Change Vulnerabilities: Case Studies of the Maldives and Kenya. Honors Scholar Theses. Paper 383.

Pernetta, J.C. 1992. Impacts of climate change and sea-level rise on small island states. National and international responses. Global Environmental Change 2(1), 19-31.

Presley, T. K. (2005). Effects of the 1998 drought on the freshwater lens in the Laura area, Majuro Atoll, Republic of the Marshall Islands (No. 2005-5098). Geological Survey (US).

Rajasuriya AH, Zahir EV, Muely BR, Subramanian K, Venkataraman MVM, Wafar SM, Munjurul Hannan Khan, Whittingham E (2000) Status of coral reefs in South Asia: Bangladesh, India, Maldives and Sri Lanka. In: Wilkinson C (ed) Status of coral reefs of the world: 2000. Aust Inst Mar Sci, Townsville, pp 95–116, http://www.reefbase.org/references/ref_Literature.asp?searchactive=yes&ID=11755

Richmond, B.M., Jaffe, B.E., Gelfenbaum, G., Morton, R.A., 2006. Geologic impacts of the 2004 Indian Ocean Tsunami on Indonesia, Sri Lanka, and the Maldives. Zeitschrift für Geomorphologie N.F., Suppl.-Vol. 146, 235–251.

Sovacool, B. K. (2012). Perceptions of climate change risks and resilient island planning in the Maldives. Mitigation and Adaptation Strategies for Global Change, 17(7), 731-752.

Spennemann, D. (2006). Freshwater lens, settlement patterns, resource use and connectivity in the Marshall Islands. Transforming Cultures eJournal, 1(2).

Srikanthan, R. "Stochastic generation of daily rainfall data." MODSIM2005, Melbourne, 12 (2005): 1915-1921.

Srikanthan, R., & McMahon, T. A. (2001). Stochastic generation of annual, monthly and daily climate data: A review. Hydrology and Earth System Sciences, 653-670.

Stoer, J., & Bulirsch, R. (1980). Introduction to numerical analysis: New York, Springer-Verlag, 609p.

Taylor, K. E., Stouffer, R. J., & Meehl, G. A. (2012). An Overview of CMIP5 and the experiment design. Bulletin of the American Meteorological Society 93, 485-498.

Terry, J. P., & Falkland, A. C. (2010). Responses of atoll freshwater lenses to storm-surge overwash in the Northern Cook Islands. Hydrogeology Journal, 18(3), 749-759.

Terry, J. P., & Thaman, R. R. (2008). Physical geography of Majuro and the Marshall Islands. The Marshall Islands: environment, history and society in the atolls. Faculty of Islands and Oceans, The University of the South Pacific, Suva, Fiji, 1-22.

Terry, James P., and Ting Fong May Chui. "Evaluating the fate of freshwater lenses on atoll islands after eustatic sea-level rise and cyclone-driven inundation: a modelling approach." Global and Planetary Change 88 (2012): 76-84.

The World Bank. (2011). Maldives. Retrieved 11 10, 2012, from The World Bank: http://www.worldbank.org/en/country/maldives.

Thurber, D., Broecker, W., Blanchard, R., & Potratz, H. (1965). Uranium-Series Ages of Pacific Atoll Coral. Science 149, 55-58.

Todorovic, P., & Woolhiser, D. A. (1975). A Stochastic Model of n-Day Precipitation. Journal of Applied Meteorology, 17-24.

Tsyban, A.V., J.T. Everett, and J.G. Titus (1990), World oceans and coastal zones. In: UNESCO (1991), Hydrology and Water Resources of Small Islands: a practical guide. Studies and Reports in Hydrology. No. 49. Falkland A. (editor), Custodio E. (1991) with contributions from other authors. Unesco, Paris, France.

Underwood, M.R., F.L. Peterson, and C.I. Voss. 1992. Groundwater lens dynamics of atoll islands. Water Resources Research 28, no. 11:2889–2902.

Urish, D. W. (1974), Fresh water on the coral atoll island. The Military Engineer, Jan.-Feb., 25-27.

Vacher, H.L. (1997), Introduction: Varieties of carbonate islands and a historical perspective. In Geology and Hydrogeology of Carbonate Islands. Developments in Sedimentology 54, eds. H.L. Vacher and T. Quinn, 1-33.

Volker RE, Mariño MA, Rolston DE (1985) Transition zone width in ground water on ocean atolls. J Hydraul Eng 111(4):659–676

Voss, C. I. (1984). A finite-element simulation model for saturated-unsaturated, fluid-density-dependent ground-water flow with energy transport or chemically-reactive single-species solute transport (No. 84-4369). US Geological Survey,.

Voss, C.I. and A.M. Provost (2010), SUTRA, A model for saturated-unsaturated variable-density ground-water flow with solute or energy transport. USGS Water-Resources Investigations Report 02-4231. Reston, Virginia: USGS.

White, I., Falkland, T., Metutera, T., Metai, E., Overmars, M., Perez, P., Dray, A., 2007. Climatic and human influences on groundwater in low atolls. Vadose Zone J. 6, 581 – 590.

WHO (World Health Organization) (1972), International standards for drinking-water. WHO (U.N.), Geneva.

WHO(World Health Organization), 2009. Guidelines and Manual for Rain Water Harvesting in Maldives. Male, Maldives: Ministry of Housing Transport and Environment Government of the Republic of Maldives Technical Support.

Wilkinson C, O. Linden, H. Cesar, G. Hodgson, J. Rubens, and A.E. Strong, 1999. Ecological and socioeconomic impacts of 1998 coral mortality in the Indian Ocean: An ENSO impact and a warning of future change? Ambio 28, 188-196.

Winston, Richard B. ModelMuse: a graphical user interface for MODFLOW-2005 and PHAST. US Geological Survey, 2009.

Woodroffe C. D and Falkland A.C. (1997). Geology and hydrogeology of the Cocos (Keeling) Islands, Chapter 31, Geology and Hydrogeology of Carbonate Islands, Developments in Sedimentology 54 (editors Vacher, H.L. and Quinn, T.M., Elsevier, Amsterdam.

Woodroffe, C.D. 2008. Reef-island topography and the vulnerability of atolls to sea-level rise. Global and Planetary Change 62, 77-96.

Woodworth, P.L. 2005. Have there been large recent sea level changes in the Maldive Islands Global and Planetary Change 49, 1-18.

Woodworth, P.L., C. Le Provost, L.J. Richards, G.T. Mitchum and M. Merrifield (2002), A review of sea level research from tide gauges during the World Ocean Current Experiment. Oceanogr. Mar. Biol., 40 , 1-35.

APPENDIX I

Table A 1. Model performance results for monthly rainfall rates in Region 1 and RCP Scenario 4.5, ranking best to worst according to the total score.

GCM	Mean RE(mm)	Std RE	NRMSE	Corr	BS	S score	Kendal Slope (mm/year)	Total Score
IPSL-CM5A-MR	-0.04	-0.14	0.87	0.57	4.19	-0.04	-0.14	33
MIROC5	-0.05	0.05	0.83	0.67	5.23	-0.05	0.05	34.5
GFDL-ESM2M	-0.11	-0.04	0.94	0.56	2.93	-0.11	-0.04	44
FIO-ESM	0.07	0.01	1.09	0.41	3.79	0.07	0.01	50
HadGEM2-ES	-0.20	0.02	1.07	0.47	5.79	-0.20	0.02	58
CSIRO-Mk3-6-0	-0.16	-0.11	0.87	0.61	5.69	-0.16	-0.11	62
NorESM1-M	-0.04	0.17	1.15	0.45	4.83	-0.04	0.17	65.5
GISS-E2-R p3	-0.11	0.06	1.03	0.51	6.03	-0.11	0.06	67
IPSL-CM5A-LR	-0.16	-0.43	0.85	0.57	5.09	-0.16	-0.43	68
CESM1-CAM5	0.28	0.01	1.04	0.55	4.61	0.28	0.01	70
GISS-E2-H p3	-0.10	0.18	1.10	0.51	6.49	-0.10	0.18	70.5
GFDL-CM3	0.13	0.18	1.04	0.57	4.87	0.13	0.18	71.5
GISS-E2-H p1	-0.09	0.28	1.18	0.49	5.81	-0.09	0.28	74.5
CCSM4	0.24	0.08	1.07	0.52	4.83	0.24	0.08	77
GISS-E2-H p2	-0.06	0.29	1.16	0.51	6.51	-0.06	0.29	77.5
GFDL-ESM2G	-0.25	-0.22	1.02	0.45	4.23	-0.25	-0.22	80.5
NorESM1-ME	0.00	0.16	1.29	0.29	4.11	0.00	0.16	82
GISS-E2-R p2	-0.12	0.21	1.13	0.50	7.71	-0.12	0.21	87
GISS-E2-R p1	-0.13	0.19	1.15	0.47	7.65	-0.13	0.19	88.5
MIROC-ESM	0.55	0.46	1.39	0.63	4.11	0.55	0.46	93
MRI-CGCM3	-0.20	0.28	1.23	0.47	14.51	-0.20	0.28	95
MIROC-ESM-CHEM	0.59	0.42	1.41	0.62	4.81	0.59	0.42	95.5
HadGEM2-AO	-0.22	0.15	1.22	0.40	8.65	-0.22	0.15	111
bcc-csm1-1	0.24	0.80	1.79	0.32	12.03	0.24	0.80	135

Table A2. Model performance results for monthly rainfall rates in Region 1 and RCP Scenario 6.0, ranking best to worst according to the total score.

GCM	Mean RE(mm)	Std RE	NRMSE	Corr	BS	S score	Kendal Slope (mm/year)	Total Score
MIROC5	-0.09	0.04	0.86	0.65	4.79	99	0.0006	29
IPSL-CM5A-MR	0.00	-0.17	0.92	0.50	4.15	95	0.0013	35
GFDL-CM3	0.07	0.15	1.01	0.56	3.45	111	0.0026	36.5
CESM1-CAM5	0.24	0.01	1.01	0.56	4.75	90	0.0005	54
CSIRO-Mk3-6-0	-0.12	-0.06	0.86	0.62	6.15	84	0.0026	55
GISS-E2-H p3	-0.07	0.25	1.16	0.49	3.81	103	0.0027	58
FIO-ESM	0.07	0.01	1.11	0.39	4.05	96	0.0028	59
NorESM1-M	-0.01	0.22	1.21	0.42	5.16	99	0.0024	64.5
GFDL-ESM2G	-0.19	-0.16	1.01	0.45	3.29	103	0.0046	68
HadGEM2-ES	-0.16	0.06	1.10	0.46	5.11	99	0.0033	69
NorESM1-ME	-0.01	0.16	1.29	0.29	3.89	101	0.0032	72.5
GISS-E2-R p1	-0.08	0.33	1.24	1.24	5.91	94	-0.0009	74
GISS-E2-R p2	-0.09	0.30	1.22	0.46	6.55	90	0.0009	76
CCSM4	0.24	0.11	1.08	0.53	5.05	84	0.0045	77.5
GISS-E2-H p1	-0.04	0.47	1.34	0.46	6.09	99	0.0021	77.5
GISS-E2-R p3	-0.10	0.21	1.20	0.43	4.29	98	-0.0019	79.5
IPSL-CM5A-LR	-0.13	-0.23	0.99	0.42	4.21	97	0.0089	83.5
GFDL-ESM2M	0.07	0.26	1.40	0.25	4.01	107	0.0052	91.5
GISS-E2-H p2	-0.11	0.45	1.33	0.47	5.75	94	-0.0007	93.5
MIROC-ESM-CHEM	0.58	0.44	1.38	0.65	5.21	90	0.0025	94.5
MRI-CGCM3	-0.22	0.27	1.25	0.46	20.95	80	0.0019	96
MIROC-ESM	0.55	0.41	1.36	0.63	4.41	92	0.0056	103
HadGEM2-AO	-0.23	0.16	1.26	0.37	10.77	84	0.0089	113
bcc-csm1-1	0.21	0.74	1.67	0.38	12.57	84	0.0055	129.5

Table A3. Model performance results for monthly rainfall rates in Region 1 and RCP Scenario 8.5, ranking best to worst according to the total score.

GCM	Mean RE(mm)	Std RE	NRMSE	Corr	BS	S score	Kendal Slope (mm/year)	Total Score
IPSL-CM5A-MR	-0.03	-0.20	0.89	0.53	3.73	101	0.0007	30
GFDL-ESM2M	-0.08	-0.02	0.98	0.52	3.37	105	0.0016	32.5
MIROC5	-0.04	0.06	0.84	0.67	5.01	97	0.0059	42
FIO-ESM	0.04	0.01	1.07	0.42	3.73	97	0.0004	47.5
CSIRO-Mk3-6-0	-0.13	-0.08	0.87	0.61	5.63	85	0.0016	52
CESM1-CAM5	0.26	0.04	1.01	0.58	4.53	92	0.0021	58.5
GFDL-CM3	0.11	0.16	1.01	0.58	4.83	105	0.0056	61
GFDL-ESM2G	-0.21	-0.23	0.98	0.47	3.49	104	0.0032	65
GISS-E2-R p3	-0.10	0.21	1.21	0.42	3.99	96	0.0012	69
NorESM1-M	0.03	0.26	1.18	0.47	4.23	99	0.0104	69.5
NorESM1-ME	0.03	0.26	1.18	0.47	4.23	99	0.0104	69.5
GISS-E2-R p2	-0.07	0.33	1.23	0.48	7.11	95	0.0015	72
GISS-E2-H p3	-0.05	0.30	1.21	0.47	3.97	108	0.0074	77
HadGEM2-ES	-0.19	0.02	1.08	0.46	6.09	89	-0.0007	77.5
CCSM4	0.24	0.10	1.09	0.52	4.99	84	0.0055	82.5
IPSL-CM5A-LR	-0.14	-0.42	0.86	0.54	5.17	90	0.0064	83.5
GISS-E2-R p1	-0.07	0.34	1.33	0.38	5.39	95	0.0016	88.5
GISS-E2-H p1	-0.04	0.44	1.31	0.47	6.15	97	0.0035	90.5
MIROC-ESM	0.53	0.39	1.32	0.64	4.47	97	0.0039	90.5
GISS-E2-H p2	-0.09	0.40	1.31	0.45	6.17	92	0.002	93.5
MIROC-ESM-CHEM	0.55	0.42	1.35	0.65	4.73	82	0.0001	98.5
HadGEM2-AO	-0.28	0.07	1.23	0.37	8.13	84	0.0023	101
MRI-CGCM3	-0.19	0.32	1.30	0.42	16.25	91	0.0038	107.5
bcc-csm1-1	0.12	0.66	1.66	0.31	12.65	86	-0.0035	126.5

Table A4. Model performance results for monthly rainfall rates in Region 2 and RCP Scenario 2.6, ranking best to worst according to the total score.

GCM	Mean RE(mm)	Std RE	NRMSE	Corr	BS	S score	Kendal Slope (mm/year)	Total Score
CESM1-CAM5	0.09	0.26	1.33	0.33	3.69	111	-0.002	34.5
MIROC5	-0.12	-0.22	0.97	0.47	4.33	104	0.0023	39
IPSL-CM5A-LR	0.19	-0.21	1.04	0.43	3.93	102	0.0007	42.5
CCSM4	-0.14	0.02	1.08	0.46	3.95	104	0.0046	43
GFDL-ESM2G	0.01	0.17	1.34	0.24	4.07	109	0.0022	43.5
GISS-E2-R p1	0.07	0.42	1.46	0.31	3.97	105	-0.0033	53
NorESM1-ME	-0.12	0.25	1.41	0.24	3.63	108	0.0034	57.5
IPSL-CM5A-MR	0.25	0.16	1.37	0.29	4.35	110	0.0054	64
GISS-E2-R p2	0.08	0.41	1.44	0.33	4.49	96	0.004	64.5
HadGEM2-ES	0.25	0.52	1.39	0.53	6.03	88	-0.0002	67.5
NorESM1-M	-0.06	0.45	1.57	0.22	4.75	99	0.0028	74
GFDL-CM3	0.14	0.57	1.45	0.45	4.93	95	0.0029	75
GISS-E2-R p3	0.12	0.54	1.61	0.27	4.93	95	-0.0011	75
FIO-ESM	0.03	0.30	1.49	0.19	3.83	101	0.0062	75.5
GISS-E2-H p1	0.16	0.55	1.68	0.22	3.35	108	0.0018	79
MIROC-ESM	0.43	-0.04	1.49	0.20	4.63	93	-0.0025	79.5
MIROC-ESM-CHEM	0.43	-0.14	1.46	0.17	4.79	85	-0.001	81.5
MRI-CGCM3	0.23	0.90	1.71	0.49	4.99	90	0.0031	93.5
GISS-E2-H p2	0.27	0.49	1.65	0.25	4.57	96	0.0056	98
GFDL-ESM2M	0.26	0.86	1.78	0.42	4.93	113	0.0105	102
CSIRO-Mk3-6-0	0.59	0.49	1.77	0.46	5.81	75	0.0051	103
bcc-csm1-1	-0.11	0.69	1.83	0.15	11.15	100	-0.0083	113
GISS-E2-H p3	0.31	0.68	1.86	0.21	4.01	99	0.0121	118.5
HadGEM2-AO	0.85	0.85	1.79	0.42	4.99	91	0.0109	119

Table A5. Model performance results for monthly rainfall rates in Region 2 and RCP Scenario 4.5, ranking best to worst according to the total score.

GCM	Mean RE(mm)	Std RE	NRMSE	Corr	BS	S score	Kendal Slope (mm/year)	Total Score
CESM1-CAM5	0.00	-0.11	0.92	0.52	3.81	103	0.0028	24.5
GISS-E2-R p1	0.05	0.06	1.10	0.43	100	100	-0.0006	43
IPSL-CM5A-LR	0.19	-0.18	1.03	0.45	3.99	103	-0.0002	46.5
GISS-E2-R p2	0.07	0.12	1.17	0.40	4.39	99	0.0008	48
GFDL-ESM2G	0.01	0.10	1.26	0.28	4.05	106	0.0022	48.5
CCSM4	-0.13	0.03	1.08	0.46	3.63	106	0.0064	50
MIROC5	-0.11	-0.19	0.96	0.47	4.07	104	0.0043	51.5
GISS-E2-H p1	0.15	0.25	1.29	0.39	3.89	97	0.0005	64
GISS-E2-R p3	0.11	0.18	1.28	0.34	4.01	101	0.0034	68
FIO-ESM	0.02	0.22	1.43	0.17	3.47	107	0.0047	70
IPSL-CM5A-MR	0.24	0.22	1.40	0.30	2.79	119	0.0033	73
MRI-CGCM3	0.20	0.91	1.70	0.50	5.27	92	-0.0012	79
GISS-E2-H p2	0.20	0.13	1.26	0.37	4.39	89	0.0057	79.5
NorESM1-M	-0.08	0.36	1.50	0.22	3.92	102	0.0031	80
GFDL-CM3	0.17	0.61	1.48	0.47	4.37	111	0.005	80.5
HadGEM2-ES	0.26	0.56	1.44	0.52	5.77	84	0.001	81
GISS-E2-H p3	0.20	0.27	1.38	0.33	4.43	89	0.0035	89
MIROC-ESM	0.44	-0.02	1.53	0.16	5.55	81	0.0002	90
NorESM1-ME	-0.10	0.36	1.49	0.24	4.41	106	0.0057	91
MIROC-ESM-CHEM	0.46	-0.15	1.47	0.20	5.33	81	0.001	93.5
CSIRO-Mk3-6-0	0.57	0.47	1.74	0.45	6.35	75	0.0038	109
GFDL-ESM2M	0.29	1.09	2.05	0.35	3.81	118	0.0173	110
HadGEM2-AO	0.28	0.89	1.76	0.46	6.33	79	0.0049	111
bcc-csm1-1	-0.09	0.69	1.82	0.16	9.43	102	-0.0086	113

Table A 6. Model performance results for monthly rainfall rates in Region 2 and RCP Scenario 6.0, ranking best to worst according to the total score.

GCM	Mean RE(mm)	Std RE	NRMSE	Corr	BS	S score	Kendal Slope (mm/year)	Total Score
CESM1-CAM5	0.01	-0.12	0.93	0.51	3.53	103	0.0033	30
GFDL-ESM2G	-0.04	0.06	1.02	0.52	3.03	109	0.0074	33.5
MIROC5	-0.12	-0.18	1.02	0.42	3.49	107	0.0018	38
CCSM4	-0.13	0.04	1.09	0.45	3.69	106	0.0053	46
GFDL-CM3	0.13	0.51	1.42	0.44	4.33	102	0.0013	57.5
NorESM1-ME	-0.11	0.33	1.48	0.22	4.17	106	0.0025	62.5
FIO-ESM	0.03	0.30	1.52	0.14	3.01	110	0.0057	64.5
MIROC-ESM-CHEM	0.44	-0.08	1.46	0.24	4.51	89	-0.0011	67
GISS-E2-H p2	0.17	0.41	1.49	0.30	3.53	103	-0.0053	68
GISS-E2-R p3	0.12	0.45	1.54	0.26	4.59	95	-0.0015	72
IPSL-CM5A-LR	0.21	0.17	1.34	0.31	4.41	98	0.0061	72.5
GISS-E2-R p2	0.07	0.41	1.49	0.28	5.33	89	0.0036	75.5
GISS-E2-H p3	0.21	0.63	1.70	0.29	3.31	109	0.001	77
NorESM1-M	-0.07	0.40	1.53	0.22	4.98	94	0.0023	77.5
GISS-E2-R p1	0.13	0.50	1.50	0.35	3.67	101	0.0066	79
MIROC-ESM	0.46	0.02	1.53	0.23	4.91	90	0.0026	83
MRI-CGCM3	0.18	0.91	1.74	0.46	5.91	93	0.0001	84.5
HadGEM2-ES	0.28	0.62	1.51	0.50	5.05	90	0.0068	92
GFDL-ESM2M	0.25	0.78	1.71	0.41	3.51	120	0.0086	92.5
HadGEM2-AO	0.19	0.83	1.74	0.39	6.47	82	-0.0023	93
IPSL-CM5A-MR	0.49	0.22	1.81	0.05	6.65	86	-0.0007	102
bcc-csm1-1	0.06	1.00	2.04	0.21	8.49	102	0.0057	106.5
GISS-E2-H p1	0.20	0.56	1.76	0.15	3.37	104	0.0089	107
CSIRO-Mk3-6-0	0.61	0.53	1.82	0.46	7.17	71	0.0087	114.5

Table A7. Model performance results for monthly rainfall rates in Region 2 and RCP Scenario 8.5, ranking best to worst according to the total score.

GCM	Mean RE(mm)	Std RE	NRMSE	Corr	BS	S score	Kendal Slope (mm/year)	Total Score
CESM1-CAM5	0.03	-0.10	0.98	0.47	3.77	101	0.0064	43.5
MIROC5	-0.11	-0.23	0.95	0.48	4.09	104	0.0023	44
CCSM4	-0.13	0.01	1.10	0.43	3.89	105	0.0062	48
IPSL-CM5A-MR	0.23	0.03	1.32	0.25	3.73	107	-0.0007	49.5
GISS-E2-R p1	0.10	0.44	1.49	0.31	2.69	116	0.0015	53.5
GFDL-ESM2G	0.02	0.09	1.30	0.23	4.29	105	0.0041	56.5
FIO-ESM	0.01	0.21	1.43	0.17	3.65	107	0.0041	61
GFDL-CM3	0.13	0.51	1.42	0.44	4.51	100	0.0016	67.5
IPSL-CM5A-LR	0.22	-0.11	1.15	0.37	4.17	99	0.0045	68
NorESM1-ME	-0.07	0.37	1.49	0.24	3.55	110	0.0081	68.5
GISS-E2-H p3	0.21	0.48	1.58	0.29	3.41	102	0.0002	72.5
MRI-CGCM3	0.18	0.82	1.61	0.50	4.53	98	0.0001	77
GISS-E2-H p2	0.18	0.54	1.65	0.25	3.87	105	-0.002	78.5
MIROC-ESM-CHEM	0.43	-0.14	1.43	0.23	4.57	92	-0.0028	80
GFDL-ESM2M	0.19	0.77	1.74	0.34	3.29	123	0.0022	83.5
MIROC-ESM	0.46	-0.03	1.49	0.26	5.65	81	0.0024	83.5
GISS-E2-R p3	0.16	0.46	1.58	0.24	4.13	96	0.0013	84.5
NorESM1-M	-0.03	0.44	1.54	0.24	4.33	96	0.0075	86.5
GISS-E2-H p1	0.14	0.51	1.64	0.21	3.61	99	0.0009	87
HadGEM2-ES	0.26	0.65	1.50	0.52	5.35	88	0.0038	90
GISS-E2-R p2	0.11	0.41	1.55	0.22	4.25	99	0.0084	91.5
HadGEM2-AO	0.21	0.82	1.71	0.42	5.71	87	0.0008	98.5
CSIRO-Mk3-6-0	0.59	0.41	1.73	0.46	6.47	73	0.0047	104.5
bcc-csm1-1	-0.09	0.47	1.89	-0.13	7.87	81	0.0104	117

Table A8. Model performance results for monthly rainfall rates in Region 3 and RCP Scenario 2.6, ranking best to worst according to the total score.

GCM	Mean RE(mm)	Std RE	NRMSE	Corr	BS	S score	Kendal Slope (mm/year)	Total Score
CESM1-CAM5	0.26	-0.24	1.07	0.28	3.73	106	0.0051	35
NorESM1-ME	0.01	0.22	1.53	0.14	2.67	111	0.0035	38
CCSM4	0.24	-0.34	1.04	0.27	5.39	100	0.0028	40.5
MIROC-ESM	0.54	-0.23	1.24	0.04	2.79	110	-0.0007	49
IPSL-CM5A-LR	-0.16	-0.14	1.30	0.15	4.57	94	0.0015	56
MIROC5	-0.07	-0.33	1.13	0.13	3.49	107	-0.0015	56.5
MIROC-ESM-CHEM	0.58	-0.23	1.21	0.08	3.43	109	-0.0019	57
FIO-ESM	0.07	-0.18	1.33	0.01	4.13	95	0.0031	60
NorESM1-M	-0.03	0.27	1.70	0.00	2.83	106	0.0033	61
GISS-E2-R p1	-0.09	0.56	1.83	0.22	3.21	105	0.0046	62.5
IPSL-CM5A-MR	-0.01	0.17	1.57	0.08	3.45	111	-0.004	66.5
GFDL-CM3	0.09	0.57	1.68	0.29	3.53	111	-0.0036	72.5
HadGEM2-ES	-0.19	1.71	1.71	0.20	3.71	103	-0.0009	79.5
HadGEM2-AO	-0.23	0.75	1.96	0.18	3.97	104	0.0073	82
GISS-E2-H p1	-0.09	0.84	2.09	0.22	4.22	100	0.0036	86.5
MRI-CGCM3	-0.21	0.92	2.02	0.18	4.21	100	-0.0011	88
GFDL-ESM2G	-0.22	0.48	1.81	0.07	3.79	103	-0.0063	91.5
GFDL-ESM2M	-0.03	0.75	2.00	0.22	3.59	103	-0.0071	92
GISS-E2-R p3	-0.09	0.64	2.02	0.13	4.05	94	0.0024	97
GISS-E2-H p2	-0.06	0.72	2.07	0.14	5.21	84	0.0045	97.5
CSIRO-Mk3-6-0	-0.12	0.55	2.08	0.18	6.63	73	0.0002	101
GISS-E2-R p2	-0.11	0.57	1.89	0.13	4.71	89	0.0137	103.5
GISS-E2-H p3	-0.05	0.88	2.25	0.13	3.91	102	0.0011	108.5
bcc-csm1-1	0.25	1.06	2.19	0.14	16.09	68	-0.0078	109

Table A 9. Model performance results for monthly rainfall rates in Region 3 and RCP Scenario 4.5, ranking best to worst according to the total score.

GCM	Mean RE(mm)	Std RE	NRMSE	Corr	BS	S score	Kendal Slope (mm/year)	Total Score
CESM1-CAM5	0.00	-0.23	1.05	0.32	4.05	101	0.0018	30
CCSM4	-0.06	-0.33	1.05	0.27	4.45	102	0.0019	42
MIROC-ESM	0.01	-0.20	1.25	0.04	2.93	107	0.0024	42.5
MIROC-ESM-CHEM	0.02	-0.20	1.18	0.14	3.49	107	0.0019	44
MIROC5	0.06	-0.27	1.15	0.15	2.67	114	-0.0001	55
IPSL-CM5A-LR	0.18	-0.16	1.26	0.19	4.57	95	0.0012	58
IPSL-CM5A-MR	0.23	0.25	1.63	0.09	3.15	111	0.004	61.5
NorESM1-ME	0.11	0.25	1.53	0.12	2.69	111	-0.0082	68
HadGEM2-ES	0.22	0.57	1.74	0.22	3.73	97	0.002	69.5
NorESM1-M	0.17	0.21	1.59	0.04	3.11	107	-0.0029	71
GISS-E2-R p2	0.28	0.38	1.68	0.21	3.79	97	0.0056	75
GISS-E2-H p2	0.31	0.54	1.86	0.17	3.39	98	0.0034	76.5
GISS-E2-R p1	0.32	0.30	1.72	0.15	3.95	99	0.002	77
FIO-ESM	0.11	-0.24	1.27	0.03	4.33	100	-0.0006	78.5
GFDL-ESM2G	0.28	0.51	1.89	0.06	3.37	101	0.0032	79
GISS-E2-H p1	0.33	0.53	1.81	0.25	4.69	89	0.0035	79
GISS-E2-R p3	0.36	0.29	1.74	0.16	4.25	93	0.0036	81
MRI-CGCM3	0.14	0.97	2.08	0.17	4.41	96	0.003	88.5
GISS-E2-H p3	0.35	0.53	1.86	0.21	4.57	92	0.0012	93
GFDL-CM3	0.22	0.61	1.81	0.19	5.37	97	0.0006	96
bcc-csm1-1	-0.07	1.00	2.08	0.17	10.51	84	0.0012	101.5
HadGEM2-AO	0.21	0.74	1.93	0.16	4.25	98	-0.0044	104.5
GFDL-ESM2M	0.36	0.70	1.96	0.24	5.11	91	0.0063	108
CSIRO-Mk3-6-0	0.51	0.45	2.04	0.20	6.03	76	0.0057	108.5

Table A10. Model performance results for monthly rainfall rates in Region 3 and RCP Scenario 6.0, ranking best to worst according to the total score.

GCM	Mean RE(mm)	Std RE	NRMSE	Corr	BS	S score	Kendal Slope (mm/year)	Total Score
CESM1-CAM5	0.01	-0.21	1.10	0.25	4.15	100	0.003	26
IPSL-CM5A-LR	0.18	0.28	1.53	0.20	2.91	112	0.0034	38
CCSM4	-0.06	-0.30	1.06	0.28	5.09	98	0.0017	43
MIROC-ESM	0.02	-0.23	1.22	0.07	3.31	108	0.0019	45
MIROC5	0.06	-0.27	1.17	0.13	3.17	109	-0.0005	48
NorESM1-M	0.20	0.27	1.62	0.08	2.97	113	0.0027	55
MIROC-ESM-CHEM	-0.02	-0.17	1.28	0.02	3.43	109	-0.0032	57.5
NorESM1-ME	0.11	0.19	1.51	0.09	2.73	116	-0.0058	58.5
FIO-ESM	0.12	-0.20	1.29	0.03	3.47	105	0.001	61
GFDL-CM3	0.22	0.54	1.69	0.26	3.93	107	-0.0012	63
HadGEM2-ES	0.17	0.58	1.79	0.15	2.59	109	-0.0024	67
GISS-E2-R p1	0.31	0.62	1.93	0.15	3.33	110	0.0063	72.5
GISS-E2-H p2	0.33	0.73	1.98	0.21	4.57	97	0.0032	77
GFDL-ESM2G	0.26	0.51	1.87	0.06	4.01	107	-0.001	85
CSIRO-Mk3-6-0	0.52	0.55	2.13	0.18	6.95	68	0.0045	89
GISS-E2-R p3	0.34	0.59	1.94	0.14	4.59	95	0.0001	91
GISS-E2-H p1	0.37	0.86	2.18	0.14	3.95	98	0.0049	95.5
HadGEM2-AO	0.16	0.82	1.97	0.16	4.77	95	-0.0091	96
MRI-CGCM3	0.12	1.16	2.28	0.12	4.77	100	-0.0012	100.5
GISS-E2-H p3	0.41	0.91	2.26	0.15	4.65	91	0.0055	102.5
GFDL-ESM2M	0.32	0.65	1.99	0.12	4.33	100	-0.004	103.5
GISS-E2-R p2	0.28	0.63	1.97	0.08	3.73	98	0.0127	103.5
bcc-csm1-1	0.03	1.26	2.34	0.13	9.41	84	0.0109	106.5
IPSL-CM5A-MR	0.07	1.41	2.46	0.16	10.75	83	0.0117	107.5

Table A11. Model performance results for monthly rainfall rates in Region 3 and RCP Scenario 8.5, ranking best to worst according to the total score.

GCM	Mean RE(mm)	Std RE	NRMSE	Corr	BS	S score	Kendal Slope (mm/year)	Total Score
CESM1-CAM5	0.00	-0.25	1.08	0.25	4.01	102	0.0022	32
MIROC-ESM	0.03	-0.21	1.24	0.05	2.65	112	0.0045	47
CCSM4	-0.06	-0.33	1.04	0.29	5.11	95	0.002	47.5
MIROC-ESM-CHEM	0.01	-0.19	1.21	0.12	3.25	106	-0.0018	48.5
NorESM1-ME	0.17	0.20	1.54	0.10	2.95	113	0.0023	49.5
HadGEM2-ES	0.21	0.66	1.75	0.29	3.45	101	0.004	53
GFDL-CM3	0.24	0.53	1.70	0.26	4.13	107	0.0042	55.5
IPSL-CM5A-LR	0.18	-0.14	1.29	0.16	4.41	96	0.001	56.5
FIO-ESM	0.11	-0.17	1.32	0.00	3.35	107	-0.0001	60
IPSL-CM5A-MR	0.21	0.15	1.55	0.08	2.89	115	-0.0017	61.5
MIROC5	0.04	-0.32	1.12	0.16	4.61	100	-0.0043	64.5
HadGEM2-AO	0.24	0.95	2.02	0.28	4.49	98	0.0038	74.5
GISS-E2-R p1	0.25	0.55	1.79	0.19	3.31	107	-0.0027	77.5
NorESM1-M	0.18	0.16	1.57	0.03	3.85	99	-0.0044	81
MRI-CGCM3	0.15	1.00	2.16	0.11	4.39	98	0.0039	84.5
CSIRO-Mk3-6-0	0.51	0.51	2.09	0.18	6.59	77	0.0025	90.5
GFDL-ESM2G	0.24	0.42	1.78	0.06	3.87	99	-0.0039	91.5
GISS-E2-H p1	0.32	0.80	2.05	0.19	4.57	86	0.0007	96
GISS-E2-R p2	0.25	0.54	1.88	0.07	4.35	89	0.0073	96.5
bcc-csm1-1	-0.08	1.08	2.16	0.16	10.79	79	-0.0007	100.5
GISS-E2-H p2	0.34	0.81	2.09	0.17	4.85	87	0.0012	101.5
GISS-E2-R p3	0.34	0.63	2.00	0.11	4.13	96	-0.0029	104
GFDL-ESM2M	0.32	0.78	2.10	0.10	4.87	100	-0.0009	106.5
GISS-E2-H p3	0.37	0.91	2.24	0.13	4.37	98	-0.0024	114

Table A12. Average lens thickness under the center of the island for each island width and geographic region, across all accepted GCMs from the RCP8.5. The first set of values is averages through the years 2011-2030, and the second set is for the years 2031-2050. The GCM index corresponds to the order listed in Table 6.

Average Lens Thickness (m)		Island Width (m)											
		200			400			600			1100		
		R1	R2	R3	R1	R2	R3	R1	R2	R3	R1	R2	R3
First 20 Years (2011-2030)	GCM 1	0.23	0.33	0.81	1.96	2.22	4.00	4.92	5.46	8.81	11.27	11.66	12.92
	GCM 2	0.23	0.19	0.93	2.06	2.27	4.02	5.15	5.59	8.70	11.45	11.76	12.99
	GCM 3	0.21	0.36	0.83	2.11	2.65	4.31	5.25	6.28	9.29	11.50	12.03	13.13
	GCM 4	0.30	0.28		2.21	2.66		5.41	6.28		11.59	12.09	
	GCM 5	0.19	0.23		2.23	2.86		5.44	6.62		11.61	12.19	
	GCM 6	0.27	0.42		2.38	2.89		5.73	6.74		11.75	12.22	
	GCM 7	0.19	0.45		2.93	2.93		5.81	6.81		11.76	12.33	
	Mean	0.23	0.32	0.85	2.19	2.64	4.11	5.39	6.26	8.93	11.56	12.04	13.01
		R1	R2	R3	R1	R2	R3	R1	R2	R3	R1	R2	R3
Last 20 Years (2031-2050)	GCM 1	0.26	0.35	0.96	2.03	1.82	3.95	5.16	4.62	8.66	11.38	11.14	12.98
	GCM 2	0.20	0.20	0.80	2.13	2.59	4.33	5.30	6.16	9.31	11.54	12.00	13.14
	GCM 3	0.22	0.34	0.95	2.22	2.69	4.39	5.41	6.30	9.37	11.61	12.10	13.16
	GCM 4	0.54	0.30		2.28	2.72		5.52	6.37		11.68	12.12	
	GCM 5	0.24	0.19		2.67	3.13		6.31	7.17		11.97	12.44	
	GCM 6	0.38	0.67		2.84	3.34		6.59	7.60		12.08	12.48	
	GCM 7	0.43	0.59		3.20	3.67		7.18	8.13		12.30	12.64	
	Mean	0.32	0.38	0.90	2.48	2.85	4.22	5.93	6.62	9.11	11.79	12.13	13.09

APPENDIX II

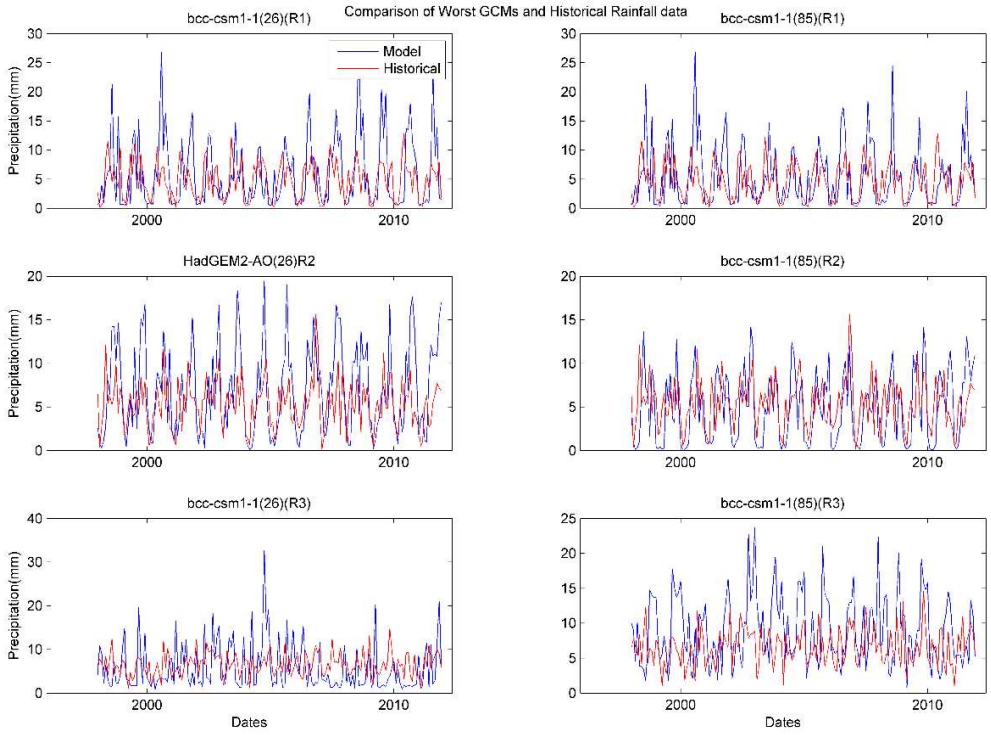

Figure B1. Comparison of historical rainfall data time series plots from worst GCMs for RCP.2.6

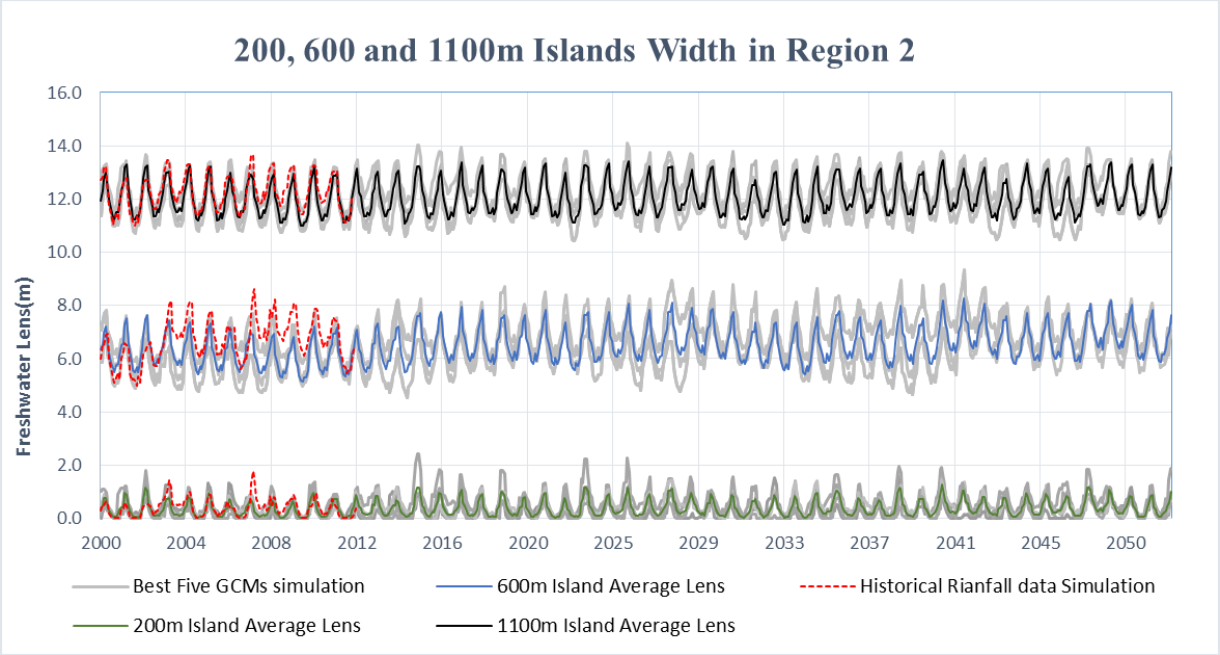

Figure B2. Time series plot of lens thickness for each accepted GCM in Region 2

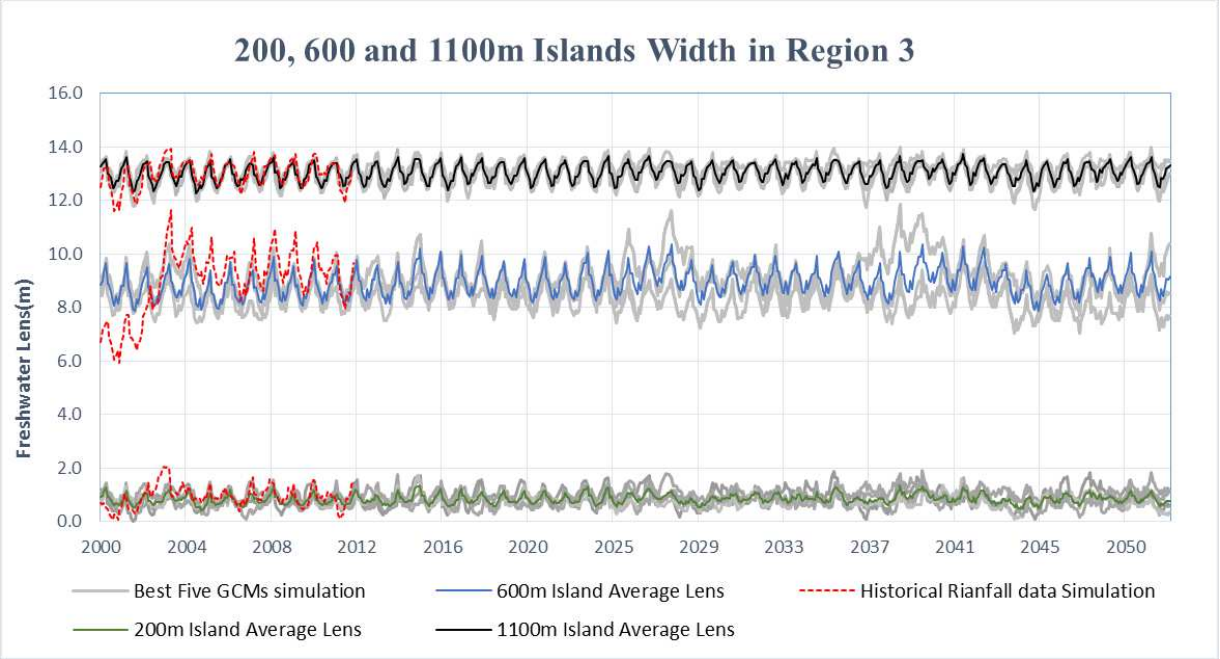

Figure B3. Time series plot of lens thickness for each accepted GCM in Region 3

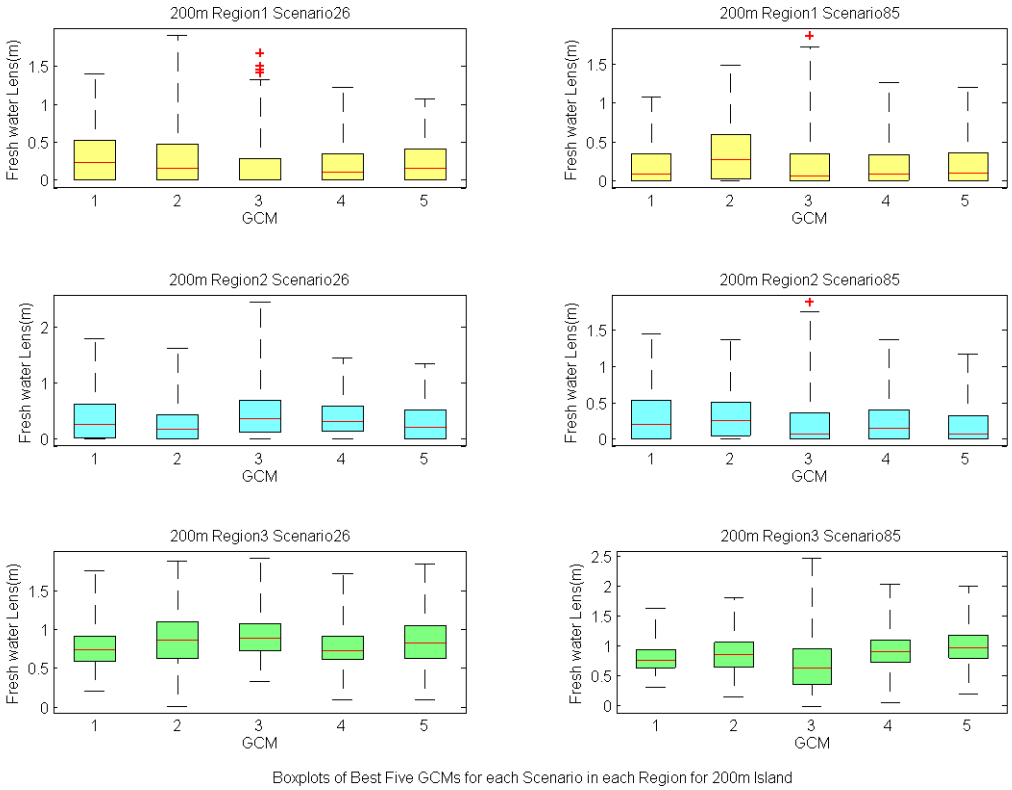

Figure B4. Boxplots of best five GCMs for each scenario in each region for 200m island

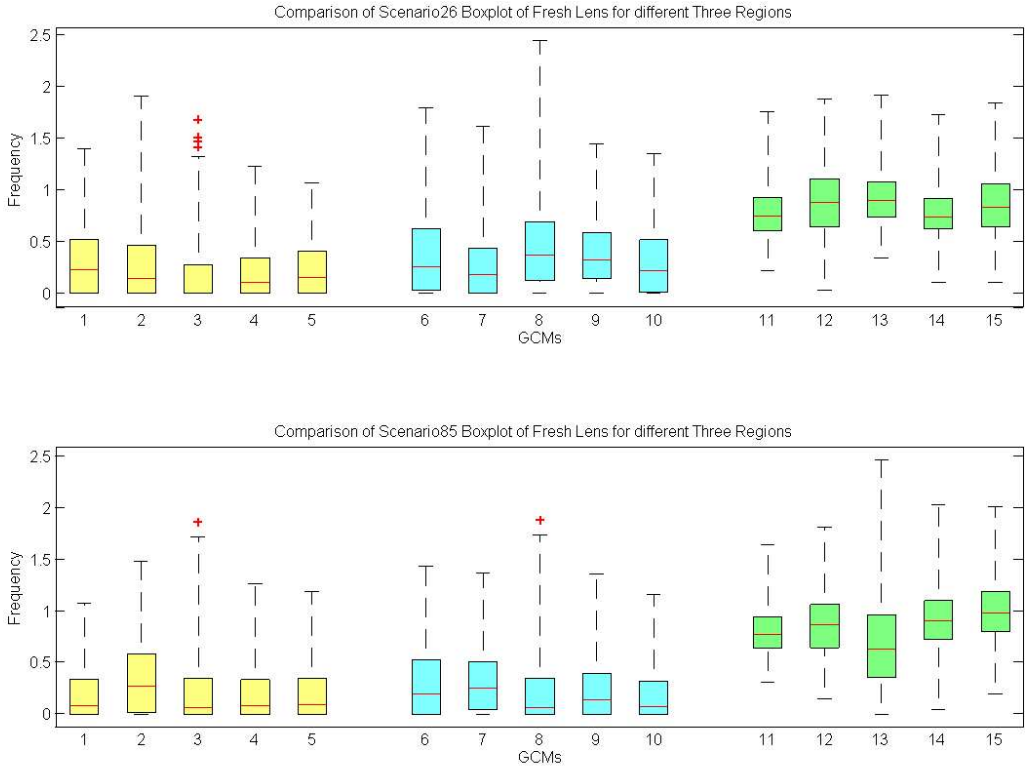

Figure B5. Comparison of scenario 26 boxplot of fresh lens for different three regions for 200 m island

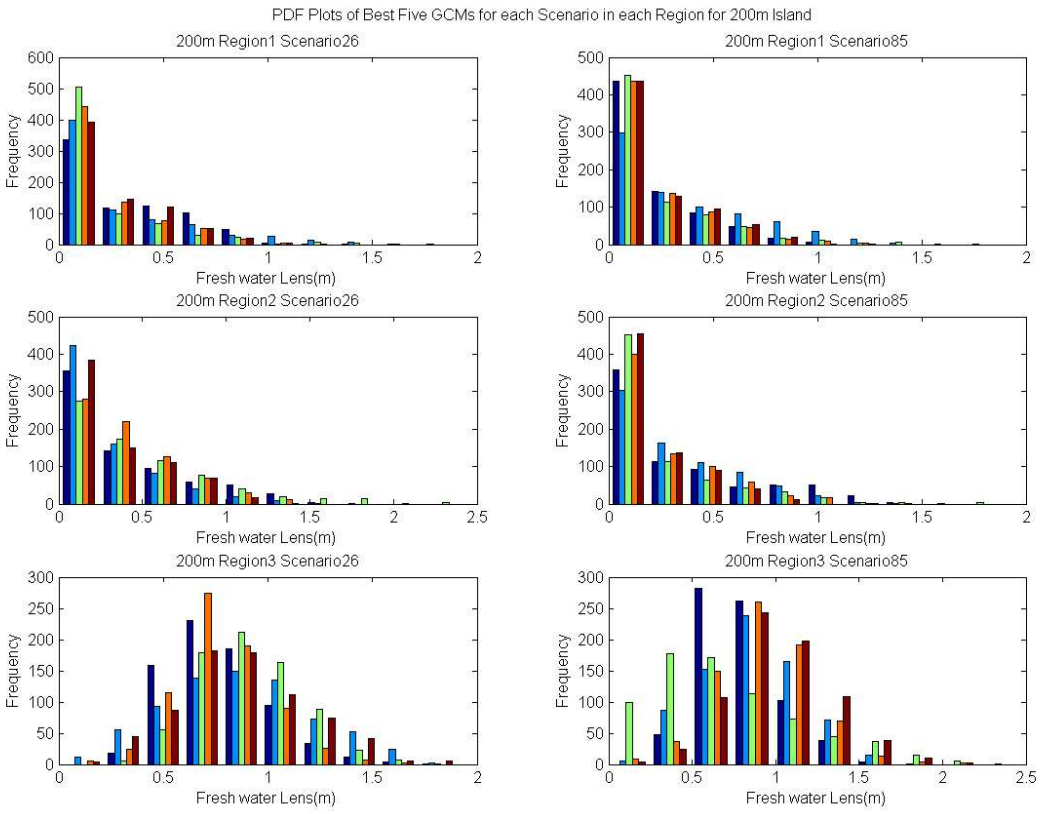

Figure B6. PDF plot of fresh lens between GCMs in 200 m island

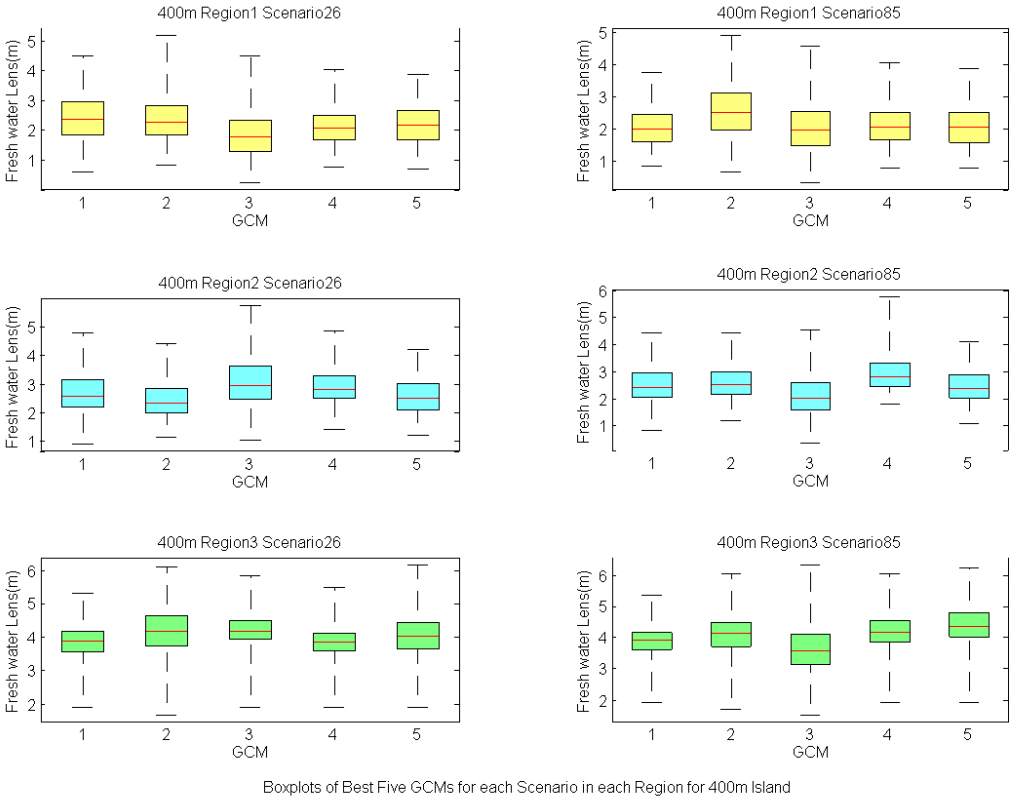

Figure B7. Boxplots of best five GCMs for each scenario in each region for 400m island

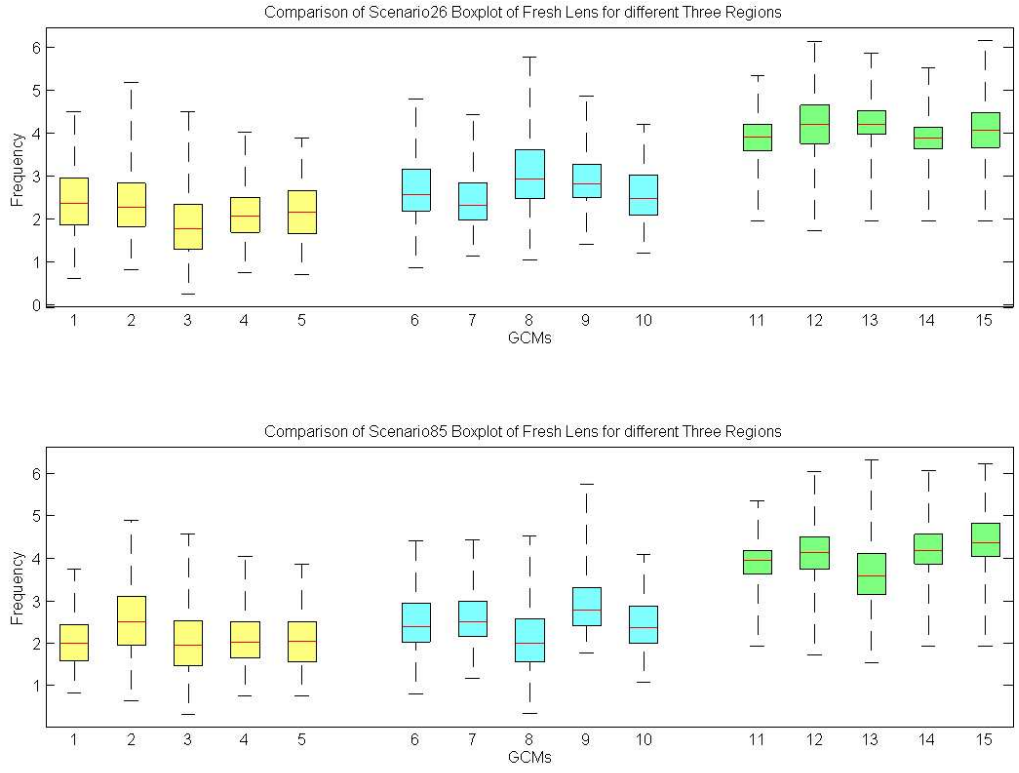

Figure B8. Comparison of scenario 26 boxplot of fresh lens for different three regions for 400 m island

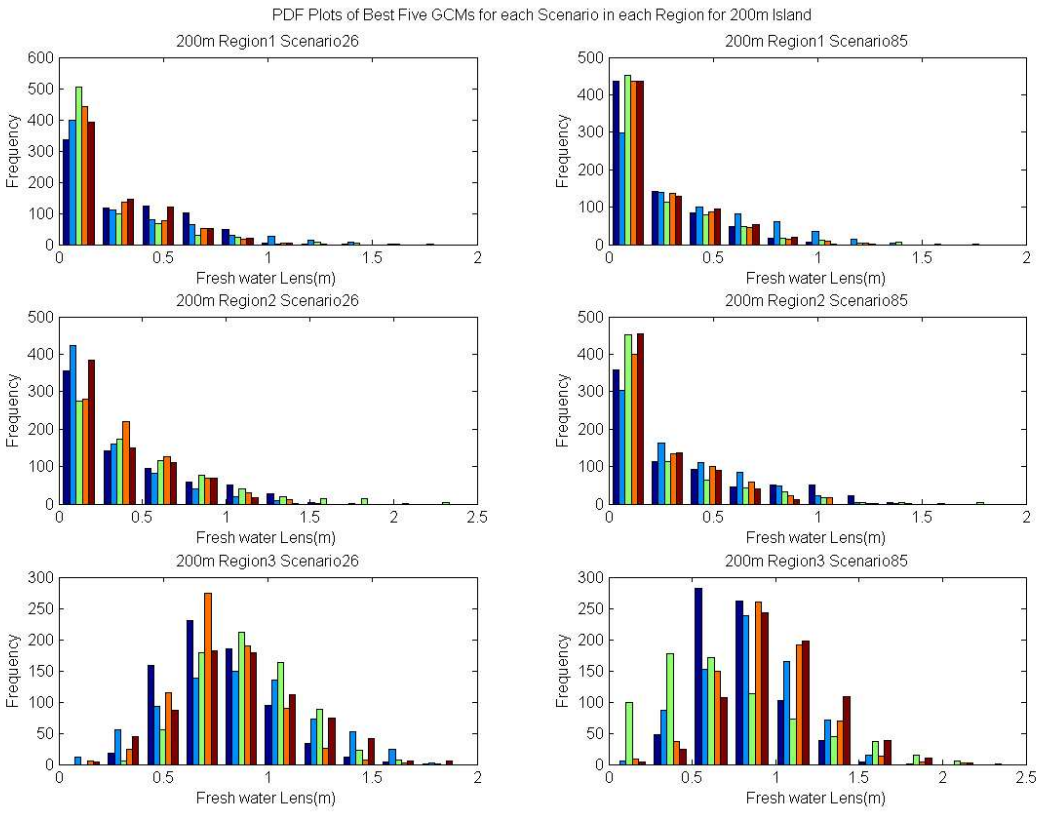

Figure B9. PDF plot of fresh lens between GCMs in 400 m island

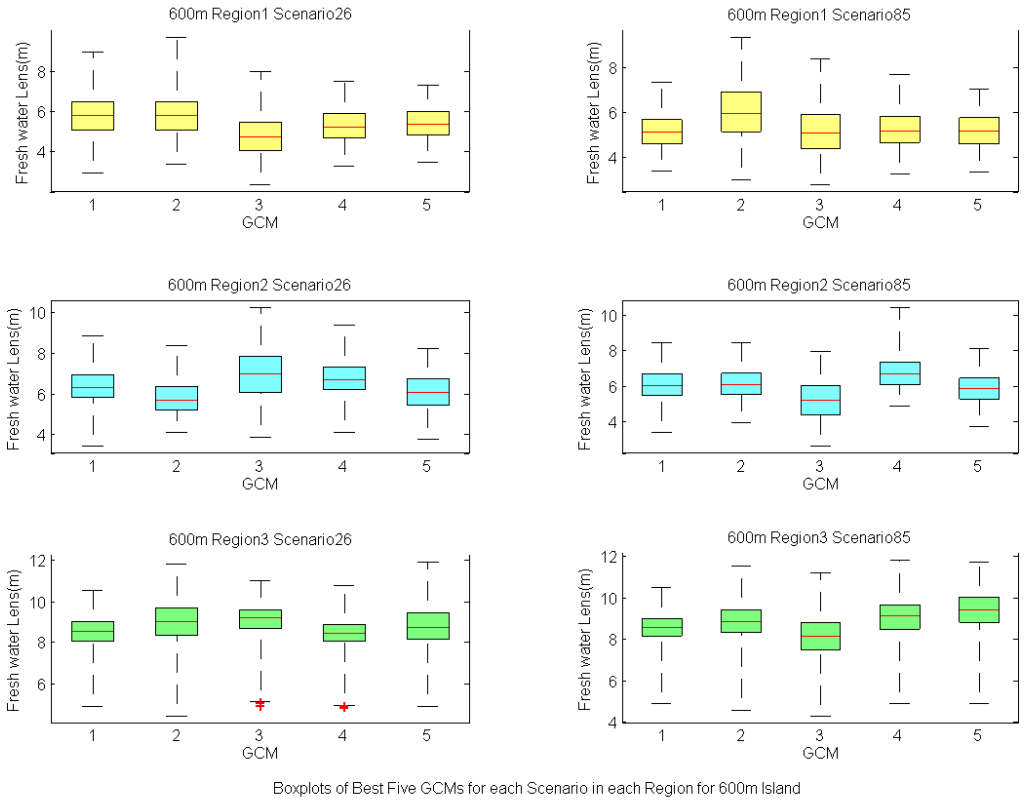

Figure B10. Boxplots of best five GCMs for each scenario in each region for 600m island

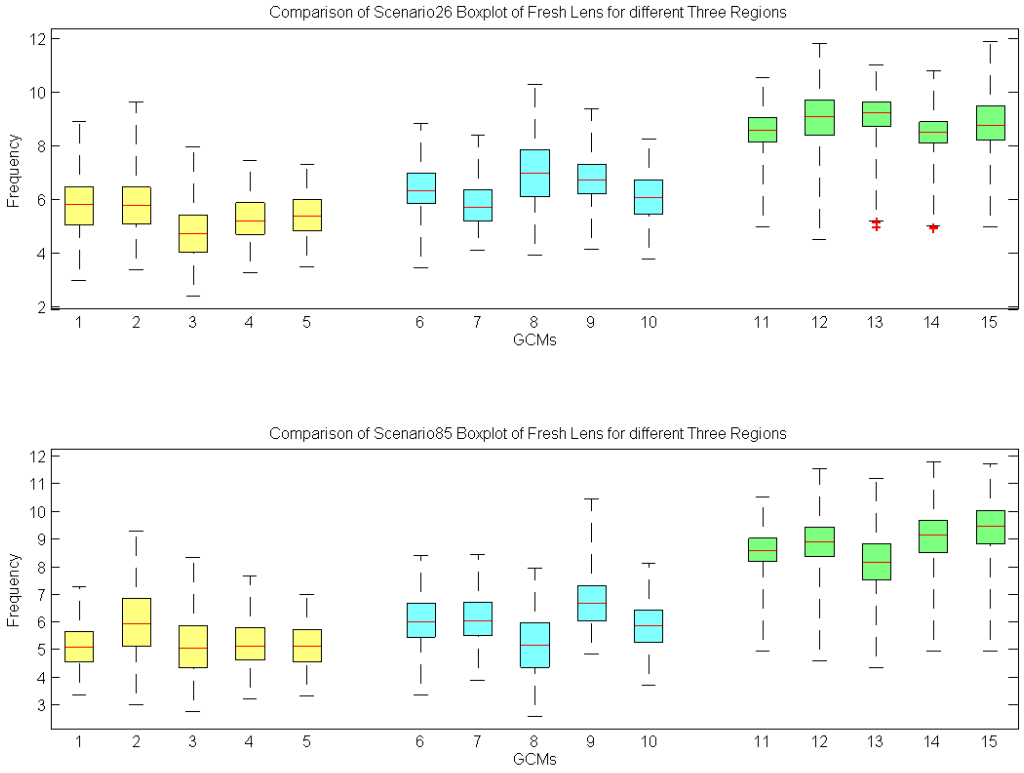

Figure B11. Comparison of scenario 26 boxplot of fresh lens for different three regions for 600 m island

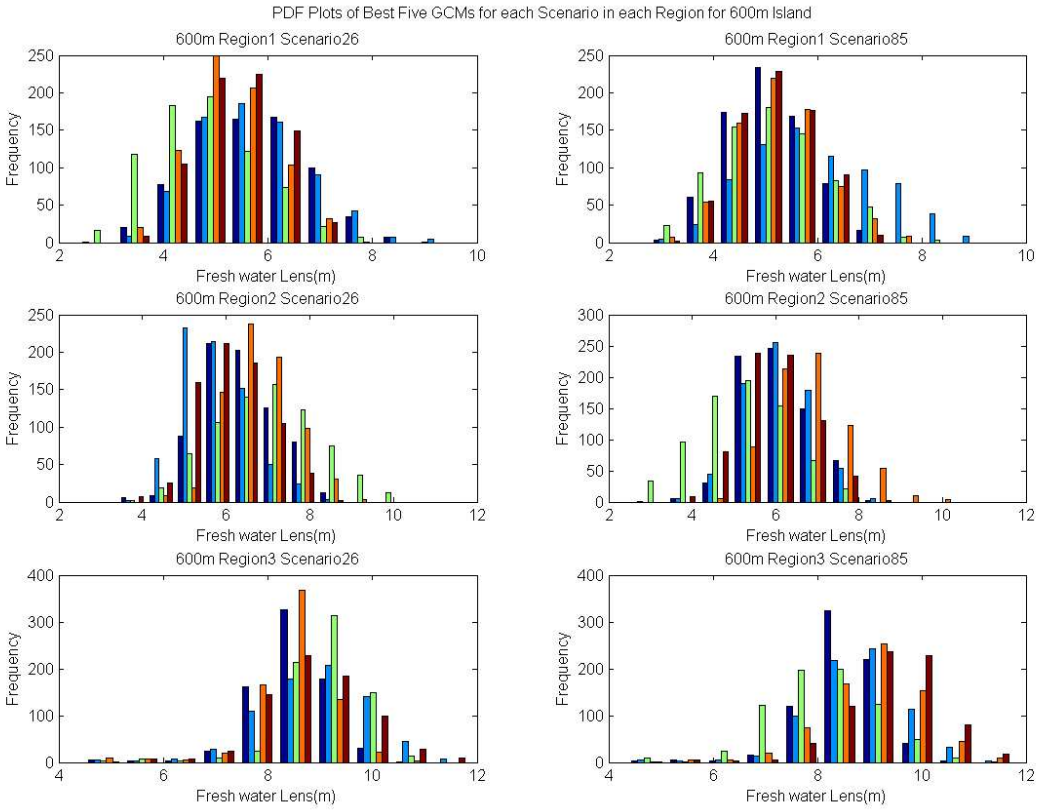

Figure B12. PDF plot of fresh lens between GCMs in 600 m island

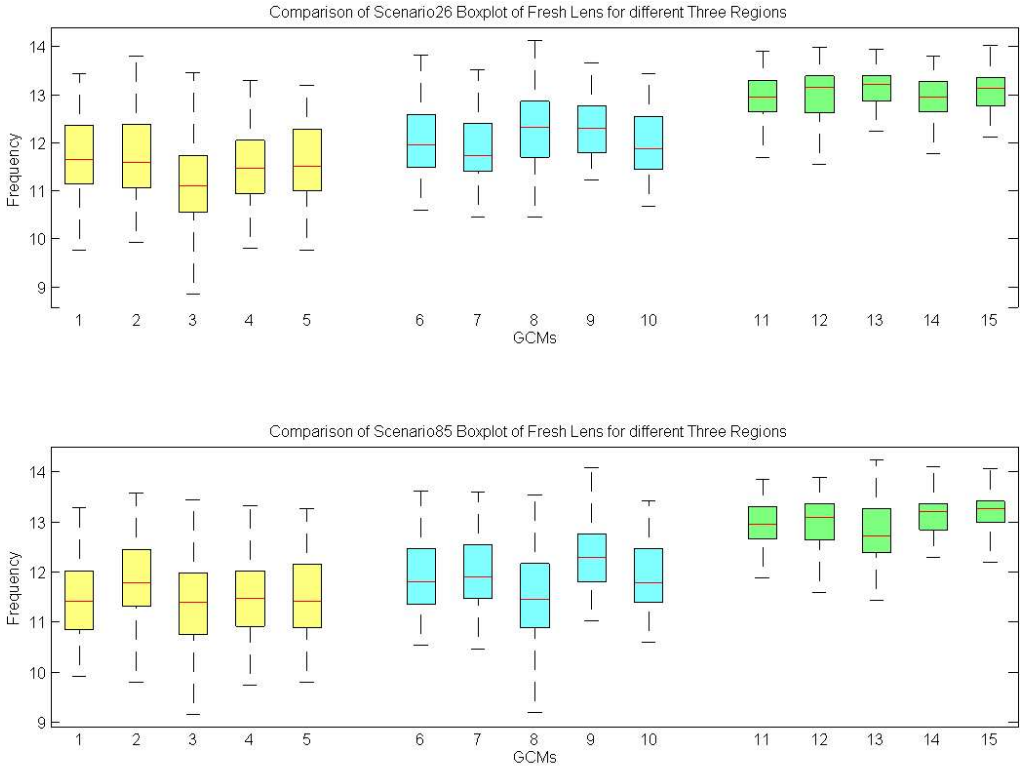

Figure B13. Comparison of scenario 26 boxplot of fresh lens for different three regions for 1100 m island

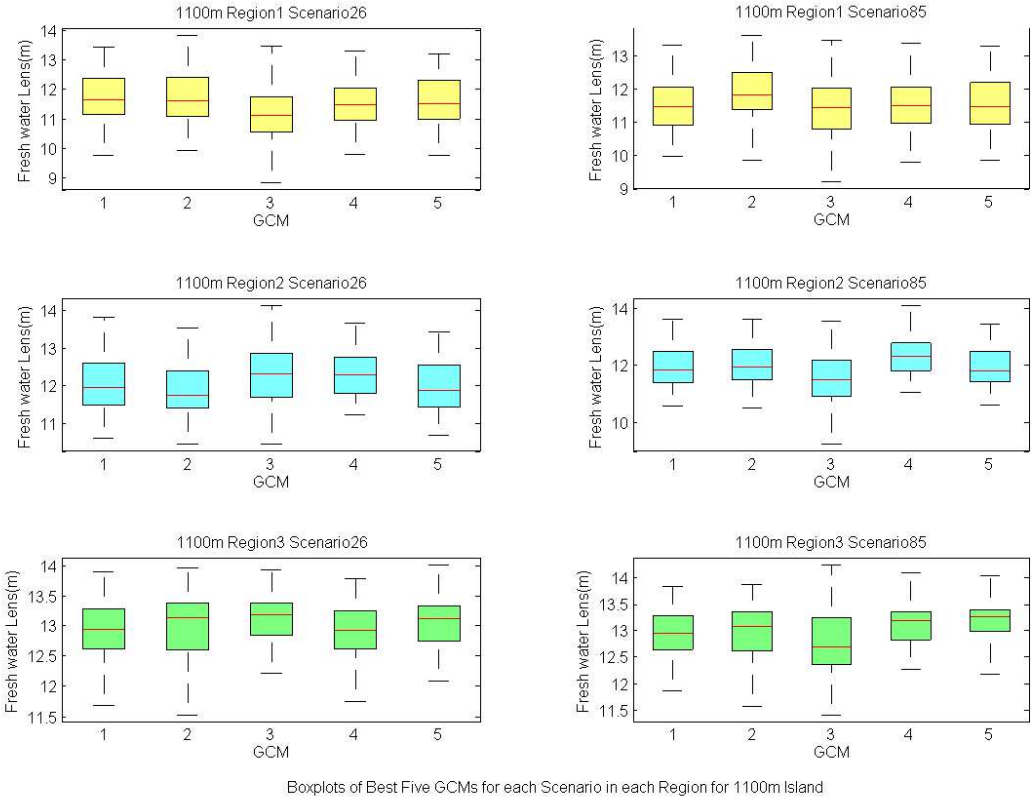

Figure B14. Boxplots of best five GCMs for each scenario in each region for 1100m island

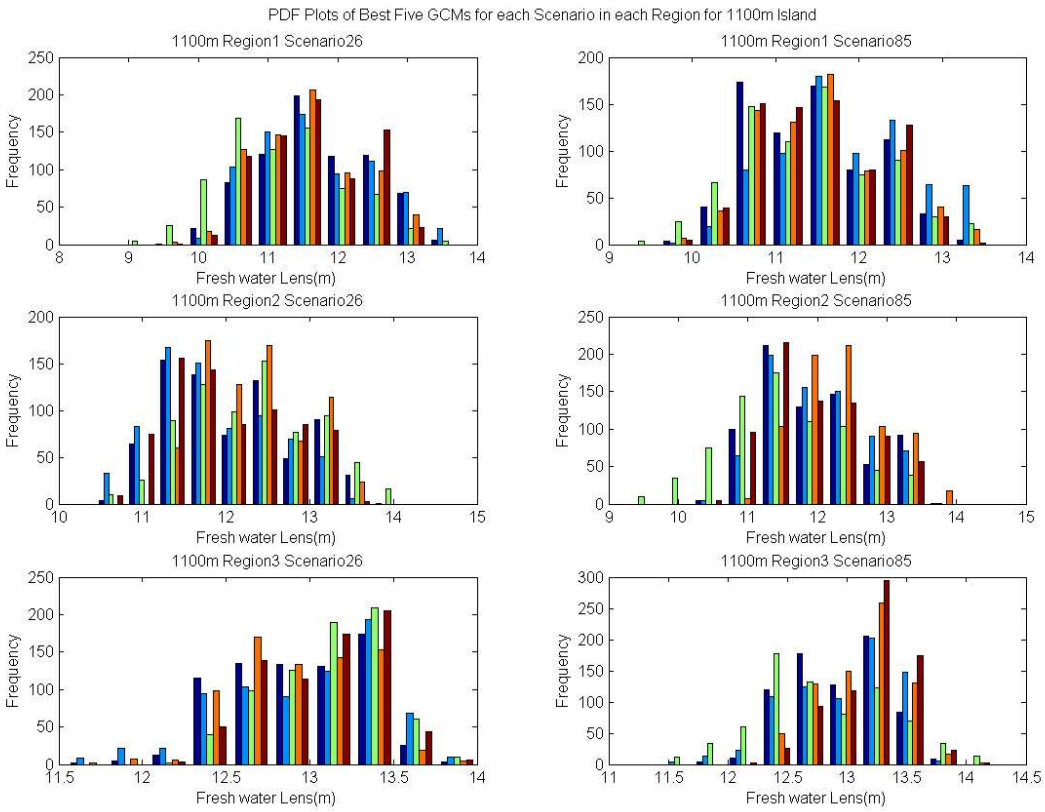

Figure B15. PDF plot of fresh lens between GCMs in 1100 m island

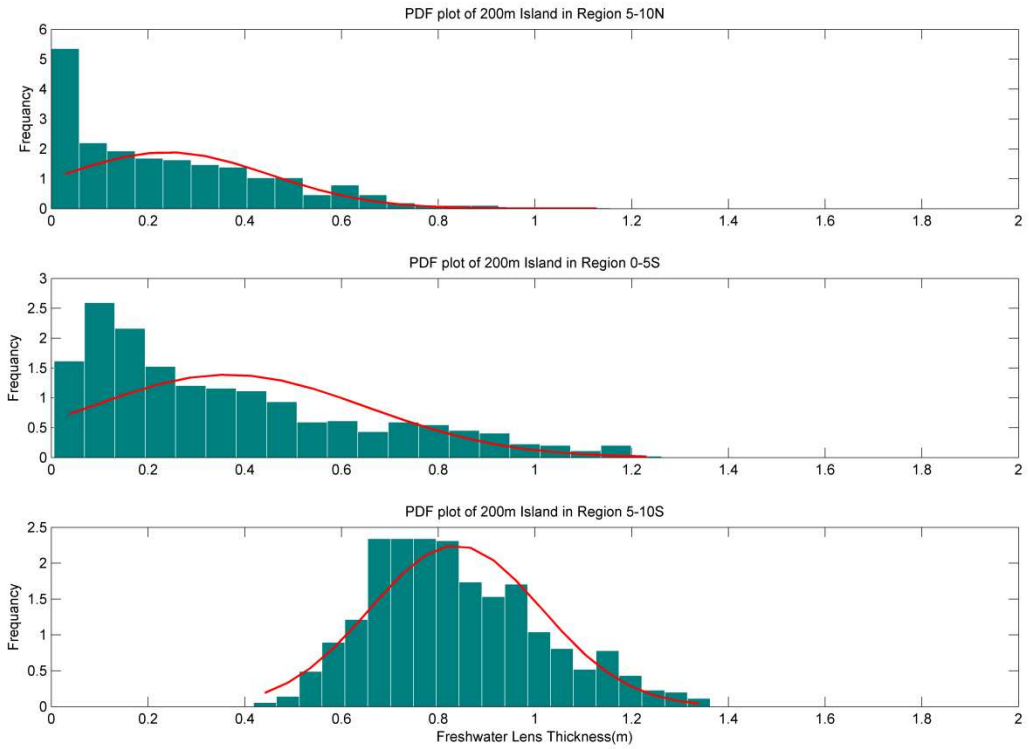

Figure B16. Lens thickness PDF plot for 200m islands

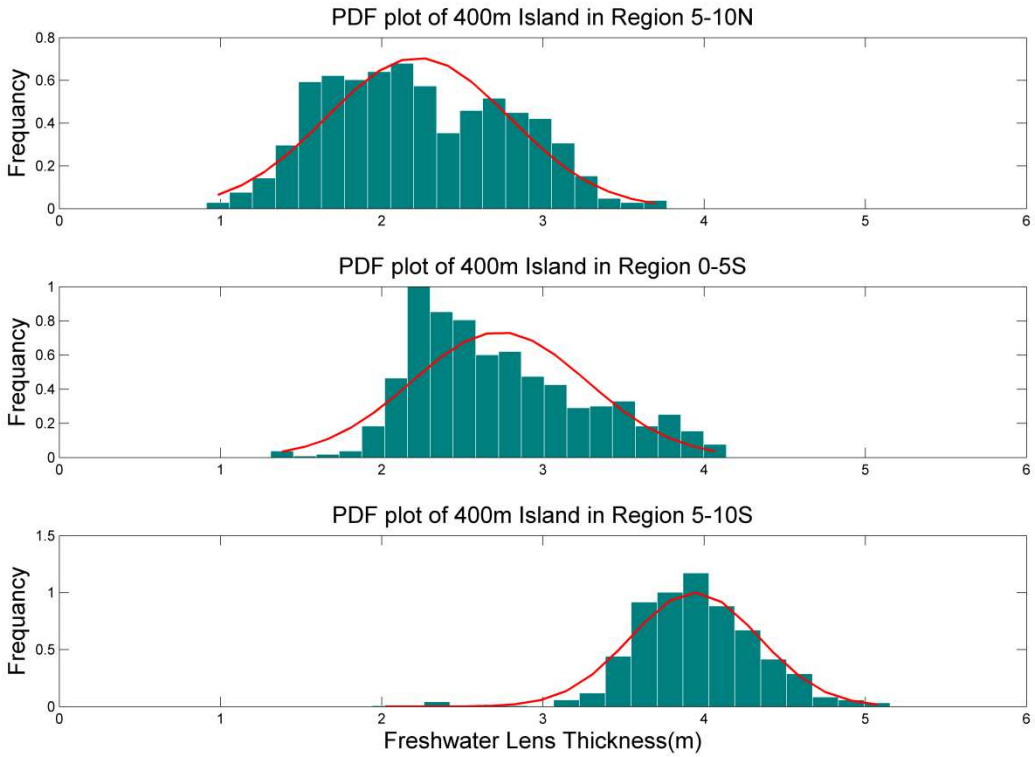

Figure B17. Lens thickness plot for 600 m islands